Technische Universität München
Fakultät für Medizin

The contribution of epithelial to mesenchymal transition (EMT) to the metastases of pancreatic cancer

Quentin Hans Albrecht Müller

Vollständiger Abdruck der von der Fakultät für Medizin der Technischen Universität München zur Erlangung eines

Doktors der Medizin (Dr. med.)

genehmigten Dissertation.

Vorsitz: Prof. Dr. Florian Eyer

Prüfer*innen der Dissertation:

1. Prof. Dr. Dieter Saur
2. Prof. Dr. Maximilian Reichert

Die Dissertation wurde am 09.01.2023 bei der Technischen Universität München eingereicht und durch die Fakultät für Medizin am 13.06.2023 angenommen.

Table of Contents

List of Tables

List of Figures

List of abbreviations

°C	degree Celsius
4-OHT	4-hydroxytamoxifen
α-SMA	alpha smooth muscle actin
AB	alcian blue
ADM	acinar-to-ductal-metaplasia
AFL	atypical flat lesion
AFN	atipamezole, flumazenil, naloxone
Ai65 mTmG	Rosa-CAG-FrtSTOPFrt-LoxSTOPLox-tdTomato
amp	ampicillin
ANOVA	analysis of variance
APS	ammonium persulphate
ATF	activating transcription factor
BLI	bioluminescence imaging
Bp	base pair
BSA	bovine serum albumin
CDKN2A	cyclin-dependent kinase inhibitor 2A
cDNA	complementary deoxyribonucleic acid
CAPL	Calcium placental Protein
Cers	ceramide synthase
CNV	copy number variation
COL6a1	collagen alpha-1 (VI) chain
COSMIC	catalogue of somatic mutations in cancer
CREB	cyclic AMP responsive element binding
CT	computed tomography
CTC	circulating tumour cells
CypA	cyclophilin
Da	Dalton
DDR	DNA damage response
DMEM	Dulbecco´s modified Eagle medium
DMSO	dimethylsulfoxide
DNA	deoxyribonucleic acid
dNTP	deoxynucleoside triphosphate
DRS	dual-recombinase system
DTT	dithiothreitol
EDTA	ethylenediaminetetraacetic acid
Elas	elastase
ELISA	enzyme-linked immunosorbent assay
EMT	epithelial mesenchymal transition
ERK	extracellular signal-related kinase
EtOH	ethanol
EV	empty vector
F18-FDG	fluorine-18-2-fluoro-2-deoxy-D-glucose
Fbp2	fructose-1,6-bisphophatase isozyme 2
FCS	fetal calf serum
FDR	false discovery rate
FISH	fluorescence *in situ* hybridisation
FOLFIRINOX	folinic acid, fluorouracil, irinotecan, oxaliplatin

FOXO	forkhead box O protein
FSF	*frt*-stop-*frt*
Fsp1	fibroblast specific protein 1
FTI	farnesyltransferase inhibitor
g	gram
GAP	GTPase-activating protein
GEF	guanine nucleotide exchange factor
GEMM	genetically engineered mouse model
GSEA	gene set enrichment analysis
GSK3	glycogen synthase kinase 3
h	hour
H&E	hematoxylin and eosin
HDAC	histone deacetylase
HEK	human embryonic kidney
Hmgcr	3-hydroxy-3-methylglutaryl CoA reductase
i.p.	intraperitoneal
IAP	inhibitor of apoptosis protein
IHC	immunohistochemistry
IKKε	inhibitory κB kinase epsilon
IPMN	intraductal papillary mucinous neoplasm
kb	kilo base pair
KO	knock-out
Kras	v-Ki-ras2 Kirsten rat sarcoma viral oncogene homolog
L	liter
LB	Luria Broth Bertani
Ldha	lactate dehydrogenase A
LOH	loss of heterozygosity
LSL	*loxP*-stop-*loxP*
M	molar
MALDI	matrix-assisted laser desorption/ionization
MAPK	mitogen-activated protein kinase
MCN	mucinous cystic neoplasm
MDCT	multi-detector CT
mg	milligram
min	minute
mL	milliliter
mm	millimeter
mM	millimolar
MMF	midazolam, medetomidine, fentanyl
MMP	matrix metalloproteinase
MRI	magnetic resonance imaging
mRNA	messenger ribonucleic acid
mTmG	membrane-targeted tandem dimer Tomato, membrane-targeted green fluorescent protein
mTOR	mammalian target of rapamycin
mts1	metastasin 1
MTT 3	(4,5-dimethyl-2-thiazolyl)-2,5-diphenyl-tetrazolium bromide
MW	molecular weight
nab	nanoparticle albumin-bound
Nf- κB	nuclear factor kappa-light-chain-enhancer of activated B-cells

ng	nanogram
NGS	next generation sequencing
nm	nanometer
nM	nanomolar
Nrf2	nuclear erythroid 2-related factor
NSCLC	non-small cell lung cancer
OD	optical density
OXPHOS	oxidative phosphorylation
PAGE	polyacrylamide gel electrophoresis
PanIN	pancreatic intraepithelial neoplasia
Parp poly	(ADP-ribose)-polymerase
PBS	phosphate buffered saline
PCR	polymerase chain reaction
PDAC	pancreatic ductal adenocarcinoma
PDEδ	phosphodiesterase delta
PDGF	platlet derived growth factor
PDK1	3-phosphoinositide-dependent protein kinase 1
Pdx1	pancreatic and duodenal homeobox 1
PET	positron emission tomography
Pfkl	phosphofructokinase, liver isoform
PH	pleckstrin homology
PI3K	phosphoinositide 3-kinase
PIP2	phosphatidylinositol 4,5-bisphosphate
PIP3	phosphatidylinositol 3,4,5-trisphosphate
PPP	pentose phosphate pathway
PPT	primary pancreatic tumour
PSC	pancreatic stellate cells
PTEN	phosphatase and tensin homolog
Ptf1a	pancreas transcription factor subunit alpha
PVDF	polyvinylidene fluoride
qRT-PCR	quantitative real time PCR
R26	*Rosa26*
RB	retinoblastoma
RNA	ribonucleic acid
ROCK	Rho Kinase
ROI	region of interest
ROS	reactive oxygen species
rpm	revolutions per minute
rRNA	ribosomal ribonucleic acid
RT	room temperature
RTK	receptor tyrosine kinase
rtTA	reverse tetracycline transactivator
SCID:	severe combined immunodeficiency
SEM	standard error of mean
SD	standard deviation
SDS	sodium dodecyl sulphate
SH2	Src homology 2
Skp2	S-phase kinase-associated protein 2
Snail	snail homolog 1
S.O.C.	Super Optimal Broth with catabolite repression

SUV	standardized uptake value
TAE	tris-acetate-EDTA
TAF	tumour associated fibroblasts
TAM	tamoxifen
TAM	tumour associated macrophages
TBST	tris-buffered saline tween-20
TCA	tricarboxylic acid
TE	tris-EDTA buffer
TEMED	N,N,N',N'-tetramethylethylenediamine, 1,2-bis(dimethylamino)-ethane
Tnc	tenascin C
TP53 / Trp53	transformation related protein 53
tTA	tetracycline transactivator
Twist	Twist related protein 1
U	unit of enzyme activity
Ubr1	ubiquitin protein ligase E3 component N-recognin 1
UV	ultraviolet
V	volt
WB	western blot
WT	wild type
w/v	weight per volume
µg	microgram
µL	microliter
µm	micrometer
µM	micromolar
zeb1	Zinc Finger E-Box Homeobox 1

1. Abstract

Malignant neoplasia is the second leading cause of death worldwide while metastatic outspread with consecutive systematic organ failure is the main reason for cancer-associated death. Pancreatic cancer is a highly malignant, highly metastatic disease with very poor prognosis and limited treatment options which remained unchanged over the last decades. Metastasis development is commonly associated with the activation of epithelial to mesenchymal transition (EMT), a genetic program which allows cancer cells to increase their ability to infiltrate the bloodstream, disseminate and detach from the primary tumour mass.

Recent studies however challenged the common metastatic pathway when the knock-out of key EMT-Transcription factors (EMT-TF) failed to suppress metastatic formation and development in pancreatic cancer. Targeting EMT-positive cells *in vivo* has been a problem for years due to the transient nature of EMT and mesenchymal to epithelial transition (MET). In this work I used a dual recombinase, dual immunofluorescence reporter system under the control of a gatekeeper of EMT in pancreatic cancer (Fsp1). This enabled tracing EMT positive and negative cells *in vivo* to all metastatic sites. To overcome interfering host-specific fluorescence signals I performed orthotopic transplantation of primary pancreatic tumour (PPT) cell lines into immunocompetent (C57BL6/J;129/S6) and immunodeficient mice (*NOD.Cg-Prkdcscid Il2rgtm1Wjl*/SzJ (SCID)). In all three approaches EMT negative metastases largely outnumbered EMT positive metastases in nearly all organ systems.

In a large-scale immunofluorescence analysis, utilizing different mesenchymal and epithelial markers the reporter system was evaluated for its veracity and its ability to reliably label EMT positive and negative cells. I showed that EMT negative labelled cells ubiquitously harboured an epithelial phenotype while recombined EMT positive labelled cells showed the whole spectrum of mesenchymal, epithelial and partial epithelial partial mesenchymal cells.

This data now provides a robust and reliable reporter system to target EMT events *in vivo* and *vitro*. Furthermore, it suggests alternative, EMT independent routes to metastases in pancreatic cancer. This opens up a new field of research which needs further attention to identify new metastatic mechanisms.

2. Zusammenfassung

Maligne Neoplasien sind die zweithäufigste Todesursache weltweit, wobei die Metastasierung mit konsekutivem, systemischen Organversagen die Hauptursache für Krebs assoziiertem Tod ist. Das Pankreaskarzinom ist eine hoch maligne, hoch metastatische Erkrankung mit infauster Prognose und limitierten Behandlungsoptionen, welche in den letzten Jahrzehnten unverändert geblieben sind. Die Entwicklung von Metastasen ist im Allgemeinen mit der Aktivierung der epithelialen zu mesenchymaler Transition (EMT) assoziiert, einem genetischen Programm, welches es Tumorzellen erleichtert, den Blutstrom zu infiltrieren, zu disseminieren und sich von der primären Tumormasse abzulösen.

Aktuelle Studien fordern jedoch die allgemein gültige Theorie der Metastasenentwicklung heraus, da knock-outs von Schlüssel EMT-Transkriptionsfaktoren nicht ausreichten, um die Entwicklung von Metastasen des Pankreaskarzinoms zu unterdrücken. EMT-Zellen *in vivo* zu verfolgen, ist aufgrund der flüchtigen Natur von EMT und der mesenchymalen zu epithelialen Transition (MET) ein langbestehendes Problem. In dieser Arbeit benutzte ich ein duales Rekombinase, duales Fluoreszenzreporter System, das von einem „Gatekeeper“ Protein für EMT im Pankreaskarzinom (Fsp1) kontrolliert wird. Dies ermöglicht es, EMT positive und EMT negative Zellen *in vivo* in alle Metastasen zu verfolgen. Um störende, wirtspezifische Immunfluoreszenzsignale auszuschließen, führte ich orthotrope Transplantationen von primären Pankreastumor (PPT) Zellen in immunkompetente und immundefiziente Mäuse durch. In allen drei Ansätzen überstieg die Anzahl von EMT negativen Metastasen die Anzahl von EMT positiven Metastasen in fast allen Organsystemen deutlich.

In einer großangelegten Immunfluoreszenzanalyse wurde unter der Benutzung von verschiedenen mesenchymalen und epithelialen Markern das Reporter System auf seine Verlässlichkeit und Richtigkeit evaluiert. Ich habe gezeigt, dass EMT negativ markierte Zellen durchgehend einen epithelialen Phänotyp exprimierten, während EMT positiv markierte Zellen das gesamte Spektrum von mesenchymalen, epithelialen und teilweise epithelial, teilweise mesenchymalen Zellen abbildeten.

Diese Daten stellen nun ein robustes und zuverlässiges Reporter System zur Verfügung, um EMT-Ereignisse *in vivo* und *in vitro* zu verfolgen. Des Weiteren geben sie zusätzliche Hinweise auf EMT-unabhängige Metastasenentwicklung. Dies eröffnet ein neues Forschungsfeld, welches mehr Aufmerksamkeit benötigt, um neue Metastasierungsmechanismen zu identifizieren.

3.Introduction

3.1 History of pancreatic cancer

Cancer is the second leading cause of death worldwide and was responsible for estimated 8,9 million deaths in 2016. In the last centuries new treatment and diagnosis options arose for many different cancer entities and greatly increased survival and the prognosis of patients. However, research mostly focused on the main tumour entities, like breast, prostate or gastrointestinal cancer. Excellent prognosis and treatment options as well as good organized early detection algorithms have been established for those cancers. Meanwhile other tumour entities remain unheeded and survival prognosis did not improve. (Roser Max und Ritchie Hannah 2018).

Among those, one tumour type should be especially regarded: pancreatic cancer. While only accounting for 3% of the global cancer cases, it is responsible for over 7% of cancer associated deaths in the United States and is therefore the 4th leading cause of cancer-related death in both sexes. Even more, in contrast to most other cancers, the overall cancer mortality did not decline for over 50 years but slightly rose and the 5-year survival rate remained unchanged low at approximately 9%, stressing the lack of innovation in this field of study (Siegel et al. 2019). Demographic simulations also suggest that pancreatic cancer will surpass most other cancer types in the following years and will be the second leading cause of cancer-associated deaths in 2030 right after lung carcinomas (Rahib et al. 2014). Its poor prognosis is mainly associated with late stage detection, early metastases, lack of surgical and pharmacological treatment options, high relapse rates and substantial chemo- and radioresistance (Ryan et al. 2014).

Pancreatic ductal adenocarcinoma (PDAC) accounts for over 90% of all pancreatic cancer types, while the rest are neuroendocrine or tumours of the pancreatic islet cells. Only 10-20% of PDAC get diagnosed at an early treatable stage, while the rest are either locally advanced or already systematic spread (Adamska et al. 2017; Siegel et al. 2019). At these late stages, the tumour has either already formed distant metastases or will do so soon. The median survival of PDAC patients greatly varies depending on the tumour stage from 26 month (resectable), to 12-18 months (borderline resectable or locally advanced) and 6-11 months (metastatic) (Neoptolemos et al. 2018). This has not significantly changed for the last few decades. Novel state of the art treatment possibilities for metastatic PDAC with FOLFIRINOX (5-fluorouracil, leucovorin, irinotecan, and oxaliplatin) or Gemcitabine and nab-Paclitaxel could only provide a marginal increase of survival of 4,3 and 1,8 months respectively (Conroy et al. 2011; Hoff et al. 2013). Additionally, surgical treatment is mostly limited due to the normally advanced tumour stage and although humans can live without a functional pancreas, the high malignancy

of this tumour and the resulting high metastatic burden subsequently leads to early organ failure (mostly liver and lung) and accounts for most of the patients' early deaths (Gupta und Massagué 2006). But even small, localised tumours, which can be completely removed by surgery have a high rate of early local (38%) or distant relapses (46%) (Fischer et al. 2012).

To recapitulate, PDAC is a highly aggressive, highly lethal tumour entity with limited therapeutically options, stagnating progress but rising cases worldwide. This marks pancreatic cancer treatment as one of the scientific challenges. There is obviously an urgent need to better understand the development of this cancer and to identify the mechanisms that contributes to its high malignancy and from that generate novel strategies to address PDAC in the future.

3.1.1 Kras driven mouse model

For further investigation it is crucial that reliable, comparable, and suitable models exist, to examine molecular patterns, genetical aberrations, and any other stage of pancreatic cancer. Multistep analyses of human PDAC samples have shown a great variety of promising genetical targets which are responsible for PDAC induction, maintenance, and progression (e.g. Kras, SMAD4, p53, CDKNA2) (Iacobuzio-Donahue et al. 2009; Hustinx et al. 2005) To implement genetically engineered mouse models (GEMM), that mimics human PDAC mostly inducer of pancreatic metaplasia and dysplasia are utilized. The most common PDAC GEMMs use the pathological activation of the oncogenic $Kras^{G12D}$ mutation. Aberrant expression and activity of Kras is observed in over 90% of PDAC and PDAC precursor lesions (pancreatic intraepithelial neoplasias (PanINs)) (Kanda et al. 2012). It was also shown that the activity of Kras is obligatory for PDAC formation, development, and maintenance (Ying et al. 2012; Pylayeva-Gupta et al. 2011; Morris et al. 2010; Seidler et al. 2008). Therefore, current GEMM for PDAC utilize a permanently active Kras mutation ($Kras^{G12D}$) knock-in, controlled by a stop cassette which is flanked by frt or loxP sites. Oncogenic activity of Kras in the pancreas is achieved by interbreed of $Kras^{G12D}$ (LSL or FSF) mice with organ specific induction of the recombinases Flp or Cre, resulting in sporadic PDAC development (Herreros-Villanueva et al. 2012). Organ specificity is achieved by the utilisation of Pdx-1 or p48 promoters to regulate the activation of the recombinases (Kim und MacDonald 2002; Kawaguchi et al. 2002). *Pdx1-Cre* ($p48^{Cre}$)*; LSL-*$Kras^{G12D}$ mice develop ductal lesions similar to all three stages of human PanINs, which subsequently progress to PDAC after approximately one year (Hingorani et al. 2003). Following this classic PDAC progression model, recently a novel Flp-based system (*Pdx1-Flp; FSF-*$Kras^{G12D}$) has been developed to further investigate on the multistep carcinogenesis of

pancreatic cancer by combining the Flp-FRT and Cre-loxP technologies (Schönhuber et al. 2014).

3.1.2 PDAC metastases

The primary tumour mass is seldom directly responsible for the death of patients (i.e. for tumours of the central nervous system). In contrast, 90% of cancer-associated death is linked to systematic organ failure due to metastatic outspread (Gupta und Massagué 2006). This is also true for pancreatic cancer (Ryan et al. 2014). Even though the pancreatic gland is necessary for an intact digestive system and responsible to produce important hormones (i.e insulin, glucagon) and growth factors, the modern medicine would be able to compensate this loss, if the pancreas had to be removed because of a neoplastic process. But the surgical difficulties contribute only for a small part of the poor patient prognosis. Even though prominent blood vessels (e.g. celiac artery or portal vein) and the close relationship of the pancreas to nearby organs (e.g. spleen, stomach or liver) make pancreatic surgery a challenge (Ryan et al. 2014), the major problem is that at the point of diagnosis only 15-20% of the tumours are accessible for primary surgery (Adamska et al. 2017). The advanced stages of the PDAC either make local surgery impossible (i.e. walling of the aorta) or senseless (systematic spread of the tumour cells).

PDAC is characterized by a great variety of metastases, most common and life limiting are its liver, peritoneum, and lung metastases. But metastazation into lymph nodes and very painful bone metastases are also usual (Iacobuzio-Donahue et al. 2009). In the rapid process of tumour development almost all patients develop metastases. PDAC cells also stand out for their ability to infiltrate into the perineural spaces surrounding nerves, one of the major reasons why even small resected tumours have a high rate of local or distant relapses (Hirai et al. 2002; Zhang et al. 2013). Treatment of metastasized tumours is a challenge for every entity, but pancreatic cancer has an especially poor response rate. Standard treatment protocols for chemo- or radio-chemotherapy fail to suppress PDAC cell growth, spread, and recurrence (Peixoto et al. 2015). New specialized multidrug anti-cancer treatment therapies for metastatic pancreatic cancer emerged in the last years but could only increase the median survival of PDAC by 4,3 months (Conroy et al. 2011). So far, current anti-cancer treatments are not suitable to repress PDAC growth, spread or colonization at any significant rate.

Until the introduction of novel possibilities for early detection of PDAC, new specialized, targeted anti-metastatic treatment options remain a promising resort for patients with late-stage

pancreatic cancer. The inhibition of invasion, dissemination, and metastatic colonization processes could lead to a great decrease in metastatic frequency and therefore greatly increase patient's survival. Therefore, the understanding of the responsible pathways that accompany each step of metastasis formation is necessary. These are primarily: motility, infiltration, invasion, extravasation, dissemination, and colonization.

3.2 Metastasis pathways

The hallmarks of cancer have been in the centre of cancer research for two centuries now (Hanahan und Weinberg 2000, 2011). Especially the step that marks the transformation of a localised, curable disease to a systematic, life-threatening, and mostly incurable one. The stage of invasion and metastasis has until now been extensively examined by any means but still no common therapy for metastatic diseases or prevention of metastases has emerged so far. However, a reasonable theory about the steps that precede metastasis has been formulated and postulated by many authors (Brabletz 2012; Kalluri und Weinberg 2009; Lambert et al. 2017). It states that in order to invade surrounding tissue and systematically spread through the circulation cancer cells have to undergo a morphologically and functional change. This change is characterized by loss of cell-cell contacts, increased motility, and the ability to degrade extracellular matrix (ECM). After gaining access to the bloodstream these cells will form micrometastases at distant organ sites and further grow into macroscopic lesions. In this last step they also regain their original epithelial properties and again resemble the primary tumour (Brabletz 2012; Kalluri und Weinberg 2009). This circuit of shaping and reshaping of the cell is described via the activation of a genetically program called epithelial to mesenchymal transition (EMT) and its counterpart mesenchymal to epithelial transition (MET).

3.2.1 EMT and MET

EMT was first described by the work of Elizabeth Hay and named "epithelial to mesenchymal *transformation"* (Hay 1995). Ongoing research in this field finally changed the name to transition to stress the reversibility of the process and to fence it off against neoplastic transformation in tumour cells (Kalluri und Neilson 2003) . EMT is a distinct genetically program which enables epithelial-like cells to converse to single, spindle-shaped, mesenchymal cells. While this program is present but silenced in most adult, terminal differentiated cells, it can be reactivated under certain conditions: physiological or pathological (Kalluri und Weinberg 2009; Nieto et al. 2016; Brabletz et al. 2018).

Prototypical EMT is characterized by an orchestrate of changes regarding most basic functions of the epithelial cell. Most commonly known and examined are the changes in cell-cell contacts, cell motility, morphology, and ECM interaction (Lamouille et al. 2014). However, especially in the context of tumour metastasis also anti-apoptotic mechanisms, cell growth restrictions, and stem cell features are described and greatly discussed (Heerboth et al. 2015; Puisieux et al. 2014; Shibue und Weinberg 2017; Arumugam et al. 2009; Rodriguez-Aznar et al. 2019).

The integrity of the epithelial barrier function - maintained by specialized surface protein complexes and apical-basal polarity - is one of the main targets of EMT changes. Cellular junction such as tight junctions, gap junctions, and desmosomes get deconstructed, relocalized and degraded to enable cellular detachment. E-Cadherin - member of the cadherin superfamily known for they role in cell adhesion - is cleaved from the cell surface and gets further degraded (Lamouille et al. 2014) as well as repressed on a transcriptional and post-translational level by EMT transcription factors (EMT-TF) (Heerboth et al. 2015). Cytoskeletal changes crucially contribute to the increased motility in EMT cells. These changes include a reorganisation of the cortical actin complex and myosin light chain phosphorylation via RHO GTPase activation of RHO associated kinase (ROCK). Also, a loss of apical-basal polarity due to relocalisation of the PAR and Scrible complex to the front rear of the cell, which are normally integrated in the normal cellular junction architecture (Lamouille et al. 2014). Closely linked to this is the activation of proteins which interact with the ECM. Mesenchymal cells have the ability to either create ECM proteins or to degrade them, mostly by using matrix metalloproteinase (MMP) on the front rear of the cell surface (Nisticò et al. 2012). In total, these three adaptations enable the cell to detach from its neighbour cell unit, gain directed motility, and the ability to make it through the layers of ECM. While all these traits contribute to the hallmarks of cancer (Hanahan und Weinberg 2000) namely invasion and dissemination, EMT is also observed in non-neoplastic cells without any form of malignant intent (Kalluri und Weinberg 2009).

In order to address these different forms of EMT, Weinberg and Kalluri proposed a context-based classification system of EMT (Kalluri 2009; Kalluri und Weinberg 2009). Type I represents the use of EMT during the embryonic development. Here, cells undergo EMT to contribute to implantation, embryo formation, and organ development via formation of primary mesenchymal cells (primary mesenchyme). The last can now further differentiate to secondary epithelial cells by employing MET. Therefore, it is not surprising that GEMM with complete knockouts of key EMT factors lead to embryonic lethality in mice (Murray und Gridley 2006; Goossens et al. 2011).

Type II EMT characterize the physiological answer of tissue to injury. Following trauma or inflammation cells get recruited via cytokines or chemokines, utilizing EMT to gain mobility and reach the site of interest. There they reconstruct damaged tissue or regenerate tissue after lesions. However, if the inflammatory signal persists the cells, mostly activated fibroblasts, can permanently and excessively produce further ECM proteins such as collagens, laminin, elastin, and tenascins (Kalluri und Weinberg 2009) subsequently leading to organ fibrosis and destruction (Kalluri und Neilson 2003).

Both type I and II EMT are not associated with the traits commonly discussed for metastatic formation, such as invasion and systemic spread of EMT cells via the circulation. This form is termed type III EMT. Type III EMT exclusively describes EMT in neoplastic cells, which have previously undergone genetic and epigenetic changes mostly regarding cell proliferation and clonal outgrowth. The results of type III EMT differs from type I and II. EMT tumour cells gain an invasive phenotype, which enables them to invade through cell barriers like the basement membrane, which is regarded as a crucial step in a tumour towards a late-stage tumour disease. In addition, neoplastic EMT cells are suspected to be those cells which eventually enter the circulation via extravasation and ultimately form micrometastases at distant organ sites (Kalluri und Weinberg 2009) . Moreover, lately EMT is not only discussed as an obligatory step in dissemination and metastasis, but also in tumour progression (Rhim et al. 2012; Craene und Berx 2013). Parts of the pathways, involved in EMT, have been shown to help tumour cells to overcome senescence, resist pro-apoptotic signals, and play an important role in chemoresistance (Arumugam et al. 2009; Shibue und Weinberg 2017; Craene und Berx 2013). It was also shown, that EMT in tumour cells can not only lead to an invasive phenotype but instead create new cancer stem cells (Rodriguez-Aznar et al. 2019; Rhim et al. 2012). Why the results of type III EMT so greatly differs from type I and II is not fully understood yet, even though the underlying molecular program is similar in all three types.

In this context, it is important to stress the transitional nature of EMT: Cells which activate EMT do not immediately become mesenchymal ones and gain all their properties. In contrast, epithelial cells gradually lose their epithelial functions and properties and consequently gain mesenchymal ones, molecularly characterized by the loss of epithelial and gain of mesenchymal markers. In this progress especially tumour cells can display all different stages of EMT, with the ability to retain many epithelial traits and gain few mesenchymal (characterized by the coexistence of epithelial and mesenchymal markers) or fully develop to mesenchymal cells (Nieto et al. 2016). This intermediate stage is regarded as “partial EMT”, or “incomplete EMT”.

Partial EMT gained increasing attention in the last years, because of its capacity of explaining the distinct different outcomes of EMT in tumour cells (Grigore et al. 2016; Aiello et al. 2018). Whether this stage is only a transitional one on the way to a complete mesenchymal state or represent an own entity in the field of EMT and MET remains to be settled in further research. The influence of EMT on the molecular phenotype of cancer cells has been proven and validated in many *in vitro* studies, also the correlation between EMT marker and cancer metastases has been shown for different tumour entities (Owusu-Ansah et al. 2019; Hartwell et al. 2006; Xue et al. 2003). Moreover, several clinical studies associated EMT marker positivity with poor prognosis in patients (Oida et al. 2006). This marks EMT as a promising and powerful new anti-cancer treatment opportunity. However, recent studies of different cancer entities failed to provide the expected results *in vivo*. Inhibition of EMT via mi-RNA200 did not result in a significantly drop in lung metastases in breast cancer (Fischer et al. 2015). GEMM knock-outs of important EMT-TF failed to reduce the metastatic frequency in pancreatic cancer (Zheng et al. 2015) and several other studies challenge the common belief that the EMT-MET pathway is an obligatory step for cancer metastasis (Chen et al. 2018; Jolly et al. 2017). This raises the question, whether the employed methods were insufficient to block EMT successfully or whether cancer cells have the ability to metastasize without the utilization of the EMT program.

3.2.2 EMT pathways in cancer

To further grasp the concept of EMT in cancer cells, it is crucial to better understand the underlying circumstances that triggers the EMT cascade and the molecular pathways that lead to this cell differentiation. This includes three different fields that are all linked to EMT on a different level: external factors and circumstances, EMT inducing pathways, and EMT effector proteins.

External factors can be a variety of conditions which all eventually activate EMT pathways. Most commonly known and examined are hypoxia, inflammation, oncogenic, physical or metabolic stress (Heerboth et al. 2015). But also, the secretion of certain growth factors (e.g.TGF-β, PDGF-α, etc.) by surrounding cells like tumour stroma cells will lead to EMT activation (Lamouille et al. 2014). Eventually, all the mentioned above will lead into the activation of one or several of those pathways: wnt, Hif1/2, NOTCH, NF-kB, RAS-ERK1/2 or TGF-β. Even though all of these pathways will induce different changes in the cell they all have in common that they affect one or several of the key EMT-TF: TWIST1/2, SNAI1, SNAI2

(Slug) or ZEB1/2. Each one is able to fully activate the EMT cascade (Lamouille et al. 2014; Puisieux et al. 2014).

The pathway that is probably the best understood and examined is the TGF-ß pathway via the TGF-β2-receptor. External TGF-ß binds the TGF-β2-receptor which activates the type 1 transmembrane kinase which then phosphorylate the C termini of intracellular SMAD proteins. The activated SMAD2 and SMAD3 bind SMAD4 to form trimeric SMAD complexes. After translocation into the nucleus the SMAD complex binds DNA-binding TF at regulatory sequences. SMAD now mediates EMT through the three major families of EMT-TF: SNA1L, TWIST, and ZEB, which not only get enhanced in their expression but are also increased in their activity (Lamouille et al. 2014; Zavadil und Böttinger 2005; Xu et al. 2009). Moreover, SMAD is able to induce the expression of certain mesenchymal gene, like vimentin or collagen 1a, independently from EMT-TF (Xu et al. 2009).

However, TGF-ß is able to surpass the SMAD pathway and induce EMT through various non-SMAD dependent downstream effector pathways. This includes signalling through Raf-MEK-Erk, PI3K, or RHO-like GTPase and several others, which each individually regulate distinct processes linked to EMT, like cytoskeletal organisation, cell survival, growth, or migration (Xu et al. 2009; Zavadil und Böttinger 2005). These pathways are far from being TGF-ß exclusive and more likely represents prototypical responses to receptor tyrosine kinase activation. In addition, several other known EMT inducers like NOTCH or Wnt pathways interact with the TGF-ß signalling, making TGF-ß one of the key regulators of EMT induction (Lamouille et al. 2014). TGF-ß signalling can be easily used to induce EMT *in vitro*. Administration of small doses of recombinant TGF-β1 into cell media will trigger epithelial cells to convert from a cell cluster to single spindle-shaped mesenchymal cells and greatly increases expression of mesenchymal and EMT markers while reducing the expression of epithelial ones.

3.2.3 EMT in pancreatic cancer

Early and frequent metastases are characteristic of pancreatic cancer. Therefore, a close link between EMT and pancreatic metastases seems to be consistent. However, existing studies investigating the influence of EMT to PDAC, and its metastases provided controversial data. Rhim and colleagues showed that EMT^+ cells are already present in pancreatic precursor lesions (PanIN 2-3) and own the ability to disseminate into the bloodstream. This suggested that EMT precede tumour formation and might also play an important role in tumour progression (Rhim et al. 2012). However, the study could not provide direct evidence that those EMT^+

disseminated cells ultimately give rise to distant metastases. Another report could show that inhibition of the pro-invasive NF-kB pathway decreases the expression of several EMT-TF and lead to reduced tumour growth and overall metastases. Also, the potential of neural invasion seems to be impaired (Nomura et al. 2016). In contrast to these findings, Zheng et al. provided evidence that upon knock-down of the key EMT-TF *Twist and Snai1,* no significant reduction of metastases in the KPC model (*Pdx1-cre; LSL-Kras^{G12D}; P53^{R172H})* could be observed. Also, *Snai1* and *Twist* deletion did not significantly alter tumour progression or its histopathology features and had no effect on overall survival. Therefore, they concluded that EMT is dispensable for pancreatic metastasis. In addition, they found that EMT contributes to chemoresistance by reducing cancer cell proliferation and suppression of drug transporters, subsequently leading to anti-proliferating drug resistance (Zheng et al. 2015). This corresponds with earlier studies which could also link especially *Zeb1* mediated EMT with multidrug resistance (Arumugam et al. 2009). However, a more recent study conducted by Krebs et al. challenged this opinion. A knock-down of the third key EMT-TF *Zeb1* in the same KPC model, resulted in a great decrease in overall metastases. Also, *Zeb1* depletion impaired formation of precursor lesions (PanIns and ADM), high grade carcinomas, and invasion. *In vitro* a loss of cell plasticity and reduced stemness properties could also be observed. The authors demonstrated that different EMT-TF exhibit distinct functional differences and stress the importance of *Zeb1* in EMT associated metastases in PDAC (Krebs et al. 2017).

Whether EMT is responsible for pancreatic metastases or not, several independent studies strongly correlated the presence of EMT markers (e.g. *Zeb1*, S100A4) with poor patient' survival (Oida et al. 2006; Jia et al. 2019; Owusu-Ansah et al. 2019; Fei et al. 2017; Chen et al. 2017). Also, the loss of E-Cadherin is highly associated with EMT and poor prognosis (Oida et al. 2006).

Regarding these studies, the precise role of EMT in pancreatic cancer is not yet identified but it has significant clinical implications for patient prognosis. If this now accounts due to its contributions to cancer development, progression, metastasis, or chemoresistance remains to be clarified by further research.

3.3 Fibroblast-specific-protein (Fsp1, S100A4)

Fsp1, also known as S100A4, metastasin, calvasculin, CAPL, pEL98, p9Ka and mts1 is part of the S100 protein family. Members of this family are low molecular weight (10-12kDa) CA^{2+} binding proteins with no enzymatic activity, which exert their effects by interacting with their

target proteins and alter and modulate their activity. Generally, they exist in homo- or heterodimers inside the cell cytoplasm or nucleus, but also multimeric forms have been described and associated with extracellular activity (Boye und Maelandsmo 2010).

Human S100A4 consists of 101 amino acids and has a molecular weight of 11,5 kDa. Its gene is located on a gene cluster on chromosome 1q21, which is composed of four exons, of which the first two are non-coding. S100A4 can normally be found in the nucleus or the cytoplasm, where it interacts with its binding partners. Several proteins have been identified to interact with S100A4 directly or indirectly. Mostly the homodimer of S100A4 facilitates the functional cross link of two homologous or heterologous target proteins. Included in this are proteins of the cytoskeletal system like actin, non-muscular myosin IIa and IIb or tropomyosin, but also p53, p37, or methionine aminopeptidase. Apart from direct interaction increased levels of S100A4 have also been linked to the presence of increased levels of MMPs (MMP2, 3, and 9), repression of E-Cadherin, and activation of nuclear factor – kB (NF-kB) (Boye und Maelandsmo 2010; Bresnick et al. 2015).

Since those are also characteristic events in EMT, S100A4 is assumed to be closely linked to the pathways that induce EMT or play a key role in EMT activation itself (Xue et al. 2003; Bresnick et al. 2015). Subsequent studies provided plenty of evidence supporting this hypothesis (Helfman et al. 2005; Xie et al. 2009; Mishra et al. 2012; Fei et al. 2017). Key EMT-TF *Snail* was reported to directly induce S100A4 expression. The expression of S100A4 is also induced by the invasion promoting pathway of ß-catenin. Moreover, S100A4 activated NF-kB directly leads to the activation of essential EMT-TF like *Snail* or *Twist*. The key role of S100A4 in cell motility highly suggests S100A4 as a key EMT player (Boye und Maelandsmo 2010).

The distinct physiological function of S100A4 is not completely understood so far. However, S100A4 gained increasing attention in the last decades due to its link to metastases development in various cancers (Helfman et al. 2005; Xue et al. 2003; Fei et al. 2017). Several studies have shown the influence of altered S100A4 levels to metastasis, whereas increased levels of S100A4, always correlated with increased metastatic capacity (Boye und Maelandsmo 2010). Additionally, S100A4 has been utilized and established as a gatekeeper marker for EMT detection *in vivo* and *in vitro* (Xue et al. 2003; Mishra et al. 2012), also in pancreatic cancer (Rhim et al. 2012; Chen et al. 2018).

3.4 EMT independent pathways for metastasis development

Apart from the popular EMT-MET metastasis theory, several other routes of metastasis formation have been described. Some employ the concept of EMT but not as an essential part for tumour cells but rather for the surrounding tumour stroma cells. Hereby, fibroblasts or other mesenchymal cells serve as promoter for nearby tumour cells and facilitate their movement and invasion. The activation of the EMT program is facilitated via secreted growth factors (e.g. TGF-β) from the EMT negative tumour cells (Wen et al. 2019; Murakami et al. 2019; Thomas und Radhakrishnan 2019; Ren et al. 2018).

Circulating tumour cells (CTCs) are the main representatives of disseminated cells which can form distant metastases. However, in blood analyses not only single CTCs but also CTC clusters could be observed (Arnoletti et al. 2018). The composition of these cell clusters can vary extensively. Tumour-stroma or tumour-tumour cell doublets, triplets or even greater constructs have been described and found in the circulation priori to metastasis (Hong et al. 2016). CTC clusters do not follow the prototypical EMT pathway but are known to show epithelial properties to a different extent (Cheung et al. 2013; Aiello et al. 2018).

Other authors suggest that tumour cells can gain access to the circulation solemnly through their self-induced angiogenesis and passive shedding. It is already known that cancer cells are able to acquire their own blood supply by inducing the formation of novel small blood vessels. However, this newly formed vessels often lack the proper barrier function (and other functions) of already established vessels. Therefore, metastatic cells do not have to rely on their ability to infiltrate existing blood vessels but can passively gain access due to leakage in newly induced ones (Bockhorn et al. 2007; Krzykawski et al. 2019).

Also, neoplastic cells have other means of transportation than the blood at their disposal. Simply through the increasing tumour growth and the resulting increasing pressure on the tumour cells themselves, especially cells on the tumour surface can get detached from the primary tumour mass and regrow at the adjacent organ (Murakami et al. 2019). Also, for gastrointestinal tumours the outspread through ascites remains a possible non-EMT dependent route to metastasis. By increasing the intra-abdominal pressure and increase the amount of ascites fluid through different mechanisms (e.g., higher permeability of blood vessels) cells might get diluted into the peritoneal fluid and therefore gain access to the intraperitoneal cavity.

3.5 *In* and *ex-vivo* double fluorescence imaging

Applying a fluorescence label is an effective way of tracking cells of different origin and make them accessible for confocal or fluorescence microscopy and FACS analyses. However, in order to distinguish between different cellular states (e.g., EMT or non-EMT activated cells) a fluorescence reporter system needs certain qualities. Muzumdar et al proposed a global double fluorescent Cre dependent reporter system named mT/mG. This reporter system will ubiquitously label cells with membrane targeted tandem dimer tomato (mT) until Cre mediated excision. Afterwards it will permanently express membrane targeted green fluorescence protein (mG) (Muzumdar et al. 2007). Given Cre expression is crucially bound to the activation of EMT, EMT and non EMT cells can therefore be distinguished via their fluorescence signal. Madisen et al proposed a double recombinase dependent reporter system labelling only Cre and Flp recombined cells with tdTomato. The Ai65(RCFL-tdT) system can therefore be used in the next generation dual recombinase system of pancreatic cancer (Schönhuber et al. 2014) to reliable identify tumour cells who have activated their Cre bound protein expression. (Madisen et al. 2015).

3.6 Aim of this work

As recent studies provided controversial data regarding EMT and pancreatic cancer, further research have to be conducted. This study aims to investigate the role of EMT in pancreatic cancer metastases formation. The goal was to reliably track EMT and non-EMT cells *in vivo* and *vitro* and investigate whether EMT is obligatory or dispensable for metastasis formation (Zheng et al. 2015).

The GEMM *Pdx1-Flp; FSF-Kras* for pancreatic cancer progression was expanded by the recombinase-based immunofluorescence reporter system *mT/mG* (Muzumdar et al. 2007) or Ai65(RCFL-tdT) (Madisen et al. 2015) and the Cre recombinase under the control of the Fsp1 promoter. The resulting *Pdx1-Flp; FSF-Kras; Fsp1-Cre; $R26^{mTmG}$/$R26^{Ai\text{-}65\text{-}tdTom}$* mouse models both utilize a distinct, and permanent fluorescence switch in pancreatic cells after the initiation of the EMT program via the activation of Fsp1 (see 3.1). Therefore, making it possible to distinguish between EMT and non-EMT derived metastases. The models were validated for its reliability to detect EMT *in vivo* and *in vitro.* Furthermore, primary cell lines derived from *Pdx1-Flp; FSF-Kras; Fsp1-Cre; $R26^{mTmG}$/$R26^{Ai\text{-}65\text{-}tdTom}$* mice were used to investigate the role of EMT in pancreatic cancer metastases by immunofluorescence and FACS analyses in an orthotopic implantation model.

4. Materials

4.1 Technical equipment

Table 1. Technical equipment

Device	**Origin**
Autoclave 2540 EL	Tuttnauer Europe B.V., Breda, The Netherlands
Axio Cam HRc	Carl Zeiss AG, Oberkochen
Axio Cam MRc	Carl Zeiss AG, Oberkochen
Bag sealer Folio FS 3602	Severin Elektrogeräte GmbH, Sundern
Centrifuge Avanti® J25	Marshall scientific
Centrifuge Rotina 46R	Andreas Hettich GmbH & Co. KG, Tuttlingen
Charge-coupled device camera equipped with an image intensifier Orcall ER	Hamamatsu Photonics K.K., Herrsching
CO2 incubator HERAcell®	Heraeus Holding GmbH, Hanau
CO2 incubator MCO-5AC 17AI	Sanyo Sales & Marketing Europe GmbH, Munich
Cryostat microm hm 560	Thermo Fisher Scientific, Inc., Waltham, MA, USA
Dewar carrying flask, type B	KGW-Isotherm, Karlsruhe
Electrophoresis power supply Power Pac 200	Bio-Rad Laboratories GmbH, Munich
Gel Doc™ XR+ system	Bio-Rad Laboratories GmbH, Munich
Glass ware, Schott Duran®	Schott AG, Mainz
Heated paraffin embedding module EG1150 H	Leica Microsystems GmbH, Wetzlar
HERAsafe® biological safety cabinet	Thermo Fisher Scientific, Inc., Waltham, MA, USA
Homogenizer SilentCrusher M with tool F	Heidolph Instruments GmbH, & Co. KG, Schwabach
Horizontal gel electrophoresis system	Biozym Scientific GmbH, Hessisch Oldenburg
Horizontal shaker	Titertek Instruments, Inc., Huntsville, AL, USA

Laminar flow HERAsafe®	Heraeus Holding GmbH, Hanau
Leica SP8 Confocal Microscope	Leica Microsystems GmbH, Wetzlar
Magnetic stirrer, Ikamag® RCT	IKA® , Werke GmbH & Co. KG, Staufen
Microcentrifuge 5415 D	Eppendorf AG, Hamburg
Microcentrifuge 5417 F	Eppendorf AG, Hamburg
Microplate reader Anthos 2001	Anthos Mikrosysteme GmbH, Krefeld
Microscope Axio Imager.A1	Carl Zeiss AG, Oberkochen
Microscope Axiovert 25	Carl Zeiss AG, Oberkochen
Microscope DM LB	Leica Microsystems GmbH, Wetzlar
Microtome Microm HM355S	Thermo Fisher Scientific, Inc., Waltham, MA, USA
Microwave	Siemens AG, Munich
Mini centrifuge MCF-2360	LMS Consult GmbH &Co. KG, Brigachtal
Mini-PROTEAN® Tetra Cell	Bio-Rad Laboratories GmbH, Munich
Multipette stream	Eppendorf AG, Hamburg
Neubauer hemocytometer, improved	LO-Laboroptik GmbH, Bad Homburg
Odyssey® infrared imaging system	Li-Cor Bioscience, Lincoln, NE, USA
Paraffin tissue floating bath Microm SB80	Thermo Fisher Scientific, Inc., Waltham, MA, USA
Pipettes Reference®, Research®	Eppendorf AG, Hamburg
Pipetus®	Hirschmann Laborgeräte GmbH & Co. KG, Eberstadt
Power supplies E844, E822, EV243	Peqlab Biotechnologie GmbH, Erlangen
Stereomicroscope Stemi SV 11	Carl Zeiss AG, Oberkochen
Surgical instruments	Thermo Fisher Scientific, Inc., Waltham, MA, USA
Thermocycler T1	Biometra GmbH, Göttingen
Thermocycler Tpersonal	Biometra GmbH, Göttingen

Thermocycler UNO-Thermoblock	Biometra GmbH, Göttingen
Tissue Processor ASP300	Leica Microsystems GmbH, Wetzlar
Tumbling Table WT17	Biometra GmbH, Göttingen
Vortex Genius 3	IKA Werke GmbH & Co. KG, Staufen
Water bath 1003	GFL Gesellschaft für Labortechnik mbh, Burgwedel
Western blot system SE 260 mighty Small II	Hoefer, Inc., Holliston, MA, USA

4.2 Disposables

Table 2. Disposables

Disposable	**Origin**
Cell culture plastics	Becton Dickinson GmbH, Franklin Lakes, NJ, Usa; Greiner Bio-One GmbH, Frickenhausen; TPP Techno Plastic Products AG, Trasadingen, Switzerland
Cell scrapers	TPP Techno Plastic Products AG, Trasadingen, Switzerland
Cell strainer, 100 um, yellow	BD Biosciences, Franklin Lakes, NJ, USA
Combitips BioPur®	Eppendorf AG, Hamburg
Conical tubes, 15ml	TPP Techno Plastic Products AG, Trasadingen, Switzerland
Conical tubes, 50ml	Sarstedt AG & Co., Nümbrecht
Cover slips	Gerhard Menzel, Glasbearbeitungswerk GmbH & Co. KG, Braunschweig
CryoPure tubes	Sarstedt AG & Co., Nümbrecht
Disposable scalpels, size 11and 21	Feather Safety Razor Co., Ltd., Osaka, Japan

Glass slides SuperFrost® Plus	Gerhard Menzel, Glasbearbeitungswerk GmbH & Co. KG, Braunschweig
MicroAmp® optical 96-wells reaction plate	Applied Biosystems, Inc., Carlsbad, CA, USA
Microtome blades S35 and C35	Feather Safety Razor Co., Ltd., Osaka, Japan
Pasteur pipettes	Hirschmann Laborgeräte GmbH & Co. KG, Eberstadt
PCR reaction tubes	Brand GmbH & Co. KG, Wertheim; Eppendorf AG, Hamburg
Petri dishes	Sarstedt AG & Co., Nümbrecht
Phase lock gel light tubes	5 Prime GmbH, Hamburg
Pipette tips	Sarstedt AG & Co., Nümbrecht
Reaction tubes 0,5ml, 1,5ml and 2ml	Eppendorf AG, Hamburg
Safe seal pipette tips, professional	Biozym Scientific GmbH, Hessisch Oldenburg
Safe-lock reaction tubes BioPur®	Eppendorf AG, Hamburg
Seriological pipettes	Sarstedt AG & Co., Nümbrecht
Single use needles Sterican® 27gauge	B.Braun Melsungen AG, Melsungen
Single use syringes Omnifix®	B.Braun Melsungen AG, Melsungen
Tissue embedding cassette system	Medite GmbH, Burgdorf
Transfer membrane Immobilon-P	Milipore GmbH, Schwalbach am Taunus

4.3 Reagents and enzymes

Table 3. Reagents and enzymes

Reagent	**Origin**
1kb DNA extension ladder	Invitrogen GmbH, Karlsruhe
1,4-Dithiothreitol (DTT)	Carl Roth GmbH & Co. KG, Karlsruhe
2-Mercapthoethanol, 98%	Sigma Aldrich Chemie GmbH, Munich

Agarose	Sigma Aldrich Chemie GmbH, Munich
Ammonium persulfat	Sigma Aldrich Chemie GmbH, Munich
Blotting grade blocker non-fat dry milk	Bio-Rad Laboratories GmbH, Munich
Bovine serum albumin, fraction V	Sigma Aldrich Chemie GmbH, Munich
Bradford reagent	Serva Electrophoresis Gmbh, Heidelberg
Bromphenol blue	Sigma Aldrich Chemie GmbH, Munich
Complete, EDTA-free, protease inhibitor cocktail Tablets	Roche Deutschland Holding GmbH, Grenzach-Wyhlen
Dimethylsulfoxide (DMSO)	Carl Roth GmbH & Co. KG, Karlsruhe
dNTP mix, 10mM each	Fermentas GmbH, St.Leon Roth
Dodecylsulfate Na-salt in pellets (SDS)	Serva Electrophoresis Gmbh, Heidelberg
Dulbeccos's phosphate buffered saline, powder	Biochrome AG, Berlin
Ethanol (100%)	Merck KGaA, Darmstadt
Ethidium bromide	Sigma Aldrich Chemie GmbH, Munich
Ethylenediaminetetraacetic acid (EDTA)	Invitrogen GmbH, Karlsruhe
Gel loading dye, blue	New England Biolabs GmbH, Frankfurt am Main
GeneRuler 100bp DNA Ladder™	Fermentas GmbH, St. Leon Roth
Glycerol	Sigma Aldrich Chemie GmbH, Munich
HEPES Pufferan®	Carl Roth GmbH & Co. KG, Karlsruhe
HotStarTaq DNA polymerase	Qiagen GmbH, Hilden
Nonidet P40	Roche Deutschland Holding GmbH, Grenzach-Wyhlen
Magnesium chloride	Carl Roth GmbH & Co. KG, Karlsruhe
Methanol	Merck KGaA, Darmstadt
Orange G	Carl Roth GmbH & Co. KG, Karlsruhe

Phosphate buffered saline (PBS)	Sigma Aldrich Chemie GmbH, Munich
Phosphatase inhibitor mix I	Serva Electrophoresis GmbH, Heidelberg
Polyethylen glycol 4000	Merck KGaA, Darmstadt
Proteinase K, recombinant, PCR grade	Roche Deutschland Holding GmbH, Grenzach-Wyhlen
REDTaq® ReadyMix™ PCR reaction mix	Sigma Aldrich Chemie GmbH, Munich
Rotiphorese® gel 30	Carl Roth GmbH & Co. KG, Karlsruhe
RLT buffer	Qiagen GmbH, Hilden
Sodium chlorid (NaCl)	Merck KGaA, Darmstadt
Tamoxifen	Sigma Aldrich Chemie GmbH, Munich
TEMED	Carl Roth GmbH & Co. KG, Karlsruhe
Tissue-Tek® O.C.T.™ compund	Sakura Finetek Europe B.V, Alphen aan den Rijn, The Netherlands
Trishydroxymethyl-aminomethan (Tris) hydrochloride	J.T.Baker® Chemicals, Philipsburg, NJ, USA
Tris Pufferan®	Carl Roth GmbH & Co. KG, Karlsruhe
Triton® X-100	Merck KGaA, Darmstadt
Tween® 20	Carl Roth GmbH & Co. KG, Karlsruhe

4.4 Cell culture

Table 4. Cell culture media and their composition

Medium	**Components**
PDAC cell medium	89% DMEM 10% FCS (Biochrom AG) 1% Penicillin/Streptomycin
TGF- ß medium	99% DMEM 1% Penicillin/Streptomycin

	2ug/ml TGF-B (….)
FCS-starving medium	99% DMEM 1% Penicillin/Streptomycin
Freezing medium	70 % DMEM 20% FCS 10% DMSO

Table 5. Reagents for cell culture

Reagent	**Origin**
Collagenase type 2	Worthington Biochemical Corporation, Lakewood, NJ, USA
Dulbecco's modified eagle medium (DMEM) high glucose	Invitrogen GmbH, Karlsruhe
Dulbecco's phosphat buffered saline (PBS)	Invitrogen GmbH, Karlsruhe
Fetal calf serum (FCS)	Biochrom AG, Berlin
Penicillin (10000 units/ml) / Streptomycin (10000 units/ml) solution	Invitrogen GmbH, Karlsruhe
Recombinant human TGF-B-1	Invitrogen GmbH, Karlsruhe
Trypsin, 0,05% with 0,53mM EDTA 4Na	Invitrogen GmbH, Karlsruhe

4.5 Histology

Table 6. Reagents for histological analysis

Reagent	**Origin**
4',6-diamidino-2-phenylindole (DAPI)	Thermo Fisher Scientific
Donkey serum D9663	Sigma-Aldrich Chemie GmbH, Munich
Eosine	Waldeck GmbH & Co. KG, Münster
Goat serum G9023	Sigma-Aldrich Chemie GmbH, Munich
Hematoxylin	Merck KGaA, Darmstadt

Pertex mounting medium	Medite GmbH, Burgdorf
Rabbit serum R9133	Sigma-Aldrich Chemie GmbH, Munich
Roti® Histofix 4%	Carl Roth GmbH & Co. KG, Karlsruhe
Roti® Histol	Carl Roth GmbH & Co. KG, Karlsruhe
Sucrose (saccharose)	Merck KGaA, Darmstadt
Vectashield® mounting medium	Vector Laboratories, Inc., Burlingame, CA, USA
Vectashield® mounting medium with DAPI	Vector Laboratories, Inc., Burlingame, CA, USA

4.5.1 Antibodies used in histology

Table 7. Primary and secondary antibodies

Antibody	**Origin**
Alexa Fluor® 568 donkey anti-sheep IgG. A-21448	Invitrogen GmbH, Karlsruhe
Alexa Fluor® 594 donkey anti-rabbit IgG, A-21207	Invitrogen GmbH, Karlsruhe
Alexa Fluor® 594 donkey anti-rat IgG, A-21209	Invitrogen GmbH, Karlsruhe
Anti-S100A4, HPA007973	Sigma-Aldrich Chemie GmbH, Munich
Anti-S100A4, CPTC-S100A4-3	Development Studies Hybridoma Bank, IA, USA
Anti-rabbit IgG (H+L), (DyLight™ 680 Conjugate), #5366	Cell Signaling Technologie, Inc., Danvers, MA, USA
DyLight™ 650 donkey anti-mouse IgG (H+L) SA5-10169	Invitrogen GmbH, Karlsruhe
E-Cadherin, mouse 610181	BD Biosciences, Franklin Lakes, NJ, USA
E-Cadherin, Sc-59778 (DECMA-1)	Santa Cruz Biotechnologie, Inc., Dallas, TX, USA
N-Cadherin, AF6426	R&D Systems, Inc., MN, USA

Zeb1, HPA027524	Sigma-Aldrich Chemie GmbH, Munich

4.6 Molecular biology

All buffers were prepared with bidistilled H2O.

Table 8. Buffers and solutions for molecular biology

Buffer	**Components**
IP Buffer, pH 7.9	50 mM HEPES 150 mM NaCl 1 mM EDTA 0.5% Nonidet P40 10% Glycerol Phosphatase inhibitor (add prior to use) Protease inhibitor (add prior to use)
Running buffer	25 mM Tris 192 mM Glycine 0.1% SDS
Transfer buffer pH 8.3	25mM Tris 192 mM Gylcine 20% Methanol
5x Protein loading buffer (Laemmli), pH 6.8	10% SDS 50% Glycerol 228 mM Tris hydrochloride 0.75 mM Bromphenol blue 5% 2-Mercaptoethanol
6x Loading buffer orange G	60% Gylcerol 60 mM EDTA 0.24% Orange G
10x Gitschier's buffer	670 mM Tris 8.8 166 mM (NH4)2SO4

	67 mM MgCl2
Soriano lysis buffer	0.5% Triton® X-100 1% 2-Mercaptoethanol 1x Gitschier's buffer 400ug/ml Proteinase K (add prior to use)
SucRot solution (for PCR)	1.5 mg/ml Cresol red 100mM Trsi, pH 9.0 30% Saccharose

4.6.1 Primers

Oligonucleotides were synthesized by Eurofins MWG GmbH (Ebersberg) and diluted to a concentration of 10 uM

Table 9. Primers used for genotyping

PCR name	**Primer**	**Sequence (5' → 3')**
Pdx1-Flp	Pdx1-Flp forward	AGAGAGAAAATTGAAACAAGTGCAGGT
	Pdx1-Flp reverse	CGTTGTAAGGGATGATGGTGAACT
	Gabra forward (Ctrl)	AACACACACTGGAGGACTGGCTAGG
	Gabra reverse (Ctrl)	CAATGGTAGGCTCACTCTGGGAGATGATA
FSF-Kras^{G12D}	FSF-Kras common forward	CACCAGCTTCGGCTTCCTATT
	FSF-Kras WT reverse	AGCTAATGGCTCTCAAAGGAATGTA
	FSF-Kras mut reverse	GCGAAGAGTTTGTCCTCAACC
FSF-Kras^{G12D} recombination	FSF-Kras del forward	AGAATACCGCAAGGGTAGGTGTTG
	FSF-Kras del reverse	TGTAGCAGCTAATGGCTCTCAAA
Frt-stop-Frt (FSF)	FSF forward	TGAATAGTTAATTGGAGCGGCCGCAATA
	FSF reverse	CAGGGTGTTATAAGCAATCCC
FSF-recombination	FSF-Cre stop del forward	GTTCGGCTTCTGGCGTGT

	FSF-Cre stop del reverse	CGATCCCTGAACATGTCCATC
Fsp1-Cre	Fsp1-Cre forward	CAGAACTAAAGGAGCTGCTGACC
	Fsp1-Cre reverse	CTTGGAAGTCCACCTCGTTGTC
LSL-Kras^{G12D}	LSL-Kras common forward	CACCAGCTTCGGCTTCCTATT
	LSL-Kras WT reverse	AGCTAATGGCTCTCAAAGGAATGTA
	LSL-Kras mut reverse	CCATGGCTTGATAAGTCTGC
LSL-Trp53^{R172H}	Trp53^{R172H} forward	AGCCTTAGACATAACACACGAACT
	Trp53^{R172H} mut forward	GCCACCATGGCTTGAGTAA
	Trp53^{R172H} reverse	CTTGGAGACATAGCCACACTG
Trp53^{frt}	p53 frt forward	AGCCTTAGACATAACACACGAACT
	p53 frt reverse	CTTTCTAACAGCAAAGGCAAGC
Td-Tomato	Td-Tomato forward	CAAGGGAGAGGAGGTCATCAAAG
	Td-Tomato reverse	GCTTGGTGTCCACGTAGTAGTAGC
LSL-Rosa26$^{Tva-lacZ}$	R26-Tva-GT-UP	AAAGTCGCTCTGAGTTGTTAT
	R26-Tva-GT-SA-mut-LP	GCGAAGAGTTTGTCCTCAACC
	R26-Tva-GT-WT LP	GGAGCGGGAGAAATGGATATG
	Tva-LP-353	CATCTCACCAGCTCACAGCAA
EGFP	EGFP forward	TGCCCGAAGGCTACGTCCAG
	EGFP reverse	CCATGTGATCGCGCTTCTCGT
Ai65(RCFL-tdT)	Ai65 forward	GCA ATA GCA TCA CAA ATT TCA C
	Ai65 reverse	TCT AGC TTG GGC TGC AGG T

4.7 Software

Table 10. Software

Axio Vison 4.8	Carl Zeiss AG, Oberkochen
Excel	Microsoft Corp., Redmont, WA, USA
FlowJo®	FlowJO LLC, Ashland, OR, USA
GraphPad Prism 5	La Jolla, CA, USA

LAS X	Leica Microsystems GmbH, Wetzlar
Odyssey® v1.2	Li-Cor Biosciences, Lincoln, NE, USA
OpenOffice Calc	Apache Software Foundation, DE, USA
OriginPro 2017	OriginLab Corp., Northampton, MA, USA

5. Methods

5.1 Cell Culture

Primary murine pancreatic cancer cells were established from tumour mice (see 2.1.1) and were maintained in PDAC cell medium (see Tabl. 1.6) at 37°C, 5% CO_2 and 100% humidity.

5.1.1 Generating of primary murine PDAC cell lines

To generate primary murine PDAC cell lines all conditions were kept as sterile as possible to prevent any contamination. During the mouse dissection (see 2.3.4) a small part of the tumour tissue was isolated and put into sterile PBS. Subsequently the tissue was cut up into small pieces under a biological safety cabinet using a sterile disposable scalpel and incubated for 24-48h in PDAC cell medium with 200 U/ml Collagenase type II at 37°C. Afterwards the specimen was centrifuged with 1200rpm for 5 minutes and the pellet was stored in the smallest cell culture flask with PDAC cell medium for further cultivation.

When sufficient growth of tumour cells was observed via microscopy the medium was aspirated and the cells were trypsinized with trypsin/EDTA at 37°C for a sufficient time. When detachment of the cells was observed, the trypsin was antagonised with PDAC cell medium and the diluted cells were transferred into the next vessel according to the future experimental needs. If not used for further experiments, the cells were then cryopreserved (according to 2.1.6) and stored at -80°C.

5.1.2 DNA harvest from cell culture

All steps were performed under a biological safety cabinet. Cells were cultivated until they reached 70-80% confluency. The medium was aspirated, the cells were thoroughly washed in sterile PBS and an appropriate amount (e.g. 200ul for a 10cm plate) of PBS was added. The cells were then removed from the plate using a cell scraper and transferred into an Eppendorf tube. The tube was centrifuged at 1500 rpm for 5 min, the supernatant was discarded and the pellet stored for further use at -20°C.

5.1.3 Protein harvest from cell culture

All steps were performed under a biological safety cabinet. All reagents and protein specimens were cooled with ice. IP-buffer was prepared prior to use. Cells were cultivated until they reached 70-80% confluency. The medium was aspirated, the cells were thoroughly washed in sterile PBS and an appropriate amount (e.g. 200ul for a 10cm plate) of IP-buffer was added. The cells were then removed from the plate using a cell scraper and transferred into an eppendorf tube. The tube was centrifuged at 1500 rpm for 5 min and 4°C, the lysate was transferred to another tube, snap frozen in liquid nitrogen and stored for further use at -80°C.

5.1.4 TGF-B treatment in cell culture

All steps were performed under a biological safety cabinet. Cells were cultivated until they reached 50-60% confluency. The medium was aspirated and then replaced by either TGF- ß or FCS-starving medium (see.1.4). The cells were imaged using the Axio vison microscope on day 0-7 and prepared for FACS analysis on day 3 or 7 (see. 2.1.5).

5.1.5 FACS analysis of cell lines

All preparation steps were performed under a biological safety cabinet. Cells were cultivated until they reached 70-80% confluency. Then the medium was aspirated, the cells washed in sterile PBS and then trypsinized with trypsin/EDTA until a detachment of the cells was observed. The trypsin was antagonised with PDAC cell medium and the diluted cells were centrifuged at 1500 rpm for 5 min. The supernatant was discarded, the cell pellet diluted in PBS and again centrifuged at the same conditions. The resulting cell pellet was diluted in 1-2ml of PBS according to the amount of cells and transferred to a FACS analysis tube.

FACS analysis was performed to detected tdTomato and EGFP signal. The data were analysed using the FlowJo® software. FACS settings were determined by using control specimens of each tdTomato and EGFP cells prior to the analysis.

5.1.6 Cryopreservation of cell lines

All steps were performed under a biological safety cabinet. For cryopreservation trypsinized cells were diluted in PDAC cell medium and centrifuged at 1500rpm for 5min. The cell pellet was dissolved in ice-cold freezing medium, transferred to a CryoPure tube and frozen at -80°C. After 24h the specimens were transferred to liquid nitrogen tanks for further storage.

5.2 Histology

5.2.1 Paraffin sections

Tissue samples meant for histological analyses were fixated in Rotil Histofix 4% for 24h directly after mouse dissection, dehydrated using the ASP300 Tissue Processor, embedded in paraffin and stored at room temperature for further use. The samples were cut serially into 2.5-3um thick slides using the Microtome Microm HM355S. If not used directly for further stainings, the slides were stored at -20°C.

5.2.2 Cryo sections

Tissue samples meant for histological analyses were fixated in Roti® HistoFix 4% for 24h directly after mouse dissection, dehydrated for 24h each, first in a 30% succrose, 70% PBS solution, second in a 15% succrose, 85% PBS solution. The samples were embedded in TissueTek, snap frozen in liquid nitrogen and stored for further staining at -80°C. The samples were serially cut into 7,5-10um thick slides using the Cryostat microm hm 560 and stored for further use at -20°C.

5.2.3 H&E staining

Paraffin-embedded section were stained according to the following protocol and were afterwards covered in Pertex mounting medium:
Dewaxing for 2x5min in Roti® Histol, rehydration in a decreasing ethanol series (2x99%, 2x 96%, 2x80%). Staining in hematoxylin for 5 seconds and subsequently blueing in tap water for 5 min. Afterwards staining in eosin for 20 seconds and washing in distilled water, before given into an ascending ethanol series (2x80%, 2x96%, 2x99%). In the end the slides were incubated in Roti® Histol for 2x5min.

5.2.4 Immunofluorescence staining

To preserve the endogenous fluorescence of the tissue all steps were performed to keep the light exposition as low as possible. The cryoslides were thawed in an opaque container for 12-24h at room temperature. Afterwards they were fixated with Rotil Histofix 4% and washed two times with PBS for 5min. Then an appropriate amount of solution C (PBS with 3% BSA, 1% Saponin, 1%Triton X-100) e.g. 100-200ul for one tissue slide was administered and incubated for 1h at room temperature. The primary antibody was diluted to an appropriate staining concentration in solution C according to manufacture instruction. 100-150ul of the antibody were added to

the slides and incubated for 48h at 4°C. Then the slides were washed in PBS four times for 15min, the secondary antibody (diluted in solution C) was added and incubated for 24h at 4°C. Finally, the slides were washed 4 times with solution C for 15min, 2 times in PBS for 5min and then covered with VectaShield® mounting medium with DAPI and sealed with black nail polish. The samples were directly analysed according to 2.2.5.

5.2.5 Immunofluorescence imaging

All immunofluorescence analyses were made using the Leica SP8 confocal microscope and the LAS X software. The absorption and emission spectra were determined by the manufacture instruction of each antibody (see Table 7). Emission detectors were set to only recognise the emission maximum of each fluorochrome to prevent spillover detection. Additionally, the images were taken sequentially to avoid cross-excitation of the fluorophores. To guarantee comparability and enable further statistically analyses, default settings for each used fluorochrome were established.

5.2.6 Immunofluorescence statistical analysis

For statistical analyses of the immunofluorescence images the LAS X and OriginPro2017 software were used. Each individual cell was counted and assigned to one of the following categories: Recombined or non-recombined, and positive, partially positive, or negative. The following table (Tabl. 11) shows the criteria used to determine each single category.

Table 11. Criteria for immunofluorescence analysis

Antibody	Positive	Partially positive	negative
ECAD	Signal continuously >= 50% of the membrane no artefacts Intensity>= 40	Signal continuously >= 10% of the membrane no artefacts Intensity >=20	Signal < 10% of the membrane; discontinuously or intracellular signal, or artefacts Intensity <20
Zeb1	Signal intranuclear >50% of the nucleus no artefacts	Signal intranuclear > 10% of the nucleus no artefacts	Signal intranuclear <10% of the nucleus,

	Intensity >= 40	Intensity >=20	non-nuclear signal, or artefacts Intensity <20
Fsp1	Signal intranuclear or perinuclear >50% of the nucleus no artefacts Intensity >= 40	Signal intranuclear or perinuclear >10% of the nucleus no artefacts Intensity >=20	Signal intranuclear or perinuclear <10% of the nucleus, non-nuclear signal, or artefacts Intensity <20

5.3 Mouse experiments

All animal studies were conducted in compliance with the European guidelines for the care and use of laboratory animals and were approved by the local authorities. Mice were on a mixed C57BL6/J;129/S6 background.

5.3.1 Mouse strains

Cre/*loxP* and Flp/*frt* mouse models were used in this study. Mice carrying genes which are flanked by *loxP*/*frt* sites or silenced by an *LSL*/*FSF* cassette can be interbred with a mouse strain expressing Cre or Flp recombinase under the control of a tissue-specific promoter to allow inactivation of genes or deletion of the *LSL* or *FSF* cassette to activate expression of genes. By using the mTmG and Ai65 reporter cells were labelled according to their recombination status. Combining the Flp/*frt* recombination system for tumour initiation and the Cre/*loxP* system under the control of the Fsp1-promoter together with the two different reporter systems created a dual recombinase dual fluorescence reporter system which is able to specifically and permanently label EMT events *in vivo* and *in vitro*

LSL-KrasG12D/+ (Hingorani et al. 2003): This knock-in mouse strain was kindly provided by Prof. Tyler Jacks (Massachusetts Institute of Technology, Cambridge, MA, USA). *LSL-KrasG12D/+* mice carry a point mutation in codon 12, which corresponds to the mutation frequently found in human PDAC leading to an amino acid substitution of glycine by aspartate. After Cre-mediated deletion of the *LSL* cassette, the GTPase activity of Kras is impaired resulting in constitutive Kras signaling.

LSL-Trp53R172H/+ (Hingorani et al. 2005): This knock-in mouse strain was kindly provided by Prof. Tyler Jacks (Massachusetts Institute of Technology, Cambridge, MA, USA). *LSL-Trp53R172H* mice carry a missense mutation in codon 172 of endogenous *Trp53*, which corresponds to the human R175H mutation often found in patients with the Li-Fraumeni syndrome and in spontaneous human tumours. After excision of the *LSL* cassette, dominant-negative oncogenic Trp53 is expressed (Vries et al. 2002).

Pdx1-Flp (Schönhuber et al. 2014***):*** This transgenic mouse strain was generated in the laboratory of Prof. Dieter Saur. The codon-optimized Flp-o recombinase is expressed under the control of the *Pdx1* promoter, which is active in pancreatic progenitor cells and in adult pancreatic acini, ducts and islets.

FSF-KrasG12D/+ (Schönhuber et al. 2014): This knock-in mouse strain was generated in the laboratory of Prof. Dieter Saur. Expression of the *FSF* silenced oncogenic *KrasG12D* allele from its endogenous locus can be activated by Flp expression.

Trp53frt/+ (Lee et al. 2012): This mouse strain was kindly provided by Dr. David Kirsch (Duke University School of Medicine, Durham, NC, USA). Exons 2 to 6 of the *Trp53* gene are flanked by *frt* sites and p53 can be inactivated by Flp expression.

Fsp1-Cre (Bhowmick et al. 2004): The Fsp1-Cre line was obtained from Jackson Laboratories (# 012641). Fsp1 (S100A4) is a member of the S100 calcium binding family and promotes motility, angiogenesis and invasiveness via the induction of EMT in tumour cells (Boye und Maelandsmo 2010). Activation of the Fsp1 promoter leads to Cre-recombinase expression. This transgenic Cre line allows lineage tracing of cells expressing the Fsp1.

LSL-Rosa26$^{Tva\text{-}lacZ/+}$ (Seidler et al. 2008): The mouse strain was generated in PD Dr. Dieter Saur's group (Klinikum rechts der Isar, Technical University of Munich). Here, the *Rosa26* locus is targeted to get Cre-loxP-based conditional expression of tumour virus A (Tva) receptor as well as nuclear lacZ (β-galactosidase). Due to the Tva receptor, which is normally expressed endogenously in avian cells, these mice and isolated tumour cells from these animals can be transduced with the gene of interest by the RCAS-Tva system.

R26$^{mTmG:}$ *(Muzumdar et al. 2007)*: *R26^{mTmG}* mice will ubiquitously express a membranous tandem-dimer of tdTomato. After Cre recombination the LSL flanked tdTomato sequence gets removed and permanent EGFP expression replaces the tdTomato signal.

R26$^{CAG-FSF-LSL-Ai65-tdTom}$ (Madisen et al. 2015): This dual reporter mouse line for Flp and Cre recombinases was obtained from Jackson Laboratories (# 021875). tdTomato expression is blocked by an frt-flanked STOP cassette and by a STOP cassette flanked by loxP sites. The whole construct was introduced as a knock-in into the R26 locus.

5.3.2 Genotyping

Around 2-3 weeks after birth samples for genotyping were taken. Samples were taken as a 1mm long tail biopsy from the previously anaesthetized mouse. Each mouse also received an explicit ear marking. DNA was extracted from the specimen according to 2.4.1.

5.3.3 Orthotopic implantation

The mice (NOD Scid Il2 receptor gamma-/- (*NOD.Cg-PrkdcscidIl2rgtm1Wjl*/SzJ) or wildtype C57BL6/J) were anaesthetized using weight adapted MMF (5 mg/kg midazolam, 500 µg/kg medetomidine, 50 µg/kg fentanyl) via intraperitoneal injection (Tabl). A small left sided subcostal aslant (left to right) incision was made with a sterile scalpel, the peritoneum was punctured, and the spleen was carefully exposed. A defined number of cells (2500 cells in 25ul DMEM) were administered into the adjacent pancreas body using a microliter syringe with a 27-gauge needle. The peritoneum was stitched with a surgical suture, the skin with surgical clips, particular value was on preventing adhesion of the pancreas with the peritoneum. The MMF was antagonised with AFN (750 µg/kg atipamezole, 500 µg/kg flumazenil, 1.2 mg/kg naloxone) via subcutaneous injection. The mice were monitored postoperatively, first daily then once a week. The mice were sacrificed following standard abort criteria and samples were taken according to 2.3.4-6.

5.3.4 Mouse dissection

Prior to dissection the mouse was euthanized with isoflurane, fixed and disinfected with 70% ethanol. The abdomen was opened with a media section incision, the skin was carefully separated from the peritoneum, leaving it intact. After separation the peritoneum was punctured

and any intraperitoneal liquid was aspirated in 200ul EDTA and stored for further analyses. Next the peritoneum was fully opened and a blood sample was taken from one of the two major abdominal vessels with a small 27 gauge needle with 100ul EDTA to avoid clotting and stored on ice for further use (see 2.3.5). Pancreatic tissue samples for following RNA and protein isolation were homogenized in 1mL RLT buffer supplemented with 10 µL 2-mercaptoethanol or 600 µL IP buffer using SilentCrusher, respectively. A small piece of tissue was removed for subsequent DNA isolation. All samples were snap-frozen and stored at -80 °C until use. Subsequently all major organ systems were removed and examined for metastases, the pancreas as well as all metastatic suspicious tissue were imaged as described in 2.3.6. The size and the weight of the pancreas, liver and spleen tissue was determined. Pancreas, liver, lung, heart, kidneys, intestine, peritoneum, diaphragm and every suspicious lymphnode were isolated and fixated in Roti Histofix 4% for 24h for further histological analyses.

5.3.5 FACS analysis of blood/ascites samples

The blood and ascites samples were taken during the mouse dissection as described above and stored on ice. The samples were centrifuged at 1200rpm for 5min, the supernatant was discarded and the appropriate amount of EL-buffer was added (5x the volume of the initial sample). After 15 min of incubation on ice the samples were centrifuge at 1200rpm for 10min and the cell pellet was diluted in PBS with 3%FCS and filtered through a 100um sterile Cell strainer.
FACS analyses and FACS sort for tdTomato and EGFP were performed with help of a technician.

5.3.6 Fluorescence analysis of organs

Organ tissue was examined directly after dissection with the Axio Vison Microscope (see Table 1) for bright light (BL), tdTomato and EGFP. For documentation purposes and further analyses (e.g. metastases counting) images were taken using the AxioVison Cell Viewer v1.2. Representative images are displayed in the result part. Pancreas, liver and lung tissue were always, all other tissue only when metastatic suspicious, examined and photographed under standardized conditions.

5.4 Molecular biology

5.4.1 Isolating of DNA

Genomic DNA was isolated from the samples won as described in 2.1.2 or 2.3.2. 50-200ul of Soriano lysis buffer was added to the specimens and incubated in a thermocycler at 55°C for 90min. After heat inactivation of Proteinase K at 95°C for 15min, the samples were vortexed and centrifuged at 14000rpm for 10min at 4°C. The DNA-containing supernatant was then transferred into a new tube and stored at -20°C for further use.

5.4.2 Polymerase chain reaction (PCR).

For standard genotyping or recombination PCR (Mullis et al., 1986) a PCR pre-mix containing buffer, polymerase and dNTPs was used (Table 12). The standard PCR reaction setup and conditions are shown in Table 13. Primer amounts were optimized depending on the PCR product. If necessary, DMSO was added to improve PCR outcome. PCR products were stored at 4 °C until further analysis by gel electrophoresis.

Table 12. Composition of PCR pre-mix

Solution	**Volume/reaction**
distilled water	4,375 ul
10x buffer S	2,5 ul
30% succrose	2,5 ul
SucRot	2,5 ul
PeqTaq	0,125 ul
dNTPs (10uM each)	0,5 ul

Table 13. Standard PCR conditions and reaction mix

Reaction mix		**Conditions**		
12,5 ul	PCR pre-mix	95°C	3min	
0,25-2ul	forward primer 10uM	95°C	45s	40x
0,25-2ul	reverse primer 10uM	55-72°C	60s	

1,5ul	DNA	72°C	90s	
ad to 25ul	distilled water	25°C	hold	

Genotyping PCR. To determine the genotype of a mouse, tail DNA, which was isolated as described in 2.3.2, was used. For each allele, specific primers were designed (Table 9). Annealing temperatures and PCR products are indicated in Table 14.

Table 14. Annealing temperature and PCR products of standard PCR for genotyping and recombination

Mut= mutated allele, WT = wild type allele, rec= mutated allele without translational stop element after recombination

PCR name	**Annealing temperature**	**PCR products [bp]**
Pdx1-Flp	55°C	620 (mut); 300 (internal control)
FSF-KrasG12D	55°C	350 (mut); 270 (WT)
FSF-Kras^{G12D}recombination	60°C	196 (rec)
FSF	60°C	600 (mut)
FSF recombination	60°C	490 (rec)
Fsp1-Cre	58°	390 (mut); 290 (internal control)
R26-CAG	62°C	450 (mut); 650 (WT)
R26^{mTmG}	62°C	450 (mut); 650 (WT)
LSL-Trp53^{R172H}	55°C	270 (mut); 570 (WT)
Trp53frt	57°C	292 (mut); 258 (WT)
Td-Tomato	60°C	580 (mut)
EGFP	64°C	380 (mut)

5.4.3 Agarose gel electrophoresis

Nucleic acids were separated by electrophoresis in 1% agarose gels. Agarose was dissolved in 1x TAE buffer by boiling in a microwave. Ethidium bromide which intercalates into DNA was

added to the gel prior to gelling. DNA samples were pipetted into the gel pockets and separated at 120 V. For documentation nucleic acids were visualized by excitation with UV light with GelDoc™.

5.5 Protein biochemistry

5.5.1 Protein concentrating estimation

The protein concentrations of the cell lysate were determined by using the Bradford assay (Bradford, 1976). The protein samples (see 2.1.3) were carefully thawed on ice, centrifuged at 13200rpm for 20min and the supernatant was transferred into a new tube. 300 µL of Bradford reagent diluted 1:5 in water were placed into a well of a 96-well plate. 1 µL of the sample of interest was added. After 10 min of incubation, absorbance was measured at 600 nm with the microplate reader Anthos 2001 and protein concentration was estimated using a defined BSA dilution series as reference. Each sample was measured in triplicates. By adding protein loading buffer (Laemmli, 1970) and IP buffer, protein concentration of all samples were adjusted to one level. Protein samples were subsequently denatured at 95 °C for 5 min and stored at -20 °C.

5.5.2 SDS polyacrylamide gel electrophoresis (SDS-PAGE)

SDS-PAGE (Laemmli, 1970) using 10% or 12% separating gels depending on the size of the protein of interest was performed to separate the proteins concerning their molecular weight.
At first the reagents for the separating gel were mixed, as shown in (Table 15). After pouring into a gel caster, the gel was covered with a layer of 2-propanol and allowed to polymerize. After the stacking gel mixture was prepared, poured and polymerized, 80–120 µg of the protein samples were loaded on the SDS polyacrylamide gel. For concentration of the proteins in the stacking gel, electrophoresis was carried out at 80 V for about 45 min. Then proteins were separated at 120 V.

5.5.3 Immunoblot

After separation with SDS-PAGE the proteins were blotted onto a PVDF membrane which was activated previously by incubation in 100% methanol for 30 s and then equilibrated in transfer buffer (Towbin et al., 1979). The proteins were electro-blotted in a tank blot system onto the activated membrane at 100 V and 4°C for 2h or at 30V and 4°C for 16h. After protein transfer the membranes were blocked by incubation in 5% BSA in PBS or 5% milk at RT for 30–60 min to prevent unspecific binding of the antibody. Subsequently, the membranes were transferred

into a specific primary antibody solution diluted in 5% BSA and incubated at 4 °C over night. After three washing steps with PBS-Tween for each 15 min the membranes were incubated with the secondary antibody diluted in 5% BSA in PBS or 5% milk for 1 h at RT in the dark. Membranes were again washed three times with PBS-Tween for each 15 min and scanned at 700 nm or 800 nm wavelength using Odyssey® infrared imaging system.

Table 15 Composition of SDS polyacrylamide gels (3times)

Compounds	**10% separating gel**	**12% separating gel**	**Stacking gel**
H2O	6150ul	5100ul	4500ul
Separating gel buffer	3900ul	3900ul	-
Stacking gel buffer	-	-	1950ul
Rotiphorese® gel 30	4950ul	6000ul	1125ul
10%SDS	150ul	150ul	75uk
10% APS	75ul	75ul	37.5ul
TEMED	22.5ul	22.5ul	15ul

5.6 Statistical analyses

Graphical depiction, data correlation and statistical analysis were performed with GraphPad Prism 5 or OriginPro 2017. Generally, cell-culture based assays were performed threefold. For survival analysis, Kaplan-Meier estimator were used. Log-rank test was done for statistical analysis of survival curve. $p<0,05$ was considered statistically significant. For correlations spearman and pearson correlation coefficient were evaluated. For immunofluorescence analysis cells were manually counted using the LAS X software counting tool with the preestablished criteria seen in Table 11.

6. Results

6.1 A dual recombinase dual fluorescence reporter system for EMT detection *in vivo*

While observation of EMT events *in vitro* can easily be performed, examinations of EMT *in vivo* has been a problem for years. Cell plasticity and consecutive mesenchymal to epithelial transition (MET) made it difficult to access the steps that precede metastatic formation. While inducing EMT *in vitro* leads to a more invasive phenotype in tumour cells increasing motility, angiogenesis, and degradation potential (Thiery et al. 2009; Kalluri und Weinberg 2009), blocking EMT with therapeutic intent did not lead to the expected decrease in metastases (Fischer et al. 2015; Kalluri 2016; Thomas und Radhakrishnan 2019). This indicates that tumour cells possess multiple possibilities to form metastases. In order to observe metastatic processes and EMT events *in vivo,* we utilized a dual recombinase dual fluorescence reporter system which is capable of permanently labelling EMT-events *in vivo*.

Pdx1-Flp; FSF-Kras^{G12D}; Fsp1-Cre mice were crossed with mice which harbour the *R26^{mTmG}* or the *R26$^{Ai\text{-}65\text{-}tdTom}$* reporter system. The resulting mouse models *Pdx1-Flp; FSF-Kras^{G12D}; Fsp1-Cre; R26^{mTmG}* and *Pdx1-Flp; FSF-Kras^{G12D}; Fsp1-Cre; R26$^{Ai\text{-}65\text{-}tdTom}$* will henceforward be referred to as Fsp1^{mTmG} and Fsp1$^{Ai\text{-}65\text{-}tdTom}$ (Figure 1 A, B).

The Fsp1^{mTmG} system ubiquitously labels cells with the tdTomato fluorochrome only until Cre-recombination, which permanently changes the fluorescence signal to EGFP due to the activation of the Fsp-1 promotor. In our evaluation the vast majority of pancreatic tumour cells were non recombined, however also a small sub population of EGFP positive tumour cells exist in the primary pancreatic tumour (PPT) (2,94%, analysed via FACS). Confocal microscopy of PPT tissue showed tdTomato positivity in tumour cells and EGFP positivity in the surrounding stroma (Figure 1 C).

While *mTmG* labelling is ubiquitous, the aim was to specifically target pancreatic tumour cells in order to examine the influence of EMT on the metastatic processes in pancreatic tumours. We approached this goal with two different solutions. With the Fsp1$^{Ai65\text{-}td\text{-}Tom}$ system's property of only labelling Flp and Cre recombined cells with tdTomato (Figure 1 B) we limited the fluorescence signal in mice of the endogenous model due to the tissue specificity of Pdx1 to pancreatic cells. Leading to the fact that every fluorescence signal in other organ systems belongs to pancreatic tumour cells, but without the possibility to track non-EMT cells.

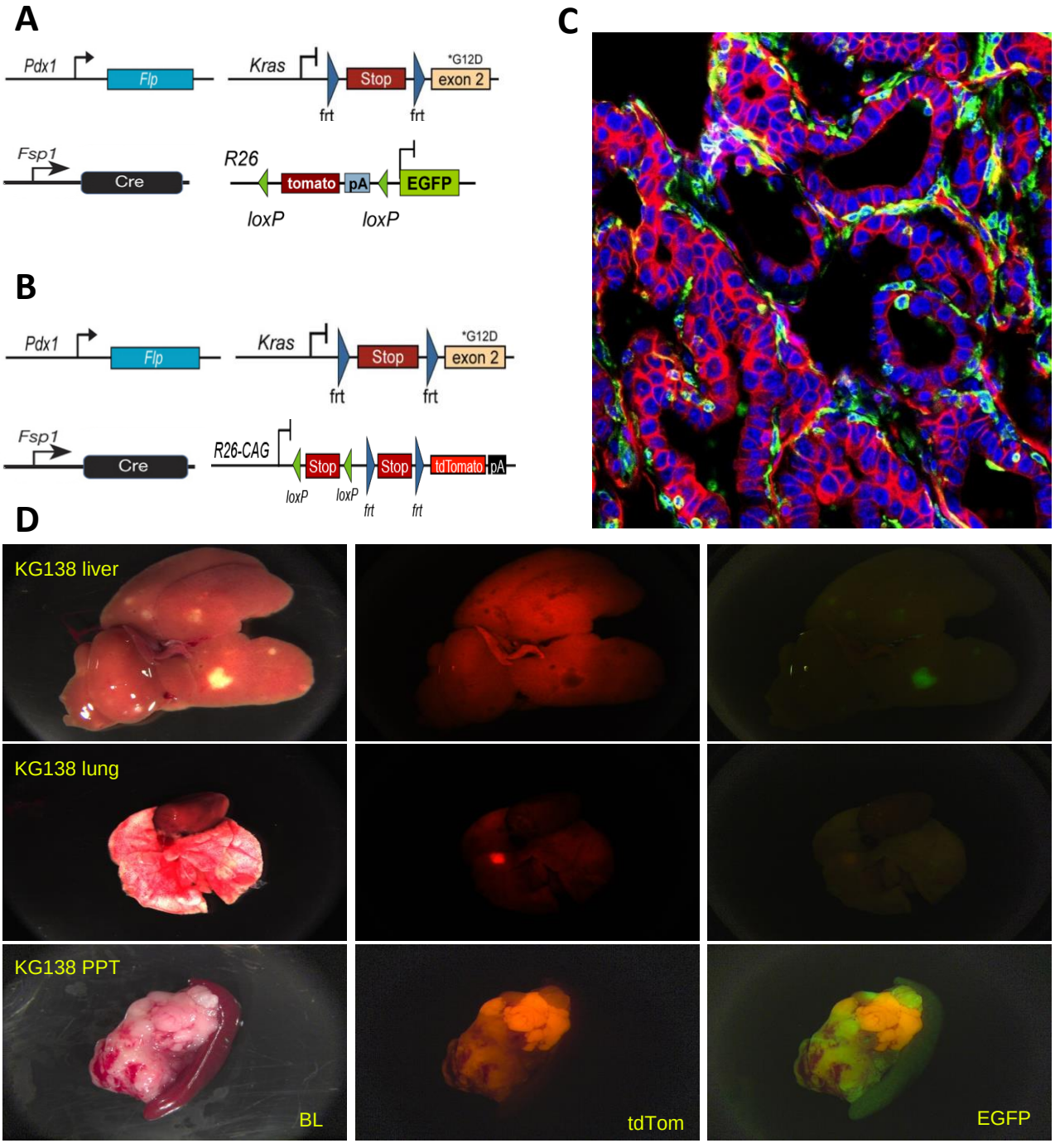

Figure 1. Dual recombinase dual fluorescence reporter system for EMT detection in vivo

(A) Genetic strategy to label EMT and non EMT cells. Pdx1-Flp-activated expression of $KRAS^{G12D}$ induces pancreatic cancer. Fsp1-Cre activation leads to a permanent shift in the fluorescence profile from tdTomato to EGFP expression.

(B) Genetic strategy to specifically label recombined tumour cells. Pdx1-Flp-activated expression of $KRAS^{G12D}$ induces pancreatic cancer. Fsp1-Cre and Pdx-Flp activation leads to permanent tdTomato expression.

(C) Representative image of confocal microscopy of PPT in $Fsp1^{mTmG}$ shows tdTomato positivity in epithelial cluster cells and EGFP positivity in the surrounding stroma cells. (blue:DAPI, red:tdTomato, green:EGFP)

(D) Representative images of macroscopic PPT and metastases in the $Fsp1^{mTmG}$ system show recombined and non-recombined metastases in the same mouse. (BL:bright light)

To overcome both problems we performed orthotopic implantation of PPT cells of both reporter systems into immunocompetent C57BL6/J wildtype (WT) and immunodeficient NOD Scid Il2 receptor gamma-/- (*NOD.Cg-PrkdcscidIl2rgtm1Wjl*/SzJ) (SCID) mice (Figure 2 A). The resulting mouse model ensured us that every fluorescence signal exclusively correspond to tumour activity, making it possible to observe and examine EMT and non-EMT cells in all compartments (blood, ascites, tissue). This also included the possibility of a statistical quantification of recombined and non-recombined tumour cells.

6.2 Influence of the EMT-status to the metastatic distribution

To analyse the metastatic pattern the two reporter systems were used in the endogenous, implanted WT, and implanted SCID mouse models.

Mice were dissected according to 2.3.4, primary pancreatic cells lines were generated (2.1.1) for further cell culture analyses and orthotopic transplantations. The recombination frequency in the primary tumour was determined by FACS analysis (see 2.1.5). All organ systems were thoroughly searched for macroscopic metastatic lesions immediately after dissection and documented using the AxioVison microscope (Table 1) with bright light, tdTom and EGFP (only for $Fsp1^{mTmG}$) filters under standardized conditions.

6.2.1 Endogenous mice

Three mice of the $Fsp1^{Ai\text{-}65\text{-}tdTom}$ and 22 of the $Fsp1^{mTmG}$ system have been analysed. In Figure 2 B is depicted the metastases distribution in the $Fsp1^{mTmG}$ system after manually evaluation of all lesions in all suspected organ systems. 59% of all mice developed metastases, with liver metastases being the most common type occurring in 36,36%, followed by lung and lymph node lesion both occurring in 13,64% of the cases. Peritoneal infiltration was only present in 9% of all mice. The metastatic burden was highest in the liver (47% of all metastases), followed by the lung (36%) (Figure 3 A). In total 47% of all metastases were recombined (Figure 3 A). 50% of mice had ascites. Primary tumours consisted mostly of unrecombined areas, with small parts of recombined cells (Figure 1 D). FACS analyses of the isolated PPT cell lines revealed a mean recombination frequency of 2,94%. Regarding the recombination behaviour of the metastatic cells, we could observe that recombined and unrecombined metastases occurred simultaneously in different as well as in the same organ systems in both reporter systems (Figure 1 D). In regard to the low numbers of PPT and metastasis in the $Fsp1^{Ai\text{-}65\text{-}tdTom}$ system no statistical analyse was performed in the endogenous model.

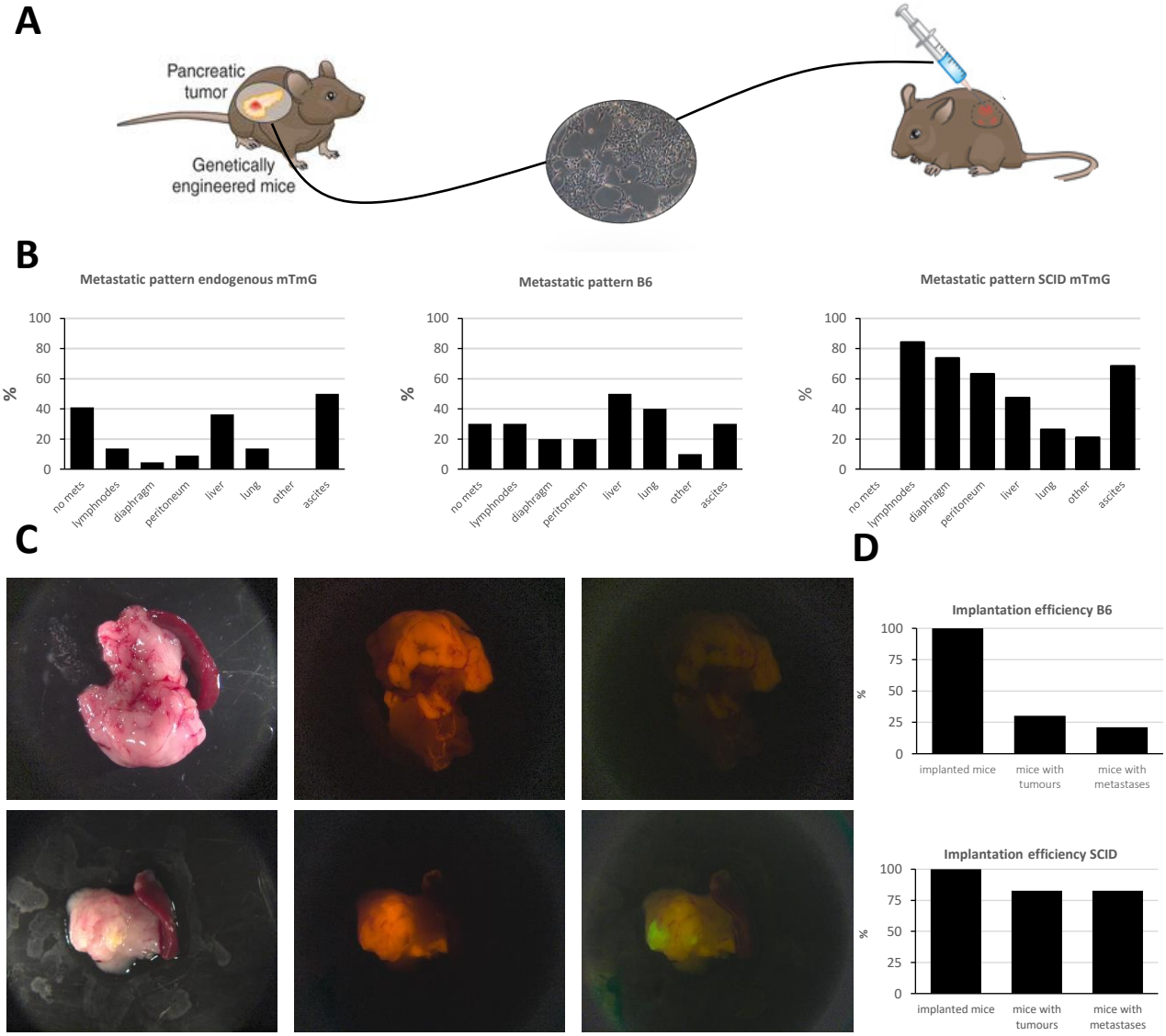

Figure 2 Orthotopic implantation model for metastazation analyses

(A) Scheme of orthotopic transplantation of endogenous PPT cells into B6 or SCID mice. PPT cells are harvested and raised in cell culture; after FACS analysis of the recombination rate a distinct number of cells (2500) were orthotopic implanted into B6 or SCID mice (see 2.3.3.)

(B) Analyses show the percentage of mice having at least one metastasis in the named organ system for endogenous, implanted B6, and implanted SCID mice in the mTmG reporter system (from left to right)

(C) Representative macroscopic images of PPTs after orthotopic implantation in B6 (top) and SCID (bottom) mice; bright field, tdTom, EGFP (from left to right)

(D) Implantation efficiency and metastastic frequency in the B6 (top) and SCID (bottom) implantation series

6.2.2 Implanted wildtype mice show predominately unrecombined metastases

In order to further investigate the findings described above and address the obstacles (low metastases rate, long breeding time, systematic underestimate of tdTom positive metastases) of the endogenous model, we implanted 33 mice from a mixed C57BL6/J;129/S6 background with

PDAC cells from the Fsp1^{mTmG} and Fsp1$^{Ai65\text{-}tdTom}$ systems (Figure 2 A) according to 2.3.3. FACS analyses of all implanted cell lines were performed directly before implantation to determine the number of recombined cells per cell line and to be able to correlate the metastatic frequency with the preimplantation recombination count.

The implantation efficiency of this approach was unsatisfactory low with only 30,3% of the mice developing a PPT (Figure 2 D). Figure 2 B shows the result of the metastases distribution in the Fsp1^{mTmG} system after manually and mechanically counting of all lesions in all suspected organ systems of all mice. 70% of all mice developed metastases, with liver metastases being the most common type occurring in 50%, followed by lung (40%) and lymph node (30%) lesions. Peritoneal infiltration was present in 20% of all mice. Additionally, 20% of the mice showed diaphragm alteration, conclusive with metastatic nodules. Regarding the overall metastatic burden liver (39,13%) and lung (25,4%) metastases were most frequent followed by diaphragm (12,3%), lymph node (11,6%), and peritoneal metastases (10,9%). Recombination percentage was at a mean 2,17% while being highest (5,7%) in lung metastases and lowest with 0% in diaphragm, lymph node, and peritoneal metastases (Figure 3 B). Against common expectation non-EMT metastases (unrecombined) significantly outnumbered EMT metastases without being exclusive (135 to 3).

The overall results of this implantation series correspond with the findings of the endogenous model. Liver and lung metastases were equally common and distributed. PPTs were similar configured (Figure 2 C) with mostly unrecombined part. However, non-EMT metastases largely outnumbered EMT-metastases. Notable is that the number of recombined metastases was significantly lower than in the endogenous mice. No correlation between the number of recombined cells in the implanted cell lines and the occurring recombined metastases could be found. Overall, the model of implantation in wildtype mice mimics and further supports the results of the endogenous model. It shows that metastatic processes are not necessarily EMT dependent.

6.2.3 Analysis of implanted immunodeficient mice

To increase the implantation efficiency and examine the influence of the immune system on the metastatic process and EMT we implanted 30 immunodeficient SCID mice with 5 mouse lines (5 mice each) from the Fsp1^{mTmG} and 1 from the Fsp1$^{Ai65\text{-}td\text{-}Tom}$ system (Figure 2 A). FACS analyses of all implanted cell lines were performed directly before implantation to determine

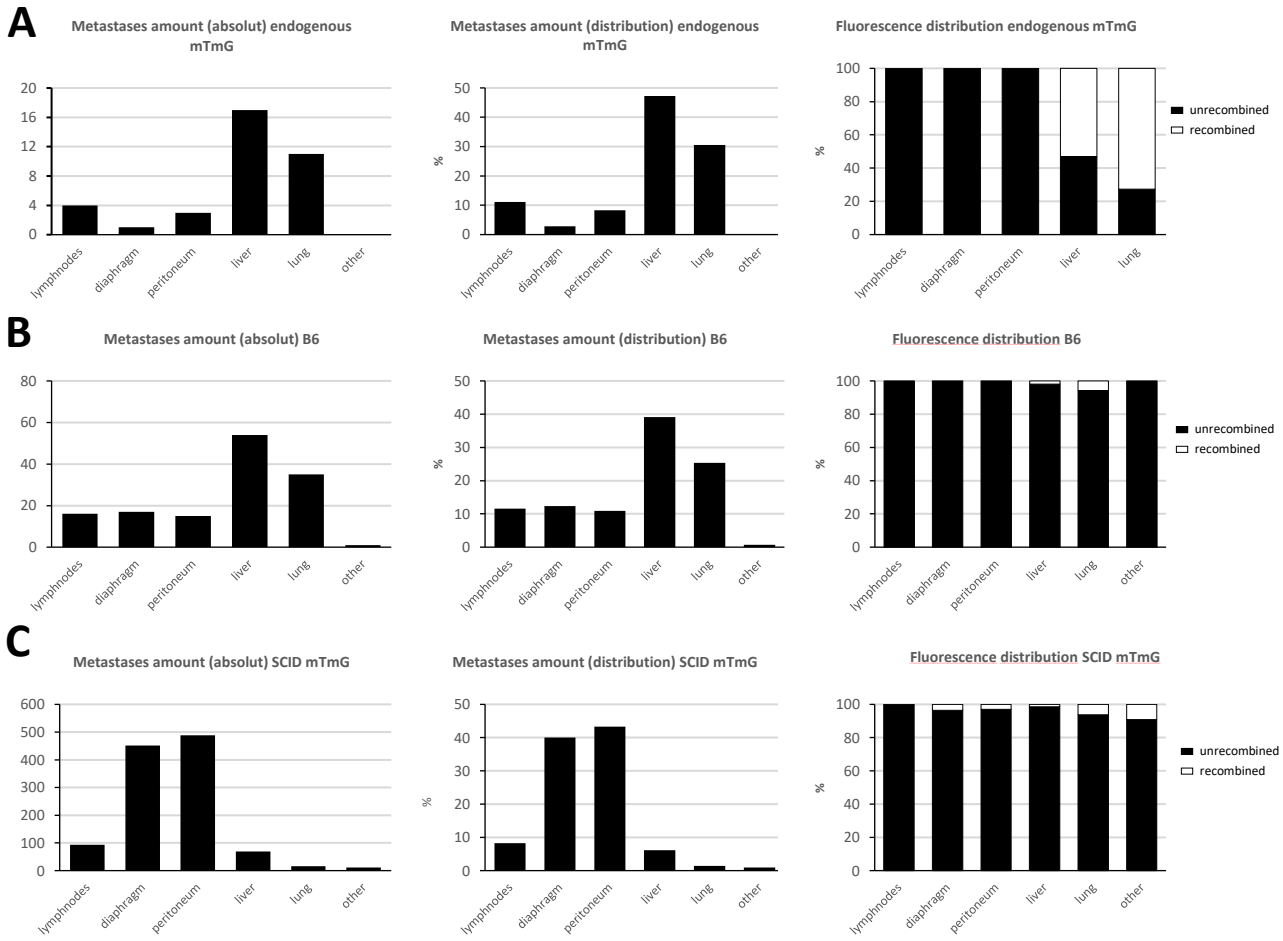

Figure 3 Metastases distribution of endogenous and implanted mice in the mTmG reporter systems

(A) Analyses show the absolute number of metastases found in all evaluated organs, the percentage distribution of all metastases and the distribution of recombined (white) and unrecombined (black) metastases for each organ system for endogenous mice (from left to right); n=22 mice; note the different scaling in column one

(B) Analyses show the absolute number of metastases found in all evaluated organs, the percentage distribution of all metastases and the distribution of recombined (white) and unrecombined (black) metastases for each organ system for implanted B6 mice (from left to right); n=11 mice

(C) Analyses show the absolute number of metastases found in all evaluated organs, the percentage distribution of all metastases and the distribution of recombined (white) and unrecombined (black) metastases for each organ system for implanted (from left to right); n=19 mice

the number of recombined cells per cell line, due to time dependent change of recombination rate *in vitro* (see result part 3.6).

Figure 2 B shows the result of the metastases distribution in the Fsp1^{mTmG} system after manually and mechanically counting of all lesions in all suspected organ systems of all mice. Compared to the results in the endogenous and implanted WT model, there was a significant increase in metastatic frequency and a great decrease in survival as expected in an immunodeficient model. All mice developed at least one metastasis. 47,4% developed liver and 26,3% lung metastases, mirroring the results in the endogenous (36,36% and 13,64%) and wildtype implantation model

(50% and 40%). However peritoneal (63,2%), diaphragm (73,7%) and lymph node (84,2%) metastases were significantly more frequent than in the other models used. This also affected the overall metastatic burden. Given these findings, peritoneal (43,3%) and diaphragm lesions (40,0%) accounted for the vast majority of all metastases in this model (Figure 3 C). When affected those metastatic sides ubiquitously harboured enormous numbers of metastases of all sizes (Figure 4 B). Liver (6,1%) and lung (1,4%) metastases accounted only for a small margin of the total number of metastases. 8,2% of metastases were found in lymph nodes. Recombination percentage was comparable to the previous models at a mean 3,01% while being

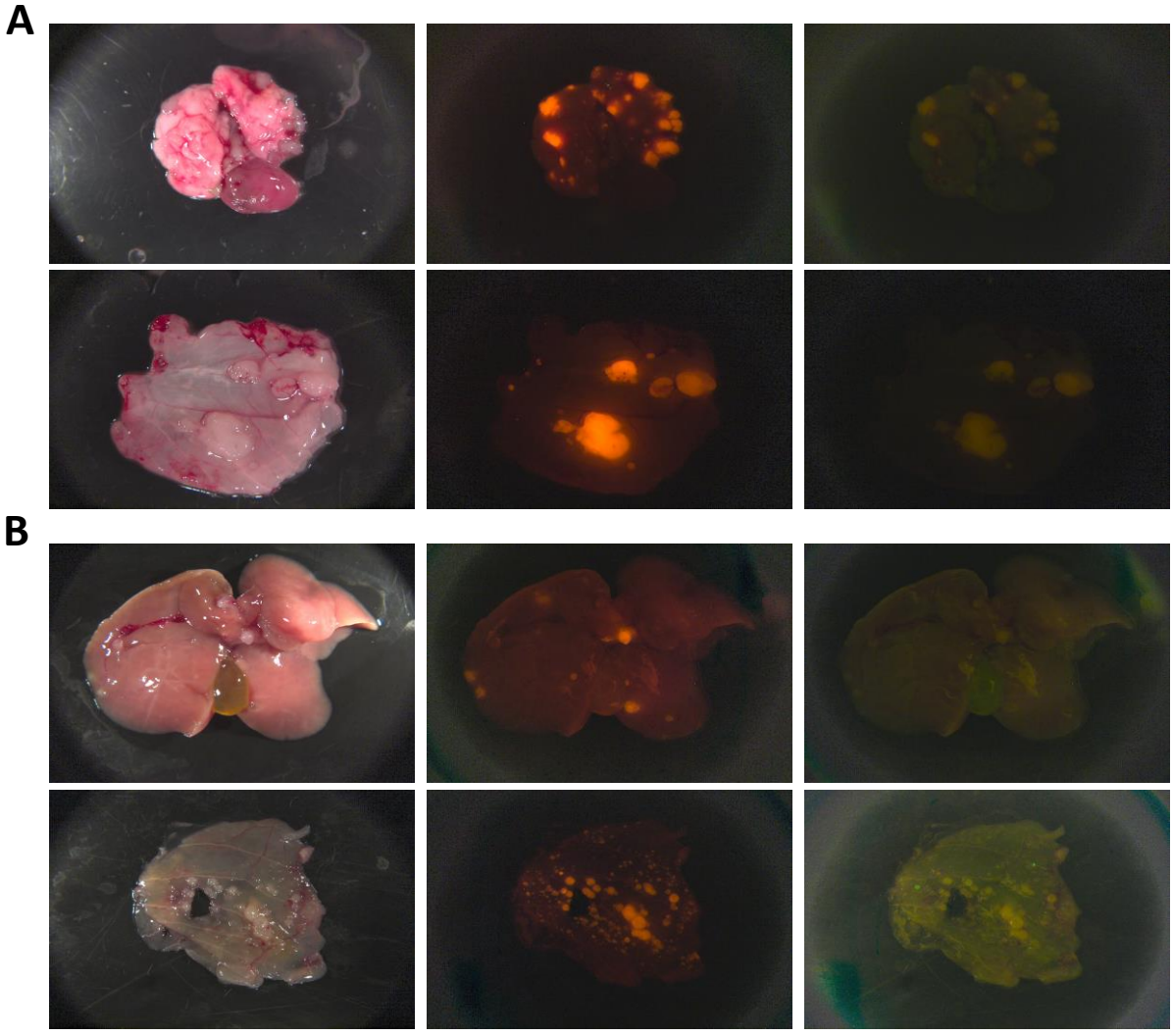

Figure 4 Macroscopic images of implanted B6 and SCID metastases

(A) Macroscopic image of an implanted B6 mouse from the Fsp1^{mTmG} reporter systems shows several unrecombined lung metastases (top) and unrecombined peritoneal metastases (bottom); bright field, tdTom, EGFP (from left to right)

(B) Macroscopic image of an implanted SCID mouse from the Fsp1^{mTmG} reporter systems shows several unrecombined liver metastases (top) and unrecombined and recombined peritoneal metastases (bottom); bright field, tdTom, EGFP (from left to right)

highest (6,25%) in lung metastases and lowest with 0% in lymph node metastases. 68,4% of mice had ascites (Figure 3 C). The macroscopic aspect of the PPTs was similar to the endogenous ones (Figure 2 C) as well as their recombination rate evaluated via FACS analysis in the isolated cell lines resembled theirs (2,15% vs. 2,94%). Additionally, FACS analyses of the isolated ascites cell lines could find that their recombination frequency was only slightly higher (2,76%) compared to 2,15% in the PPT cell lines, also indicating that no activation of the EMT program is required for cells to emigrate into the peritoneal cavity fluids.

As found in the wildtype implantation model, non-EMT metastases significantly outnumbered EMT metastases without being exclusive (1096 to 34). We could still observe recombined and unrecombined metastases in the same as well as in distant organ systems simultaneously (Figure 4 B). Also, the recombination rate seems to be somewhat organ specific (lung vs. e.g., lymph node or peritoneum).

Figure 5 shows the summary of the implantation data for the $Fsp1^{Ai\text{-}65\text{-}tdTom}$ model. This is a preliminary data as so far only one cell line was used for implantation (n=5 mice). Nevertheless, this cell line was the first to exhibit an astonishing percentage of recombined metastases (80,95%) and is therefore fitting to evaluate the behaviour of EMT activated tumour cells. However, one has to consider that non-recombined cells are not labelled by a fluorescence signal and therefore non-recombined metastases are naturally underestimated in this evaluation. Compared to the results of the endogenous and implanted WT model we saw a significant increase in metastatic frequency and a great decrease in survival. All mice developed at least one metastasis. The metastatic count was highest in this experiment with a mean of 79,8 different metastases per mouse compared to 59,5 in the $Fsp1^{mTmG}$ SCID implantation model and 13,8 in the WT implantation model. Liver and lung metastases were significantly more frequent than in any other model and occurred in 80% of all mice while peritoneal (60%), diaphragm (80%) and lymph node (100%) lesions, while being slightly elevated, are comparable to the implanted SCID mice in the $Fsp1^{mTmG}$ reporter system. 43,11% of all metastases were fund in the lung with 94,77% of them recombined, followed by liver lesions (27,32% of all lesions) with a recombination rate of 75,23%. Diaphragm and peritoneal alterations only accounted for 18,80% and 0,75% of all lesions while in the $Fsp1^{mTmG}$ system – where the majority of metastases were unrecombined - they made up more than 80% of all cases. Lymph node lesions were similarly frequent with 9,27%. 60,0% of mice had ascites. Here, unlike the wildtype and $Fsp1^{mTmG}$ SCID implantation model, EMT metastases

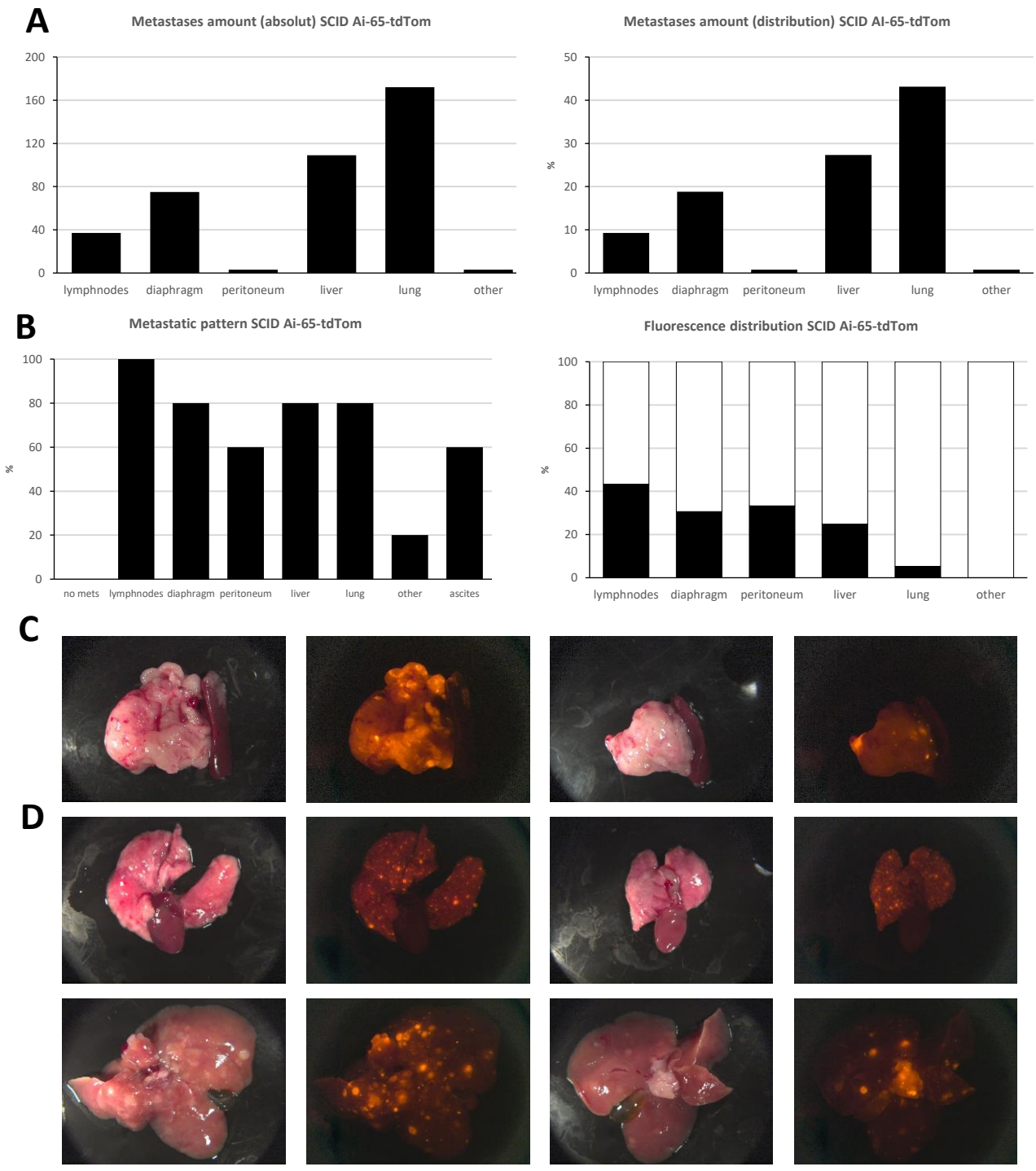

Figure 5 Metastases analyses of implanted SCID mice in the Fsp1$^{Ai\text{-}65\text{-}tdTom}$ reporter model

(A) Analyses show the absolute number of metastases found in all evaluated organs and the percentage distribution of all metastases for implanted SCID mice (from left to right); n=5 mice

(B) Analyses show the percentage of mice having at least one metastasis in the named organ system (left) and the distribution of recombined (white) and unrecombined (black) metastases (right) for each organ system for implanted SCID mice in the Fsp1$^{Ai\text{-}65\text{-}tdTom}$ reporter system, n=5 mice

(C) Representative macroscopic images of PPTs after orthotopic implantation in SCID mice shows unrecombined and recombined areas; bright field left, tdTom, right

(D) Macroscopic images of implanted SCID mouse from the Fsp1$^{Ai\text{-}65\text{-}tdTom}$ reporter systems shows several recombined lung metastases (top) and unrecombined and recombined liver metastases (bottom); bright field left, tdTom, right

significantly outnumbered non-EMT metastases without being exclusive (323 to 76). As in the endogenous and WT implanted model we found both EMT and non EMT metastases in the same and in different organ systems in the same mice (Figure 5 D). These results suggest that recombined cells exhibit a complete different metastatic pattern than unrecombined cells. With a recombination rate of over 80% we could observe a significant increase in liver and especially lung metastases, while diaphragm and peritoneal lesions greatly decreased.

6.2.4. Comparison of the metastatic behaviour of recombined and unrecombined tumour cells

To summarize in the Fsp1^{mTmG} orthotopic implantation model non-recombined metastases outnumbered recombined metastases by 32 to 1 (45 to 1) and even 78,9% (71,4%) of the mice had exclusively non-recombined metastases. This data is supported by a total amount of 19 (10) mice and 1130 (138) metastases counted in two different approaches. The numbers in brackets indicate the corresponding number in the implanted WT mice. These results support and confirm the initial findings of the endogenous Fsp1^{mTmG} mice.

The implantation of one Fsp1$^{Ai\text{-}65\text{-}tdTom}$ cell line into 5 SCID mice resulted in the highest overall recombination rate of 80,95% with 399 total metastases counted of all analysed models. It could be observed that both cell populations (recombined and unrecombined tumour cells) are able to infiltrate and metastasize every organ system, but with significantly different effectivity and organ specificity. Recombined cells were predominantly found to form metastases in the lung, while unrecombined cells spread particularly in the peritoneum and the diaphragm. Lymph nodes seem to be equally affected by both cell types. This highlight the significance of different metastatic niches according to the predominant cell type as already proposed in several studies (Reichert et al. 2018; Houg und Bijlsma 2018).

The influence of the immune system seems to be comparable for both routes since the recombination rate did not change significantly between the immunocompetent and immunodeficient mice (in the Fsp1^{mTmG} system). Also, we observed no correlation between the recombination rate of the cell lines pre-implantation and the amount of recombined and unrecombined metastases in the corresponding implanted mouse.

FACS analyses of different compartments showed low recombination rates in the primary tumours, which gradually increased in ascites and even more in the bloodstream. This again emphasises the ability of EMT positive cells to effectively invade and disseminate from the

primary tumour side, however no correlation could be drawn for an increased rate of metastasis formation (Figure 6 B).

6.3 Influence of circulating tumour cells (CTCs) to the metastatic distribution

The most important compartment and way of transportation for tumour cells is the bloodstream to infiltrate distant organs. In order to investigate this compartment and to examine the behaviour of EMT and non EMT cells, we took blood samples of tumour mice (see 2.3.6). These mice had already developed tumours and metastases, indicating a late tumour state, allowing all cell types of the primary tumour to infiltrate the bloodstream. The blood samples were prepared for FACS analysis as described in 2.3.6 and then analysed for tdTomato and EGFP positive cells using a FACS machine.

We found that the amount of tumour cells in the blood samples greatly varied from mouse to mouse. Furthermore, the recombination frequency was different between the samples. In addition to the blood samples, the isolated tumour cell lines were analysed by FACS as well and compared to the respective blood sample. For all analysed cell lines, except one, the percentage of recombined cells in the blood were significantly higher than in the corresponding tumour. Even tumours with a close to 0% recombination rate in the primary tumour cell line, showed varying amounts of recombined cells in the blood compartment (Figure 6 B). Taken together, more recombined cells were present in the blood which supports the hypothesis that cells which underwent EMT have an increased cell motility and infiltration efficiency.

Secondly, we wanted to know if the number of CTCs had any influence on the amount, distribution, or frequency of certain metastases. So, we correlated the amount of total, recombined, and non-recombined CTCs to the total, recombined and non-recombined metastases of each individual mouse. We could not observe any correlation in neither of these variables in any combination (Figure 6 A). This supports recent data showing that CTCs do not predict metastases outcome in patient with pancreatic tumour and also explains the discrepancy of the increased number of recombined CTCs, but the lack of recombined metastases.

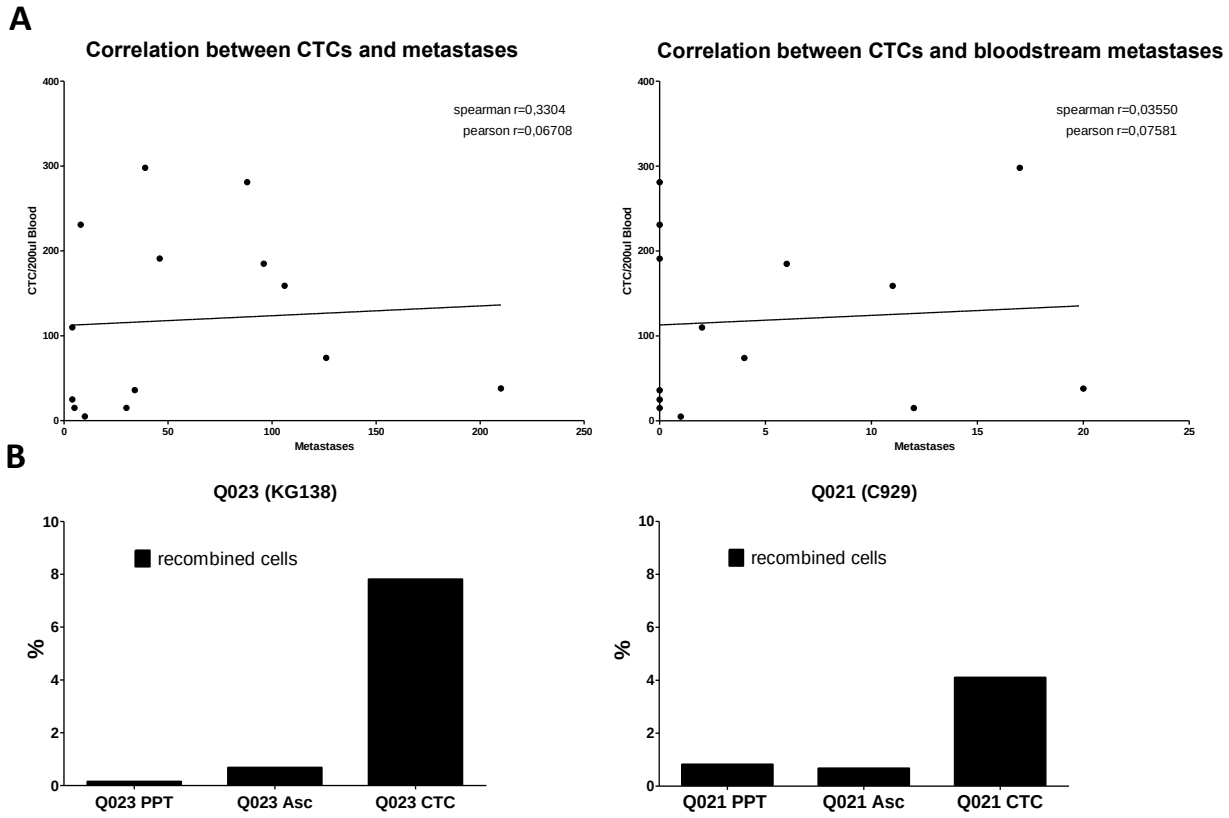

Figure 6 Correlation between CTCs and metastases and recombination frequency in PPT, ascites and blood samples

(A) Analyses show the correlation between the total amount of CTCs per 200ul blood and the total amount of metastases and bloodstream metastases (liver/lung). The pearson and spearman r are indicating no linear correlation between CTCs and metastases frequency

(B) Representative analyses of implanted Fsp1^{mTmG} SCID mice are showing the percentage of recombined cells (aquired by FACS analysis) in the primary pancreatic tumour (PPT), ascites and blood samples. Note that the amount of recombined cells is significantly increased in the blood compartment compared to the PPT

6.4 Validation of the Fsp1-Cre reporter system

Fsp1 was already used in multiple analyses as a gatekeeper for EMT (Xue et al. 2003; Chen et al. 2018) and the *mTmG* system was shown to reliable determine changes in Cre expression *in vivo* and *in vitro* (Muzumdar et al. 2007). An extensive immunofluorescence analysis for different EMT markers was performed to determine the phenotypes of recombined and non-recombined tumours cells in the primary tumour and in different metastatic tissue. To exclude non tumour cells from the analysis, we only used tissue from implanted immunodeficient mice. All tissue was stained, imaged, and analysed according to 2.2.4-6. For the phenotype analysis we used Fsp1, Zeb1, and E-Cadherin as representative EMT markers for different systems affected by the cell differentiation due to EMT.

6.4.1 Phenotype analysis of Fsp1^{mTmG} tdTomato positive cells shows consistent epithelial properties in PPT and metastases

Figure 9 A1-C1 (red) shows the result of the cell count in primary tumour tissue for non-recombined cells for E-Cadherin, Zeb1, and Fsp1. The analysis was done using 6 different primary tumours, from 3 different cell lines. A total amount of over 2000 cells were counted for each individual category. 95% of the unrecombined cells were negative for Zeb1 and Fsp1 and positive for E-Cadherin in nearly 90% of the cases. The amount of partially/uncertain positive/negative results was around 10% for E-cadherin, below 5% in Zeb1 and just around 1% for Fsp1.

The respectively results for tumour cells in different metastatic sides are shown in Figure 9 A2-C2. The following metastatic sides were evaluated: liver, lung, lymph nodes, peritoneum, and diaphragm. In total sections from 16 different metastases were evaluated. The results for each category mimic the results within the PPT. The percentage of negative cells were 93,2% for Zeb1 and 97,0% for Fsp1, and 89,5% were positive for E-Cadherin. The amount of partially/uncertain positive/negative results was around 9% for E-Cadherin, 5,1% for Zeb1 and 1,95% for Fsp1. We could not observe any significant differences in the cellular fluorescence pattern in any of the three markers between the metastatic and pancreatic tumour cells, suggesting that there is no significant shift in cellular properties regarding EMT-status during the whole process of metastases formation for unrecombined cells. This is not only true for the cumulated data from all metastases but also for each individual metastatic side compared to the PPT (Table 16), apart from the results in unrecombined lung metastases. Here, we found a significantly higher amount of only partially E-Cadherin positive (16,3%) and complete negative cells (5,1%) than in the PPT. Representative immunofluorescence images of recombined PPT and metastatic cell for all three markers can be seen in Figure 7 A-C and Figure 8 A-C respectively. In summary the non-recombined cells showed overall consistent epithelial properties in all tested markers. The amount of cells with clear mesenchymal properties were below 1% in primary pancreatic tumours and below 2% in metastatic cells. We concluded from these data that our Fsp1^{mTmG} system succeeded in labelling tumour cells with epithelial phenotype consistently with tdTomato with only a small margin of escapers (<3%).

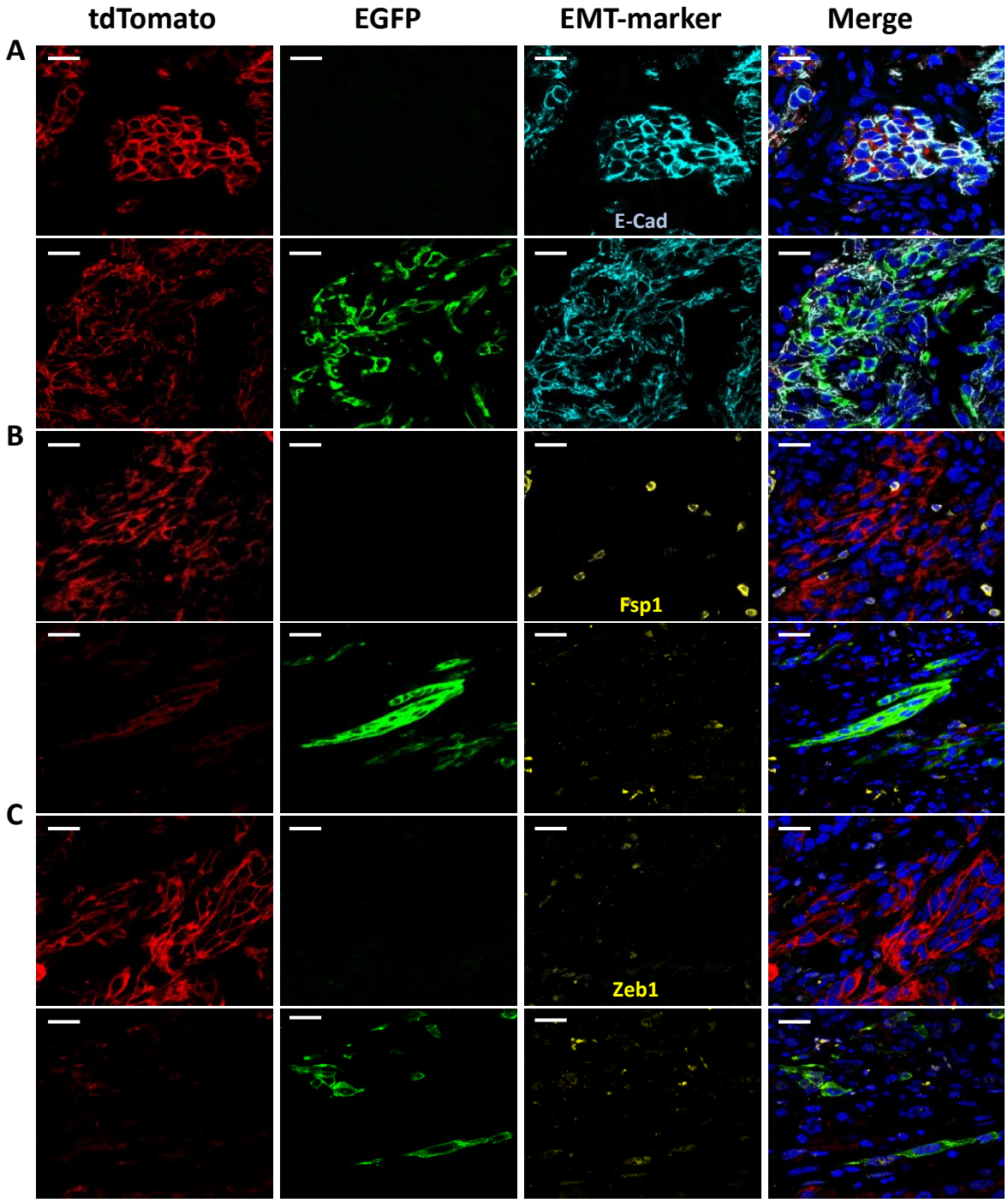

Figure 7 Confocal images of Fsp1^{mTmG} implanted SCID PPT sections, red tdtomato, green EGFP, blue DAPI,

(A) E-Cadherin staining shows E-Cadherin positivity for non-recombined (top) and positive, partial, and negative stainings for recombined cells (bottom); cyan E-Cadherin, scale bar is 20um

(B) Fsp1 staining shows Fsp1 negativity for non-recombined (top) and positive, partial, and negative stainings for recombined cells (bottom); yellow Fsp1, scale bar is 20um

(C) Zeb1 staining shows Zeb1 negativity for non-recombined (top) and positive, partial, and negative stainings for recombined cells (bottom); yellow Zeb1, scale bar is 20um

Of note, this analysis also confirmed the consistent epithelial phenotype of all non-recombined metastases in all mouse models and further supports the assumption that non EMT-dependant routes for invasion, dissemination, and metastases could play an important role in pancreatic cancer.

6.4.2 Phenotype analysis of Fsp1^{mTmG} recombined cells shows EMT and non-EMT properties in PPT and metastases

In Figure 9 A1-C1 (green) is the analysis of recombined cells for E-Cadherin, Zeb1 and Fsp1 in primary tumour depicted. 6 different primary tumours and 3 different primary murine PDAC cell lines were used for the analysis. Recombined cell showed distinctly different properties as unrecombined cells. The population of the recombined cells seems to be divided into three different subpopulations: First, we have cells which show the same properties as unrecombined tumour cells: E-cadherin positivity (49,28%), Zeb1 and Fsp1 negativity (48% and 85,16%). On the other hand, we have in contrast to the unrecombined cells a subpopulation of cells which are E-cadherin negative (26,09%), Zeb1 positive (20%) and partially Fsp1 positive (14.06%), giving them clear mesenchymal properties. Also, the amount of partial positive/negative cells for E-Cadherin (24,64%) and Zeb1 (32%) greatly increased compared to the unrecombined cells, possibly marking the transition from an epithelial to a mesenchymal phenotype, showing the transient nature of EMT.

Knowing the fluid process of EMT, partial EMT, and MET (see 1.2.1) these three population represent the different stages of a cells' transition between epithelial to mesenchymal and back. Depending on the exact moment in which a cell was captured by the immunofluorescence assay we would therefore expect the exact spectrum of phenotypes we could observe in the Fsp1^{mTmG} reporter system. Cells which have underwent the complete process from activation of EMT and MET show no differences in cell properties as non-EMT cells, however the activation of the Cre recombinase led to a permanent change from a tdTomato to an EGFP signal. While mesenchymal cells will show complete loss of E-Cadherin and more or less high levels of Zeb1 and Fsp1, cells on the brink of EMT or during the EMT process will show partially or complete changes in Zeb1, Fsp1 and E-cadherin expression. Those states could also represent states of partial EMT, where the EMT program is not fully executed. Note that there is a discrepancy between E-Cadherin negativity and Zeb1 positivity in this analysis.

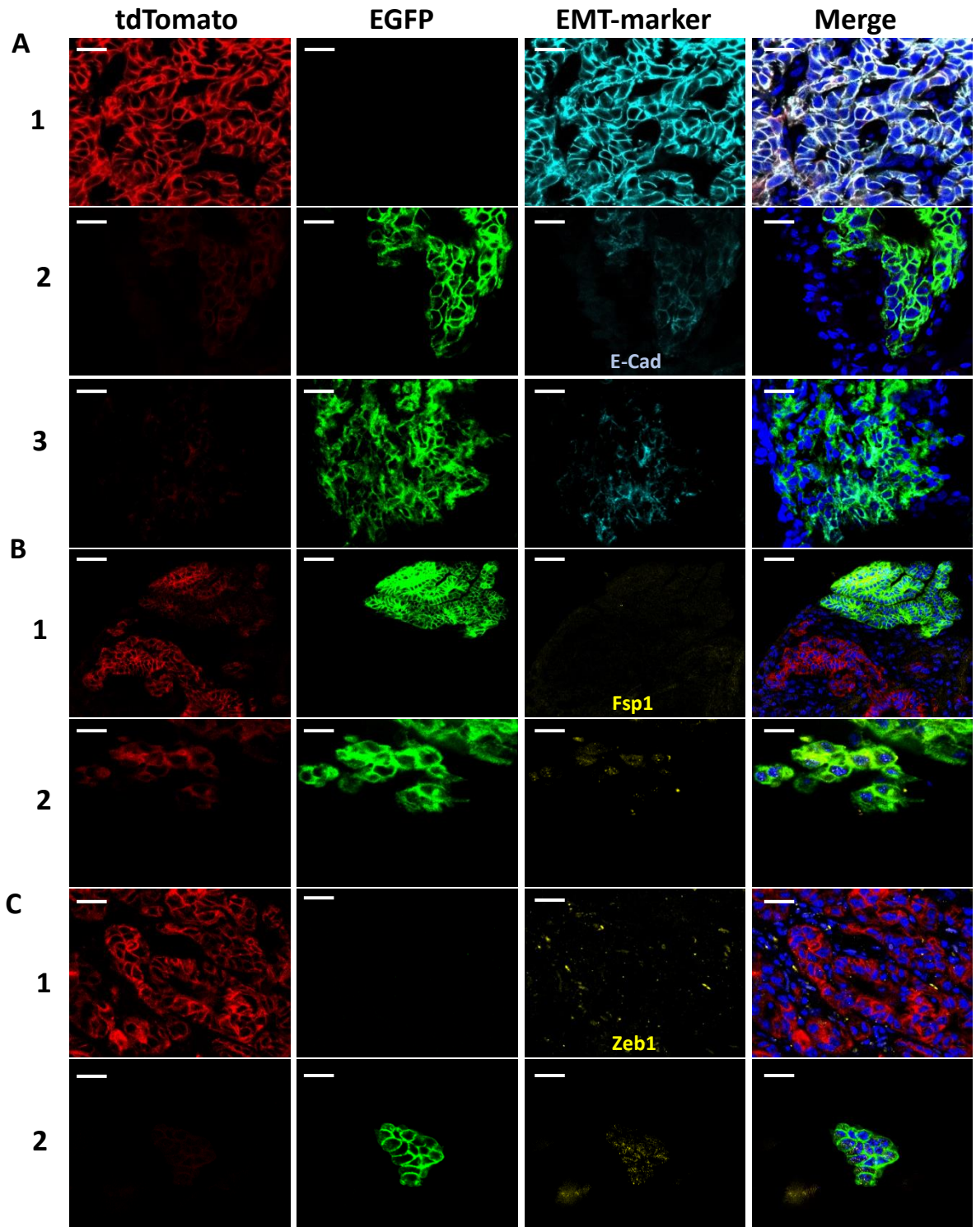

Figure 8 Confocal images of Fsp1^{mTmG} implanted SCID metastases sections, red tdtomato, green EGFP, blue DAPI

*(*A) E-Cadherin staining shows E-Cadherin positivity for non-recombined cells (top) and positive, partial, and negative stainings for recombined cells (bottom two); (1) diaphragm; (2) peritoneum; (3) lymph node metastasis; cyan E-Cadherin, scale bar is 20um

(B) Fsp1 staining shows Fsp1 negativity for non-recombined and recombined cells (top) and positive, partial, and negative stainings for recombined cells (bottom); (1) peritoneum; (2) lymph node metastasis; yellow Fsp1, scale bar is 20um for (2) and 40um for (1)

(C) Zeb1 staining shows Zeb1 negativity for non-recombined (top) and positive stainings for recombined cells (bottom); (1) lymph node; (2) peritoneum metastasis; yellow Zeb1, scale bar is 20um

In total the Fsp1^{mTmG} reporter system is capable of depicting the complete spectrum of EMT and also labels cells with EGFP even after the loss of Fsp1 gene expression and possibly reverting to an epithelial morphology.

The respective results for tumour cells in different metastatic sides are shown in Figure 9 A2-C2 (green). The following metastatic sides were evaluated: liver, lung, lymphnodes, peritoneum, and diaphragm. In total 16 different metastases from 2 different cell lines were evaluated. The results from the metastatic sides correspond well with those from the PPT. Here as well three subpopulations exist, however the distribution of the three markers is different. In contrast to the PPT, E-Cadherin level is greatly decreased (45,90% vs. 26,09% negativity) and Zeb1 levels are lower (12,89% vs. 20,0% positivity), while Fsp1 expression is significantly higher (5,93% positivity). Still partial positive/negative cells account for a significant amount of all cells (25,6% for E-Cadherin, 20,9% for Zeb1 and 8,15 for Fsp1).

These findings correlate well with the common EMT-MET theory for metastasis. Cells, which were able to infiltrate, disseminate, and metastasize by utilisation of the EMT program will certainly have activated the EMT pathways just right before becoming invasive, in contrast to recombined cells in the PPT, which could have activated the EMT program at any time from implantation to dissection. Therefore, the number of cells showing mesenchymal properties should be higher in the metastasis`s cohort. According to the theory in the last step of metastases formation (during the formation of macroscopic lesions) the disseminated cells are no longer dependent on the maintenance of the EMT program but regain their epithelial properties through MET. The mechanisms that trigger MET and the precise pathways are not completely revealed yet, but this data suggests that repression of EMT-TF (i.e Zeb1) precede the activation of certain regulatory pathways that reinduce the repressed key effector proteins like E-Cadherin. This is also a possible explanation for the missing overlap of E-Cadherin negativity and Zeb1 positivity in the recombined cell population. Independently of this E-Cadherin might also be only reexpressed at a proper level after the formation of macroscopic lesion and not at the level of micrometastasis, which have accounted for a great part of this evaluation, while Zeb1 levels are already decreasing in this state. Also, Fsp1 activation seems to be more necessary for the initiation than the overall maintenance of a mesenchymal state, given the low overall percentage of Fsp1 positivity in mesenchymal cells in metastatic sides.

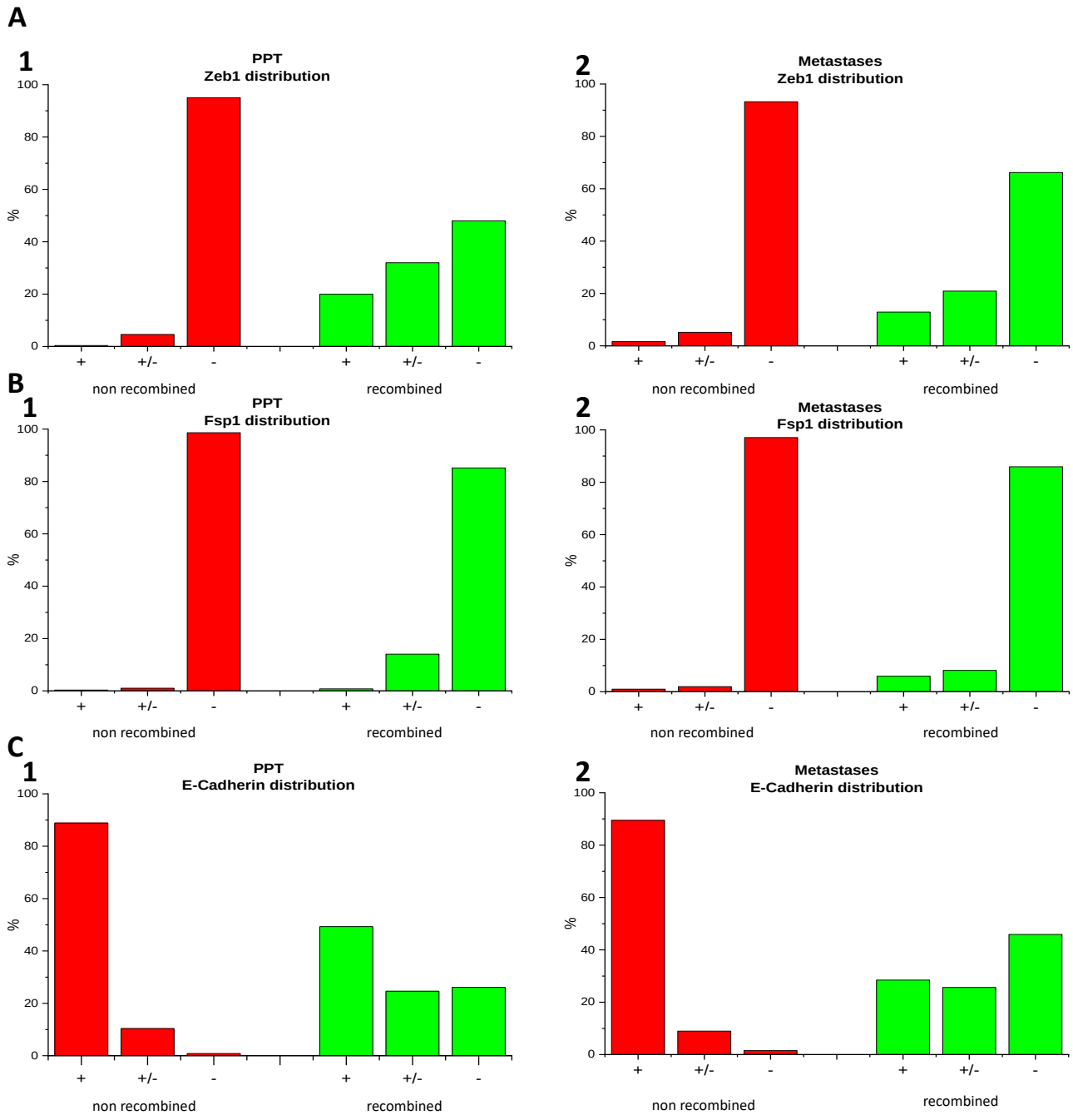

Figure 9 Quantification of the immunofluorescence distribution in Fsp1^{mTmG} implanted SCID mice for Zeb1, Fsp1 and E-Cadherin in PPT and metastatic tissue for recombined and non-recombined cells

(A) These analyses show the amount of positive, negative, and partially postive/negative Zeb1 cells in the fluorescence analysis of implanted Fsp1^{mTmG} SCID mice in PPT (1) and different metastatic tissue (2)

(B) These analyses show the amount of positive, negative, and partially postive/negative Fsp1 cells in the fluorescence analysis of implanted Fsp1^{mTmG} SCID mice in PPT (1) and different metastatic tissue (2)

(C) These analyses show the amount of positive, negative and partially postive/negative E-Cadherin cells in the fluorescence analysis of implanted Fsp1^{mTmG} SCID mice in PPT (1) and different metastatic tissue (2)

Table 16. Fluorescence distribution (in%) of Fsp1^{mTmG} cells in PPT and metastatic tissue

Primary pancreatic tumour							
	non recombined				recombined		
	+	+/-	-		+	+/-	-
Fsp1	0,34	1,05	98,62		0,78	14,06	85,16
Zeb1	0,37	4,59	95,04		20,0	32,0	48,0
E-Cadherin	88,85	10,35	0,80		49,28	24,64	26,09
Metastases E-Cadherin							
	non recombined				recombined		
	+	+/-	-		+	+/-	-
Lung	78,57	16,33	5,1		-	-	-
Liver	86,68	11,49	1,83		25,0	75,0	0
Lymph nodes	89,04	8,91	2,06		29,78	9,93	60,29
Peritoneum	86,27	10,65	3,08		7,38	19,19	73,42
Diaphragm	92,53	7,42	0,05		45,93	44,63	9,45
Absolute	89,52	8,97	1,51		28,45	25,64	45,90
Metastases Zeb1							
	non recombined				recombined		
	+	+/-	-		+	+/-	-
Lung	2,38	1,19	96,43		-	-	-
Liver	0,78	5,06	94,16		0	20,0	80,0
Lymph nodes	2,04	4,25	93,72		87,5	0	12,5
Peritoneum	0,93	8,02	91,05		10,63%	21,74	67,63
Diaphragm	-	-	-		-	-	-
Absolute	1,62	5,15	93,23		12,89	20,89	66,22
Metastases Fsp1							
	non recombined				recombined		
	+	+/-	-		+	+/-	-
Lung	-	-	-		-	-	-
Liver	1,12	3,61	95,27		0	10,0	90,0
Lymph nodes	1,06	1,21	97,73		35,8%	20,75	43,40
Peritoneum	0,27	2,52	97,20		0,30	6,23	93,47
Diaphragm	2,07	3,00	94,93		9,23	7,69	83,08
Absolute	0,99	1,95	97,06		5,93	8,15	85,93

Interestingly, while the phenotype of non-recombined cells was stable in all three marker systems in nearly all metastatic sides (apart from E-Cadherin in lung metastases) we could observe that recombined metastases showed distinct properties in different metastatic sides (Table 16). E.g. lymph node metastases showed significantly higher levels of Fsp1 (35,85%) and Zeb1 (87,5%) positivity, with overall low E-Cadherin levels (60,29% negativity),

potentially marking them as early stage EMT metastases. Whereas recombined liver metastases showed mostly a regained epithelial phenotype. However, considering the overall low number of recombined cells in certain metastatic sides compared to unrecombined cells, we should conduct further studies to obtain more data and insight on the behaviour of recombined (EMT) cells in different metastatic niches. Representative immunofluorescence images of recombined PPT and metastatic cell for all three markers can be seen in Figure 7 A-C and Figure 8 A-C respectively.

In total, the only significant number of mesenchymal cells in the whole immunofluorescence analysis could be found in recombined cells. Since epithelial cells can only acquire these properties through the activation of the EMT program we therefore concluded, that our Fsp1^{mTmG} system successfully labels EMT cells, even after the reactivation of the MET program and is able to portray the whole spectrum of the cellular changes during the EMT cascade.

6.4.3 Phenotype analysis of recombined Fsp1$^{Ai\text{-}65\text{-}tdTom}$ cells shows EMT and non-EMT properties in PPT and metastases

To investigate the comparability of the two fluorescence reporter systems we performed an immunofluorescence analysis of the recombined cells in the Fsp1$^{Ai\text{-}65\text{-}tdTom}$ system. Due to the configuration of the *Ai-65-tdTom* reporter (Figure 1 A) we could not include an analysis of the unrecombined cells as those are not labelled.

The analysis of primary tumour tissue for recombined cells is shown in Figure 11 A1-C1 for E-Cadherin, Zeb1, and Fsp1 positivity levels. The analysis was done with tissue from 3 different primary tumours all originating from one cell lines. Similar to the Fsp1^{mTmG} system we could observe three different cell populations, one with epithelial, one with mesenchymal properties, and one with mixed properties. We could observe lower E-Cadherin (45,54% negative) but higher Zeb1 (24,97% positive) and Fsp1 levels (12,78% positive) in the mesenchymal population compared to the Fsp1^{mTmG} system. Clear epithelial properties were shown in 33,55% (E-Cadherin positivity), 54,60% (Zeb1 negativity) and 71,66% (Fsp1 negativity) of all cells. Partially positive/negative cells could still be found in around 20% for E-Cadherin and Zeb1 and in about 15% of the cases for Fsp1.

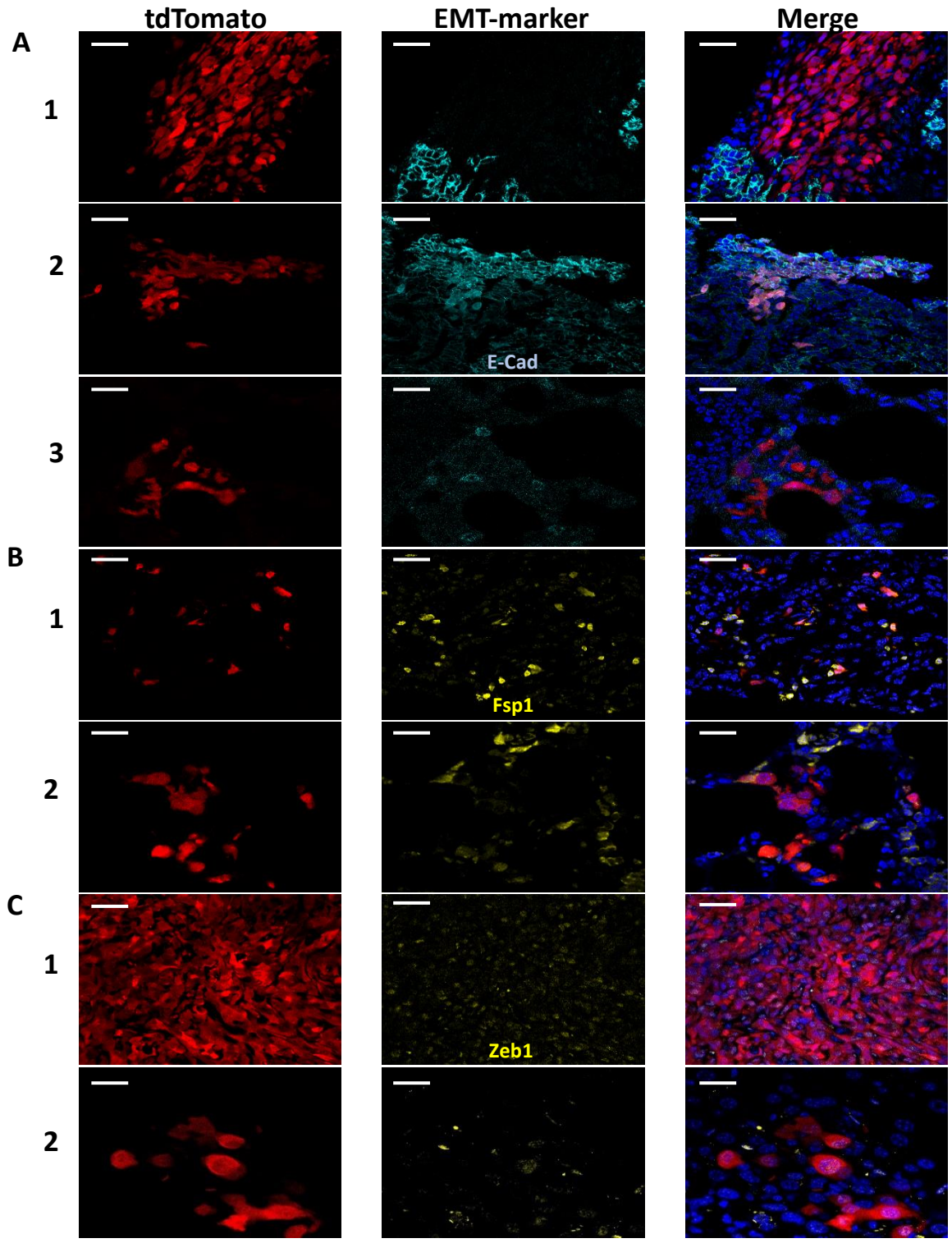

Figure 10 Confocal images of Fsp1$^{Ai\text{-}65\text{-}tdTom}$ implanted SCID PPT and metastases sections, red tdtomato, blue DAPI

(A) E-Cadherin staining shows E-Cadherin positive, partial, and negative stainings for recombined cells in PPT and metastases (1,2) PPT; (3) lung metastasis; cyan E-Cadherin, scale bar is 40um

(B) Fsp1 staining shows positive, partial, and negative stainings for recombined cells in PPT and metastases; (1) PPT; (2) lung metastasis; yellow Fsp1, scale bar is 40um for (1) and 20um for (2)

(C) Zeb1 staining shows Zeb1 positive, partial and negative stainings for recombined cells; (1) PPT; (2) liver metastasis; yellow Zeb1, scale bar is 40um for (1) and 20um for (2)

The respective results for tumour cells in different metastatic sides are shown in Figure 11 A2-C2. In total three different metastases from one cell lines were evaluated. The analysis concentrated on the most crucial metastases for human: liver and lung. Here we could confirm the findings of the PPT cells, but the mesenchymal markers were significantly higher in the metastatic sides (E-cadherin 82,44% negative, Zeb1 36,18% positive, Fsp1 26,90% positive). Comparing these two crucial metastases we could find that even though E-Cadherin level were strikingly low in both organs (90,77% for liver vs. 79,70% in lung (Table 17) the expression of Fsp1 and Zeb1 greatly dispersed. While recombined liver metastases showed repressed levels of Fsp1 (12,66%) and even less Zeb1 (4,40%), lung metastases were still maintaining significant high degrees of these EMT markers (around 36% for both (Table 17)). This might give some insight on the different metastatic niches and the necessity of maintaining mesenchymal properties in different microenvironments. This also contributes to the above-mentioned organ specificity of the EMT dependant metastasis. Representative immunofluorescence images of recombined PPT and metastatic cell for all three markers can be seen in Figure 10A-C.

Recombined cells in the $Fsp1^{Ai\text{-}65\text{-}tdTom}$ system showed the same fluorescence distribution as recombined $EGFP^{+}$ cells in the $Fsp1^{mTmG}$ reporter system with even higher levels of mesenchymal markers in both primary tumour and metastases. We therefore concluded that the $Fsp1^{Ai\text{-}65\text{-}tdTom}$ system is equally capable of successfully labelling EMT and MET cells in PPT and metastatic tissue. This now enables a comparability between the two systems in findings on EMT positive cells. However, cells with a preserved epithelial phenotype, which do not employ the EMT program during their life span evade labelling in this reporter system. Nevertheless, given the effectivity of the Fsp1-Cre recombinase in selectively labelling all EMT^{+} cells as shown in the $Fsp1^{mTmG}$ reporter system, it is reasonable to assume that tdTomato negative tumour cells in the Ai-65-tdTom system display the same epithelial properties as unrecombined cells in the mTmG reporter system.

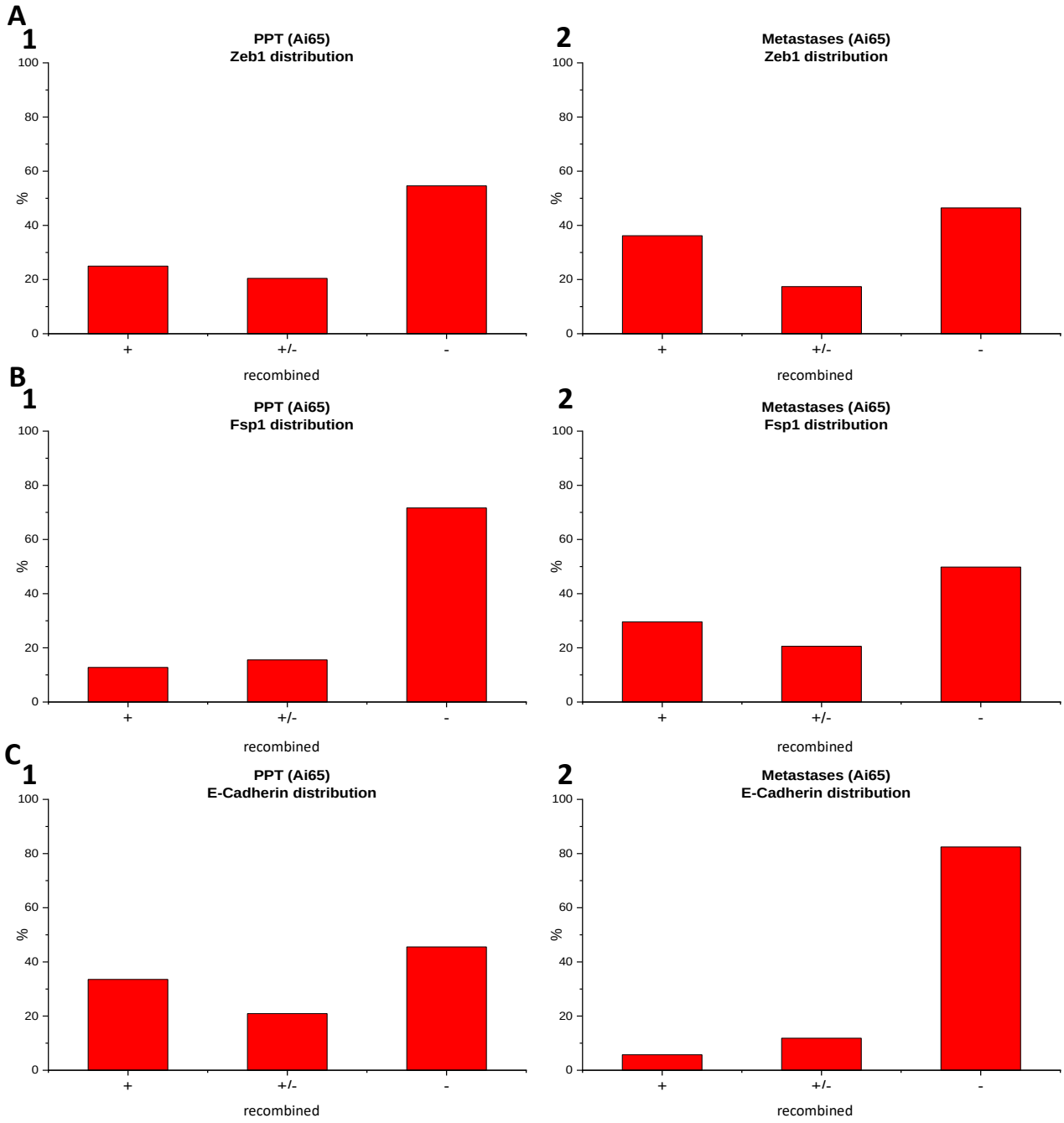

Figure 11 Quantification of the immunofluorescence distribution in Fsp1^{Ai65} implanted SCID mice for Zeb1, Fsp1 and E-Cadherin in PPT and metastatic tissue for recombined cells

(A) These analyses show the amount of positive, negative and partially postive/negative Zeb1 cells in the fluorescence analysis of implanted Fsp1^{mTmG} SCID mice in PPT (1) and different metastatic tissue (2)

(B) These analyses show the amount of positive, negative and partially postive/negative Fsp1 cells in the fluorescence analysis of implanted Fsp1^{mTmG} SCID mice in PPT (1) and different metastatic tissue (2)

(C) These analyses show the amount of positive, negative and partially postive/negative E-Cadherin cells in the fluorescence analysis of implanted Fsp1^{mTmG} SCID mice in PPT (1) and different metastatic tissue (2)

Table 17 Fluorescence distribution (in%) of Fsp1$^{Ai\text{-}65\text{-}tdTom}$ cells in PPT and metastatic tissue

Primary pancreatic tumour			
	recombined		
	+	+/-	-
Fsp1	12,78	15,56	71,66
Zeb1	24,97	20,44	54,60
E-Cadherin	33,55	20,92	45,54
Metastases E-Cadherin			
	recombined		
	+	+/-	-
Lung	6,6	13,71	79,70
Liver	3,08	6,15	90,77
Absolute	5,73	11,83	82,44
Metastases Zeb1			
	recombined		
	+	+/-	-
Lung	62,50	19,27	18,23
Liver	4,4	15,09	80,5
Absolute	36,18	17,38	46,44
Metastases Fsp1			
	recombined		
	+	+/-	-
Lung	36,36	24,24	39,39
Liver	12,66	11,39	75,95
Absolute	29,60	20,58	49,82

6.4.4 Efficiency of the reporter systems

After evaluating all the data presented above, we came to the following conclusions: the Fsp1^{mTmG} system is capable of labelling epithelial cells reliable, repetitive and with high efficiency (>90% for all three markers) with tdTomato in PPT and all kind of metastases and the rate of escaper cells (cells with positive mesenchymal markers) is satisfactorily low (<3% in PPT, <2% in metastases). Moreover, recombined cells show the complete spectrum of cell phenotypes from epithelial, over partially epithelial/mesenchymal to complete mesenchymal cell structure. Therefore, all steps of the EMT/MET process can be monitored by the recombination. Additionally, the labelling properties of the Fsp1$^{Ai\text{-}65\text{-}tdTom}$ system mirrors the findings in the Fsp1^{mTmG} system, therefore excluding significant reporter specific effects.

6.5 TGF-ß treatment induces cell differentiation *in vitro*

TGF-ß is known to be one important inducer of EMT *in vivo and vitro* (Xu et al. 2009; Lamouille et al. 2014; Zavadil und Böttinger 2005). In order to observe the behaviour of our reporter system *in vitro* we treated Fsp1^{mTmG} and Fsp1$^{Ai\text{-}65\text{-}tdTom}$ PPT cells with recombinant TGF-ß as described in 2.1.4. As internal controls we also treated *Pdx1-Flp; FSF-KrasG12D* PPT cells and cells which harbouring additionally either a hetero- or homozygous knock-out of the TGF-ß receptor type II (*BIIR +/- and BIIR +/+*). Every cell line was treated once with, once without TGF-ß medium.

Microscopic images and immunofluorescence are shown in Figure 12. After three days of treatment all cell lines apart from homozygous TGF-ß receptor type II knock-out, differentiated from an epithelial cluster like pattern to a fusiform, single cell, mesenchymal one (Figure 13 B). Surprisingly the immunofluorescence analysis could not demonstrate any significant increase in the recombination frequency, which would have correlated with the cell differentiation. Since Fsp1 is not the primary target of the TGF-ß pathway and is only activated as a second line protein after activation of the major EMT transcription factors, we expanded the treatment period from 3 to 7 days. However, seven days in FCS starved medium condition had a major impact on the cell viability and thus impaired the possibility of further analyses.

In conclusion, we could determine that TGF-ß successfully induces cell differentiation *in vitro*, but without any quantifiable effect on the recombination rate in our reporter system after 3 days. Longer treatment periods crucially decreased cell viability and therefore prevented further analyses. Overall, this experiment showed us that, even though the Fsp1^{mTmG} system successfully labels EMT events *in vivo* as shown above, it might possess a significant latency in order to do so *in vitro* and therefore probably *in vivo,* too. Moreover, further approaches should be made to determine the reaction latency of the reporter system *in vitro*.

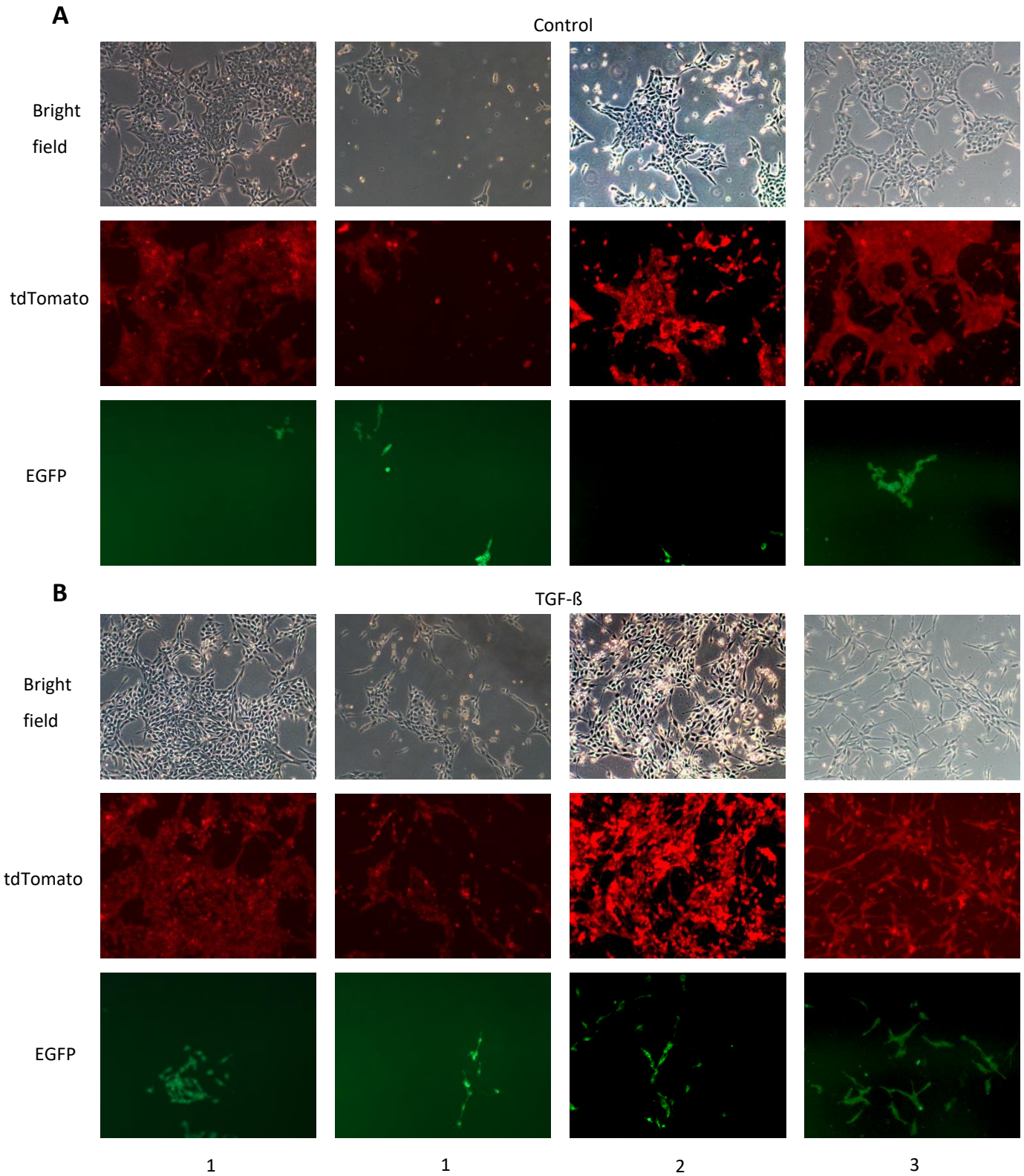

Figure 12 TGF-ß induced cell differentiation and recombination behaviour in vitro in Fsp1^{mTmG} PPT tissue

(A) Cell culture and fluorescence microscope (tdTomato and EGFP) images of Fsp1^{mTmG} PPT cells after 1 to 3 days in FCS starving medium. Representative images shown; n=2 cell lines

(B) Cell culture and fluorescence microscope (tdTomato and EGFP) images of Fsp1^{mTmG} PPT cells after 1 to 3 days in TGF-ß medium. Representative images shown; n=2 cell lines

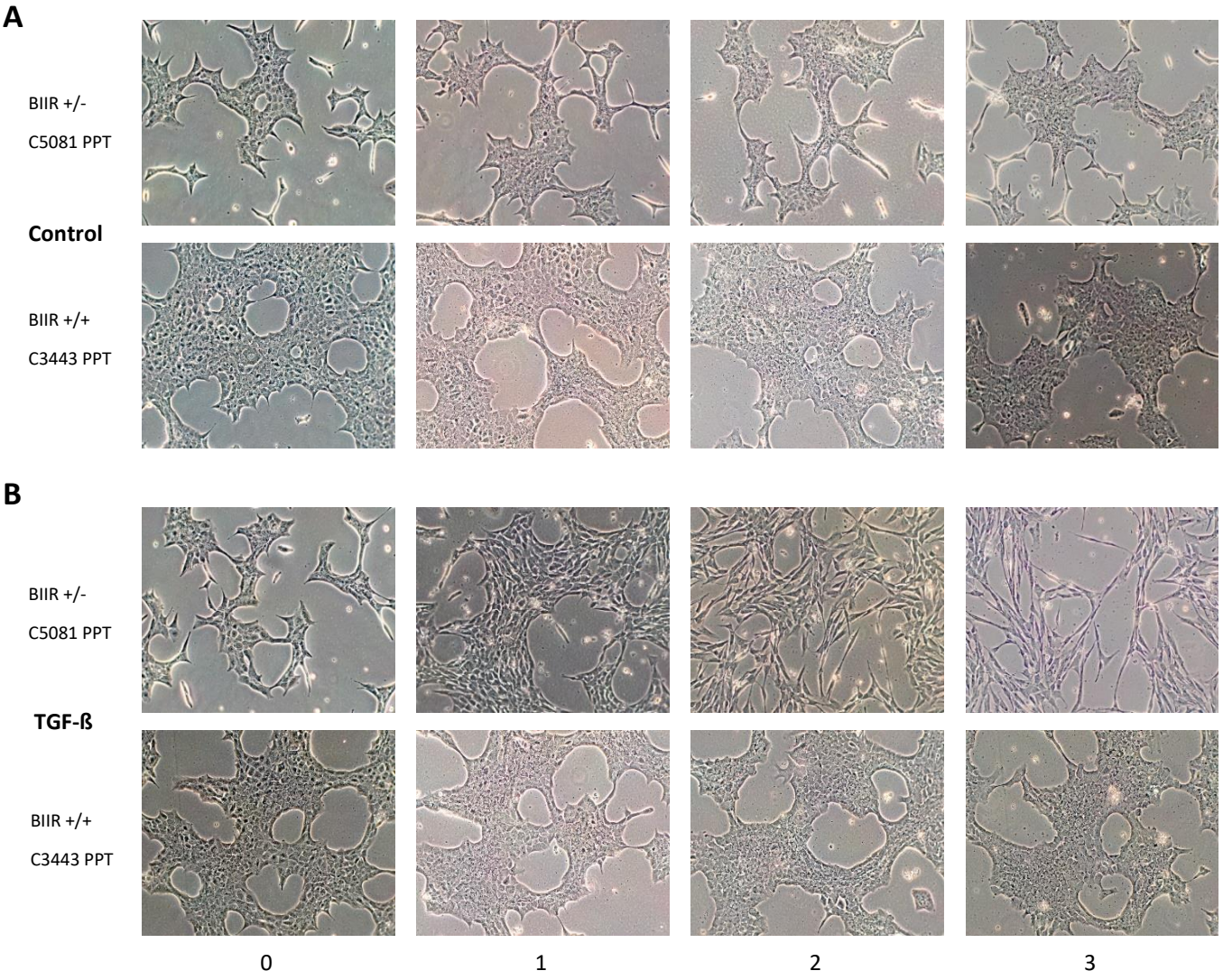

Figure 13 TGF-ß induced cell differentiation in vitro

(A) Cell culture images of Pdx1-Flp; FSF-KrasG12D BIIR +/- (top) and BIIR +/+ (bottom) PPT cells after 0 to 3 days in FCS starving medium. Representative images shown; n=5 cell lines

(B) Cell culture images of Pdx1-Flp; FSF-KrasG12D BIIR +/- (top) and BIIR +/+ (bottom) PPT cells after 0 to 3 days in TGF-ß medium. Representative images shown; n=5 cell lines

6.6 Time dependant development of recombination in the mTmG and Ai-65-tdTom system *in vitro*

Normal PDAC cell medium is known to include certain growth factors (e.g. TGF- ß, PDGF, etc.) which are capable of inducing cell differentiation and EMT *in vitro*. Also, EMT and non-EMT cells are known to differ in important properties like growth rates and cell-cell attachment. Therefore, cell lines with different passages numbers could display different cellular properties and EMT-states than the original pancreatic tumour, leading to a decrease in comparability of these cells. In order to address and quantify this difference *in vitro* we conducted a time-based experiment to determine the change of recombination rate.

Therefore, four cell lines with similar passage numbers, but different initial recombination rate was observed over a total period of 60 days and regularly FACS analysed. The resulting analysis is shown in Figure 14. In total this experiment showed that there is a time dependent change of the recombination rate *in vitro*. However, the trend of the shift seems to be cell line specific. We could observe stable (C929), decreasing (KG138) and increasing (C5197) recombination rates in the different cell lines.

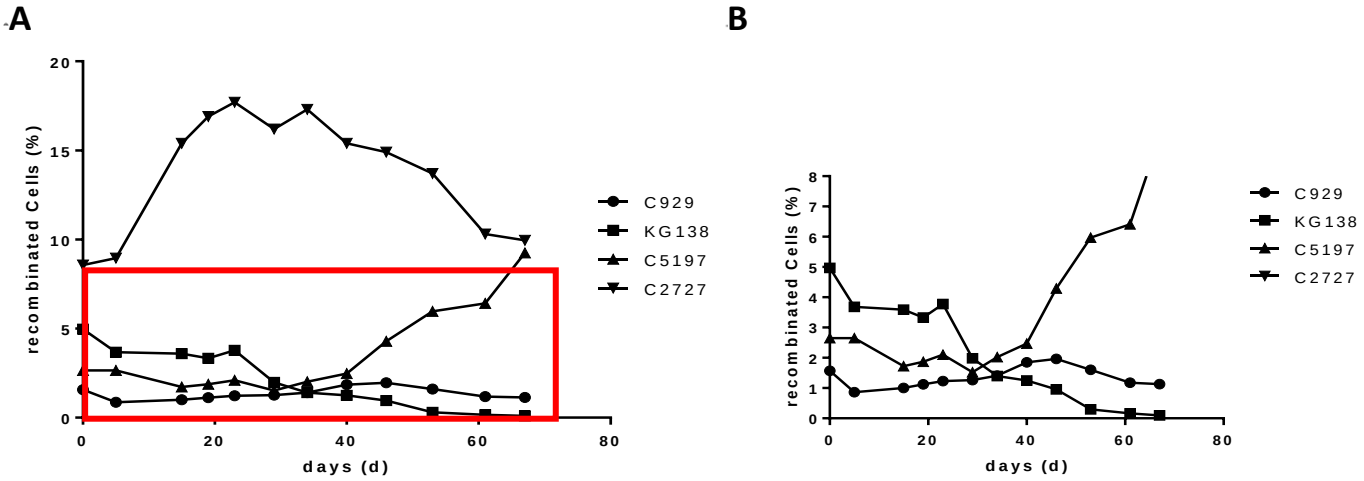

Figure 14 Time dependant development of recombination in the *mTmG* and *Ai-65-tdTom* system in vitro

3 PPT cell lines of the *mTmG* and one PPT cell line of the *Ai-65-tdTom* (C5197) system were monitored in cell culture via FACS analyses for 60 days

(A) Time dependent development of the recombination frequency in different cell lines shows stable, increasing and decreasing values after 60 days

(B) Enhanced image of (A) in red square

7. Discussion and Outlook

EMT or no EMT for metastatic outgrowth?

The fact that the activation of the EMT program enhances the ability of cancer cells for migration, dissemination, intravasation, and invasion has been sufficiently proven *in vitro* for various cancer types in a great variety of setups and identified a large number of possibly involved EMT activators, enhancers etc., whereas the number of key or essential EMT players remains small (Xue et al. 2003; Hartwell et al. 2006; Thiery et al. 2009; Kalluri und Weinberg 2009; Puisieux et al. 2014; Lamouille et al. 2014). For pancreatic cancer, an abundance of studies has been conducted that link certain proteins or marker levels to increased EMT activities and therefore to increased metastasis frequency and decreased overall survival (OS) (Cano et al. 2010). Non-coding RNA strands (ncRNA) (Lv und Huang 2019), COL6A1 (Owusu-Ansah et al. 2019) or fibroblast activation protein α (FAPα) (Wen et al. 2019) are recent and promising targets for EMT activated pancreatic metastazation. These studies usually utilize a genetically engineered mouse model to induce pancreatic cancer and design a new strain which harbours a constantly active form of the gene of interest to observe the effect in vivo, or the gene is directly enhanced by transcriptionally activating via miRNA or certain modified media *in vitro*. However, ubiquitous activation of a universal, unidirectional genetical program that gives cancer cells the properties stated above is expected to be linked to an overall poor outcome. Several of these markers have an additional impact on other crucial cell properties like proliferation rate, chemoresistance or immune evasion (Lv und Huang 2019). The questions that most of these studies fail to address is whether these enhanced levels of EMT activation correctly represent the normal tumour biology and if EMT facilitated metastazation is the predominant route of metastasizing in the physiological development of pancreatic cancer after all. These questions arise from recent findings, specifically regarding metastasis biology. An increasing amount of metastases were found to have a preserved epithelial phenotype and therefore challenge the common EMT theory (Chen et al. 2018; Zheng et al. 2015). Furthermore, sophisticated and generally applicable models to selectively monitor EMT *in vivo* are lacking.

To investigate the role of EMT in pancreatic cancer *in vivo* Zheng et al. generated KPC mice with an additional loss of Snai1 or Twist1, two of the most recognised key EMT-TF (Puisieux et al. 2014). These KPC; Twist1^{KO} and Snai1^{KO} mice were compared to control mice and evaluated in their ability to invade, infiltrate, and form distant metastases. The deletion of either Twist1 or Snai1 did not affect the primary tumour formation or histopathology and only showed

insignificant differences in overall survival compared to KPC control mice. But most interestingly no effect on the metastatic burden was found. The number of CTCs remained unchanged and no significant change in liver, lung, and spleen metastases could be observed. They concluded that metastases occur despite the significant loss of EMT capabilities and considered EMT dispensable for metastasis. However, they could find a significant contribution to chemoresistance (Zheng et al. 2015). In a different study, investigating the effect of EMT on breast cancer lung metastases, similar results were shown. Suppression of Zeb1/2, Snail1/2, and Twist via overexpression of the well-recognized EMT-inhibitor miR-200 (Gregory et al. 2008) did not significantly reduce lung metastases after orthotopic implantation. Moreover, they utilized a dual fluorescence-based lineage tracing system under the control of Fsp1-Cre to identify EMT status in metastatic cells and confirmed that lung metastases derive from non-EMT tumour cells, using a similar evaluation system as shown in $Fsp1^{mTmG}$ and $Fsp1^{Ai\text{-}65}$ mice. However, upon chemotherapy with cyclophosphamide (CTX) the majority of surviving cancer cells were EMT-positive with a preserved mesenchymal phenotype, which were able to form recurrent lung metastasis after treatment. This did not occur during simultaneous overexpression of miR-200 (Fischer et al. 2015). Therefore, EMT-independent routes to metastases might exist in various tumour entities, but EMT might still have important implications on other crucial tumour features apart from metastazation.

Krebs et al. utilized the third major EMT-TF Zeb1 and created a genetical knock out model in similar fashion. In contrast to Zheng et al they observed a significant decrease in overall metastases, especially in the formation, not colonisation, of lung metastases. Zeb1 loss reduced the metastatic competence to approximately 30% but failed to suppress metastases in general in 50% of the mice. It also strongly affected tumour differentiation with a shift to higher differentiated tumours. Krebs et al. therefore stated non redundant tissue specific subfunctions of the crucial EMT-TFs and uphold the role of EMT in pancreatic cancer (Krebs et al. 2017). As a follow up to this Chen et al. established a dual fluorescence reporter lineage tracing mouse model to identify EMT independent metastasis programs *in vivo*. Under the control of either aSMA-Cre or Fsp1-Cre a permanent fluorescence shift in EMT activated cells can be observed in mice that develop spontaneous pancreatic ductal adenocarcinomas. They found two distinct and mutually exclusive forms of metastazation. While EMT-positive cells disseminate and colonize based on single cells and micro metastases, cells with a preserved epithelial phenotype nearly exclusively made up the whole fraction of established macroscopic metastatic nodules. Similar to my findings metastases with a preserved epithelial phenotype clearly outnumbered

EMT positive metastases, not only in size but also in total numbers. Size differences could possibly be due to proliferation advantages of non-EMT cells. These findings now further support the claim that EMT-independent routes to metastasis exist and make up a significant proportion of metastases in unaffected pancreatic cancer development (Chen et al. 2018).

My work now uses Zeb1, Fsp1, and E-Cadherin as a marker for EMT in pancreatic cancer cells and utilizes a similar dual recombinase, dual fluorescent reporter system under the control of Fsp1-Cre as *in vivo* lineage tracing for EMT events as Chen et al. My results highlight the coexistence of both EMT and non EMT programs in the formation of metastases. Which program is dominantly utilized for the majority of metastasis seems to be significantly cell line (or primary tumour) specific. However, the only large proportion of lung metastases were EMT positive, which backs the findings of Krebs et al. on organ specific EMT dependency. This also gives insights on the organotropism of EMT and non EMT-cells which should be considered when addressing metastases in a clinical manner.

That epithelial plasticity and EMT-status critically affect the metastatic pattern was recently evaluated (Aiello et al. 2018). Reichert et al. showed that biallelic loss of p120catenin (p120ctn) prevented liver metastases but had no effect on lung metastases in a pancreatic cancer mouse model. P120ctn is the binding partner of E-Cadherin and responsible for stabilizing it at the membranous surface, therefore playing an important role in acquiring and maintaining an epithelial phenotype. Complete loss of p120ctn and therefore the loss of epithelial integrity restricted the capability of pancreatic cancer cells to form liver metastases dramatically. However, lung metastases were not affected, indicating an organotropism of mesenchymal cells to the lung. This is in line with my findings that the majority of lung metastases were EMT positive, and the cells lacked E-Cadherin. In contrast liver metastases mostly derived from EMT negative cancer cells and had a preserved epithelial phenotype. They concluded that these epithelial properties seem to be essential for liver metastazation (Reichert et al. 2018). Further studies on this matter are required to determine whether this phenotype is acquired via MET or if the metastatic cells preserved their epithelial properties and did not undergo EMT in the first place which is supported by the results of this study.

Fsp1 and EMT in pancreatic cancer

Even though the physiological role of Fsp-1 is not fully understood yet, its contribution to metastases and EMT in various tumour entities has been extensively studied (Boye und Maelandsmo 2010; Mishra et al. 2012; Fei et al. 2017). Fsp1 promotes an invasive phenotype

and increase metastasis ratios in a great variety of cancers (Schmidt-Hansen et al. 2004; Mishra et al. 2012). Several other functions have been associated with Fsp1, including increased chemoresistance, immune evasion, and stem-cell properties (Chen et al. 2014; Che et al. 2015). Some of these properties are the results of an enhanced EMT activity in cells, some functions might be EMT-independent effects of Fsp1 (Orre et al. 2013). Activation of the major EMT-TFs as well as common EMT-pathways regularly upregulate Fsp1 levels (Boye und Maelandsmo 2010). Therefore, Fsp1 has been stated to be a gatekeeper for monitoring EMT activation (Xue et al. 2003) *in vivo* and *in vitro*. In pancreatic cancer Fsp1 is the predominant marker for capturing EMT events (Rhim et al. 2012). Increased levels of Fsp1 are also an independent biomarker for shorter overall survival (Fei et al. 2017), increased aggressiveness, and dedifferentiation (Jia et al. 2019). Fsp1 is readily found in pancreatic stroma cells, fibroblasts, or immune cells (Boye und Maelandsmo 2010; Murakami et al. 2019), however, in line with the findings in my Fsp1 fluorescence model only a small subpopulation of cancer cells (~3-10%) are Fsp1 positive at the primary tumour site (Chen et al. 2018; Aiello et al. 2016). Given the epithelial origin of PDAC cells it is conclusive to assume Fsp1 activation as a sign of transition towards a mesenchymal phenotype. Therefore, Fsp1 has already been utilized as a marker protein for EMT in several PDAC models (Chen et al. 2018; Rhim et al. 2012).

The unknown: Partial, incomplete EMT and additional routes to metastases:

Even though EMT has been a major field of study for over two decades now a precise and all-encompassing understanding for its role in human cancer progression has not been found yet. It has become even more difficult to specifically classify its influence on various hallmarks of cancer, with new notions arising and introducing novel and even more subtle forms of EMT. Especially when different tumour entities employ distinct subtypes of this program for a variety of different tumour features (Aiello et al. 2018). The hypothesis of “partial” or “incomplete” EMT as a transitory state on the way to full EMT or as an endpoint state of EMT has recently gained increased attention. These cells maintain certain epithelial features while acquiring some mesenchymal ones (Grigore et al. 2016; Nieto et al. 2016). Whether this is an intermediate state to a complete mesenchymal phenotype or an intermediate state of epithelial-mesenchymal duality of various degree as a standalone end-state is not known yet. These cells now could combine the enhanced migratory and invasive properties of EMT activated cells while simultaneously retaining their proliferation and cell attachment advantages from their epithelial side (Jolly et al. 2017). However, these properties are not well defined in molecular terms yet

(Savagner 2015) and there is a need for a consensus on their specific roles. These new concepts have yet to prove their implications and new insight on the existing principles of EMT.

Recently, Aiello et al. proposed a partial EMT (p-EMT) program involved in metastases in a KPCY model of pancreatic cancer (Aiello et al. 2018). Using the loss of membranous E-Cadherin (M-ECAD) as an indicator for mesenchymal transition, they found a subpopulation of cells that while lacking M-ECAD showed stable levels of mRNA for E-Cadherin and other epithelial genes. They proposed that the epithelial phenotype is regulated post-transcriptionally in these p-EMT cells and could support this hypothesis by high levels of E-Cadherin in whole cell lysate and detecting an intracellular relocalization into recycling endocytic vesicles. p-EMT cells showed distinctly different properties regarding their metastatic behaviour from cells utilizing a classic EMT program (c-EMT). p-EMT cells were prone to invade as a collective group and form CTC cluster, whereas c-EMT cells exclusively form single cell CTCs. Interestingly, these clusters showed both mesenchymal and epithelial properties, lacking E-Cadherin on the surface but maintaining it at points of cell-cell contacts. Whether this new form of post-transcriptional regulation of the epithelial phenotype reflects another hybrid state of EMT and will eventually lead to the classic complete EMT program remains to be settled (Aiello et al. 2018). If it is a separate hybrid state, it would not be regulated by classical EMT-TFs or known pathways. This would implicate the existence of unknown pathways involved in the regulation of the epithelial structure of the cell and promoting metastases since CTC clusters are known to have enhanced metastatic potential compared to single cells (Aceto et al. 2014; Cheung und Ewald 2016; Maddipati und Stanger 2015).

Still, several questions arise: Why do EMT-inhibiting drugs fail to prevent metastases? Why is downregulation of the key EMT-TFs not sufficient to abolish metastases? What other means of metastazation exist for tumour cells in order to evade EMT-guided metastazation? Research suggests multiple possible answers: drugs might fail to sufficiently block all EMT related programs or drug distribution is poor in pancreatic cancer due to high grade desmoplasia and the special properties of the microenvironment as already found for classical chemotherapy (Kalluri 2016). There are additional EMT-pathways which are independent from the three major EMT-TFs (Zeb1, Snai1, Twist1). Existing mouse models fail to monitor the complete spectrum of the process of complete, partial, or incomplete EMT simultaneously (Jolly et al. 2017). However, the vast number of results on this matter suggest that there are non-EMT dependent forms of metastazation. This would be a new field of study and contradict a long-standing

paradigm of our understanding of cancer metastases formation. Some pioneer work has already been done and proposed several hypotheses on alternative metastases pathways:

The passive shedding theory supports the claim that the early stages of the metastatic process, namely intravasation, is not achieved through active migration of cancer cells. It proposes that tumour cells achieve this through passive detachment form the primary tumour side into – usually deficient – blood vessels (Bockhorn et al. 2007). This process is not dependent on any activation of an EMT program to enhance migratory or invasive potential but is guided simply by chance. A recent study supports this hypothesis and established that these principles exist in pancreatic cancer cells as well (Krzykawski et al. 2019). They also found that cells accessing the bloodstream usually intravasate as larger groups of cells, giving them significant advantages in survivability compared to disseminated single cells (Aceto et al. 2014; Maddipati und Stanger 2015; Cheung und Ewald 2016) .While this process is still highly inefficient in forming metastases the sheer mass of epithelial cells in the primary tumour side compared to mesenchymal ones could explain the astonishing difference in the metastatic outcome found in my work. Similar mechanisms were proposed for the access to the lymphatic compartment in the same studies. However, this hypothesis does not address EMT-independent seeding of disseminated cancer cells in distant organs.

Another interesting aspect of metastazation is the difference between single cell migration and the invasion of cell groups into the bloodstream. These CTCs and CTC clusters could be observed in several cancer entities and are known to exhibit distinct different metastatic properties (Hong et al. 2016). While single cell CTCs are the archetype of EMT activated cells with enhanced migratory and invasive potential, CTC cluster have been observed to maintain different degrees of epithelial properties (Cheung et al. 2013; Aiello et al. 2018; Aceto et al. 2015). The composition of these clusters seems to vary greatly between tumour entities but also between tumour types. Doublets, triplets, or even larger groups of tumour cells are described, as well as compositions of tumour cells and activated stroma cells (Hong et al. 2016). Depending on the specific formation, CTC clusters are known to have enhanced metastatic potential compared to single cells (Aceto et al. 2014; Maddipati und Stanger 2015; Cheung und Ewald 2016). Epithelial properties are regularly found within these clusters as well as several epithelial markers which could be a hint of a lack of EMT in these cells. It also points out that certain epithelial properties increase metastatic potential.

Some other mechanisms could also play a role in EMT-independent metastases in pancreatic cancer. These include the cell-in-cell phenomenon (Wang et al. 2019) as well as cell-cell

communication via extracellular vesicles (Chiba et al. 2018) or collective cell migration (Haeger et al. 2015). Both could infuse epithelial cancer cells with enhanced migratory and invasive abilities without the utilization of common EMT pathways. However, further studies are required to elucidate their precise role in human PDAC.

The contribution of the microenvironment:

The microenvironment of pancreatic cancer is known to play a crucial part in nearly every hallmark of cancer (Sun et al. 2018). Its influence on promoting metastatic outspread is - despite being extensively studied – not fully understood yet. It is known that tumour associated fibroblasts (TAFs), tumour associated macrophages (TAMs), and pancreatic stellate cells (PSCs) play an important role not only in the desmoplastic reaction which is characteristic for high grade pancreatic disorders but also have a stadium specific impact on tumour development, metastatic formation, chemoresistance, and other crucial roles in PDAC (Murakami et al. 2019; Wen et al. 2019; Ren et al. 2018; Sun et al. 2018). The outcome of drugs targeting the microenvironment were highly anticipated but so far failed to create a breakthrough in pancreatic cancer chemotherapy (Thomas und Radhakrishnan 2019; Kalluri 2016). They did however show the two-sided role the microenvironment plays for the progression of pancreatic cancer disease. Pancreatic cancer cells (PCCs) are known to exert paracrine functions and influence the formation of a tumour specific stroma. Growth factors like TGF-β1 or Platelet derived growth factor (PDGF) are only some of many factors that are known to activate surrounding fibroblast and promote EMT. Activated TAFs then not only induce further desmoplasia and increase the mechanically pressure in the ECM but also provide nourishment and promote cancer-cell migration (Murakami et al. 2019). Similar functions are described for PSCs which are a subgroup of TAFs. These cells stimulate angiogenesis and secrete matrix metalloproteases (MMPs) thereby facilitating migration and extravasation of cancer cells (Thomas und Radhakrishnan 2019). Therefore, it is possible that the main target for EMT-events in the pancreatic cancer disease are not PCCs but the surrounding stroma cells, which then support tumour cells to metastasize all while preserving their epithelial phenotype themselves. Since my work relies on the labelling of PCCs the role of the microenvironment could not be monitored simultaneously. It is therefore possible that surrounding stroma cells exhibit active EMT programs which enables epithelial and not mesenchymal tumour cells to disseminate. Another possibility is the utilization of EMT activated fibroblasts on the invasive front as so-called carrier vehicles for non-EMT cancer cells to metastasize in a cell cluster like

fashion (Hong et al. 2016). Both proposals would identify EMT as a necessary program to facilitate metastatic formation but limiting the necessity of EMT in PCCs to invasion and dissemination. This however would imply the possibility of disseminated non-EMT PCCs to colonize and grow distant metastasis without the further utilization of an EMT program. This could possibly explain the failure of EMT-inhibiting drugs to supress metastases since CTCs already existed during the start of the drug treatment. On the other hand, metastatic outgrowth could also be facilitated by previous established metastatic niches or preconditioning of target organs (Costa-Silva et al. 2015). Soluble tumour factors and circulating tumour stroma cells have been found to precede metastatic formation in certain organs and reorganize the physiological microenvironment to a more tumorigenic environment (Houg und Bijlsma 2018).

Conclusion and limitations of the different mouse models:

Confocal microscopy of PPT tissue showed tdTomato positivity in tumour cells and EGFP positivity in the surrounding stroma (see Figure 1 C). Since PDAC cells derive from epithelial ductal cells with close to no common EMT potential and stroma cells (e.g. fibroblasts) regularly undergo EMT (Sun et al. 2018) it is conclusive to the assume that the Fsp1^{mTmG} reliably labels mesenchymal cells *in vivo*. Also, the system does not seem to be impaired by early stage EMT and MET events during the embryo- and organogenesis.

The metastatic pattern analysis in the endogenous, WT, and SCID mice showed significantly more un-recombined metastases in all approaches in both reporter systems. The metastasis distribution in the endogenous mice and WT implantation model mimics the distribution found in human PDAC metastases. While the findings in the WT-implantation approach mimic and support the results in the endogenous model, it needs further improvement especially to boost implantation efficiency. This problem was overcome in the immunodeficient implantation model (efficiency > 80%).

However, a conclusive statistical analysis of metastatic distribution was not possible in the endogenous model. Due to the ubiquitous tdTomato signal in the Fsp1^{mTmG} reporter system, low intensity tdTomato positive lesions would always be disregarded and therefore EGFP positive metastases systematically overestimated. Additionally, the fluorescence signal is not tumour specific (only for Fsp1^{mTmG}), therefore only clear macroscopic organ alterations could be included in an evaluation. While giving important insights to metastatic processes, the low number of overall metastases and the long evaluation time made it hard to make conclusions from these data. These problems do not exist in the orthotopic transplantation models. That is

why only implanted mice samples were used in the validation of the fluorescence reporter systems.

However, in contrast to the endogenous and WT implantation models the immunodeficient SCID mice implantation model displayed a significant increase in peritoneal and diaphragm metastases. This might be an artefact owing to the implantation technique: Single tumour cells might get access to the intraperitoneal cavity through a leakage in the pancreas after injection of the tumour cells. Without a functional immune system SCID mice in contrast to WT mice, do not seem to be able to successfully eradicate those single tumours cells, leading to a major increase in peritoneal and diaphragm metastases simply due to simplified accessibility.

Grzelak et al. recently published a work which showed the immunogenicity of EGFP in transplantation models. Using a highly metastatic mammary tumour cells line (4TI) they showed that formation of GFP^+ lung metastases was impaired in immunocompetent mice compared to immunodeficient (SCID) mice. This was attributed to a GFP-specific $CD8^+$ T-Cells response. To overcome this a centrally tolerized mouse model for GFP restored the metastatic capacity of 4TI (Grzelak et al. 2022; Schultheiß und Binder 2022). In my work unrecombined (tdTom) metastases largely outnumbered recombined (EGFP) metastases in the wildtype and the immunodeficient model. There was no significant difference in the percentual occurrence of EGFP metastases between the wildtype (2,17 %) and the SCID model (3,01 %) suggesting no significant influence of the immunogenicity of EGFP in this approach. This might be due to the lower number of implanted cells (2500 vs. 7500) or the lower immunogenicity of GFP in C57BL6/J compared to BALB/c mice (Ansari et al. 2016). However, in the $Fsp1^{Ai65\text{-}td\text{-}Tom}$ reporter system, which naturally lacks EGFP, the recombination rate was significantly higher in the immunodeficient implantation model than in all other (endogenous, wildtype and SCID) approaches. An implantation series of $Fsp1^{mTmG}$ PPT cells into centrally tolerized GFP mice could show the immunogenicity of EGFP in pancreatic tumour cells.

We nevertheless concluded from these data, that there are first hints that metastatic processes are not necessarily EMT dependent but that there are different routes for tumour cells to invade and form metastases, which seem to coexist with the EMT route. Recent studies on this topic have already suggested that EMT is an important cellular program and might facilitate tumour chemoresistance, but failed to verify its influence on metastatic development in pancreatic tumours and suggesting alternative, EMT-independent, routes to metastazation (Zheng et al. 2015; Chen et al. 2018).

Conclusion on immunofluorescence distribution in PPT and metastases

The fluorescence analysis of the Fsp1^{mTmG} and Fsp1$^{Ai\text{-}65\text{-}tdTom}$ mouse models consistently showed epithelial properties in unrecombined (only for Fsp1^{mTmG}) and three different subpopulations in the recombined cells in PPT and metastases samples.

The existence of these three populations can easily be explained with the common concept of EMT (see 1.2.1) and supports the effectivity of the Fsp1^{mTmG} reporter system. Upon initiation of the process, cells will activate one or several EMT pathways (see 1.2.2) which will gradually lead to a morphological change of the whole cell structure by regulating downstream effector proteins. Depending on the requirements of the microenvironment, each cell will decide whether to progress, sustain or reverse (via MET) its cellular transformation. Given this everchanging state, it is apparent that the expression of several cellular markers varies greatly during this fluid process. EMT-TF (e.g. Twist, Zeb1) and key EMT player (e.g. Fsp1, aSMA) levels peak during the initiation, while downstream targets like E-Cadherin or N-Cadherin will react with different latencies. Note that after a full transition to mesenchymal cell properties only low levels of EMT-TF are necessary to maintain this state explaining the discrepancy between E-Cadherin negativity and Zeb1 positivity in this analysis (see Figure 9, 11). Since the already very low expression of Fsp1 seems to trigger the recombination in the mTmG reporter, the fluorescence signal seems to be a significantly better marker to determine Fsp1 activation, as Fsp1 levels might be too low for proper antibody detection. Also, the amount of MET events is expected to be high since remaining in an EMT state in the primary tumour tissue matrix is not beneficial for tumour cells, due to lower proliferation rates or less cell-cell interaction. This also leads to an Fsp1 expression decrease while e.g., E-cadherin levels remain only partially developed until the full regain of an epithelial state. This could explain the discrepancy in the overlap of the fluorescence distribution between Zeb1, Fsp1, and E-Cadherin in recombined PPT and metastases (see Figure 9, 11)

Regarding the partial overlap in tdTomato and EGFP signal in the confocal images Muzdumar originally published the mTmG reporter with a known mean perdurance of the tdTomato signal of approximately 4.5 days (Muzumdar et al. 2007).

With these findings the overall conclusion is that while EMT is still important for pancreatic metastases there is a significantly large number of cells which succeed in the formation of metastases without ever activating the Fsp1-Cre recombinase and therefore its EMT program. Recombined and unrecombined cells seem to utilize distinct cellular programs which enables them to metastasize but makes them prone to grow in certain organ systems. These programs

are differentiated by the activation of the *Fsp1-Cre* recombinase and therefore linked to the utilization of the EMT program. So, we concluded that there must be EMT independent routes to metastasis. These alternative routes might be the reason why several studies failed to suppress metastatic growth and formation even after inhibiting EMT-activation (Zheng et al. 2015; Fischer et al. 2015; Chen et al. 2018).

Outlook:

Based on my work several issues should be addressed in further studies, utilizing these mouse models: The Fsp1$^{Ai65\text{-}tdTom}$ system should receive more attention because only one cell line was included in the orthotopic transplantation model so far. Especially since this cell line was the only one that showed a significant high amount of recombined metastatic cells. Furthermore, the work could be extended by an additional fluorescence reporter system e.g. R26^{dual} (*Rosa26-CAG-loxP-frt-Stop-frt-FireflyLuc-EGFP-loxP-RenillaLuc-tdTomato*), which by utilizing the same general principle as the R26^{mTmG}-reporter could exclude reporter specific effects (Chen et al. 2018). Even though Fsp1 was reported to be the predominant marker for EMT events in pancreatic cancer (Rhim et al. 2012), other mesenchymal Cre lines (e.g. αSMA, Vimentin, COL6A1, N-Cadherin) could be established to successfully capture all EMT related events in pancreatic tumour cells. These mesenchymal markers could also be included in the confocal staining series to additionally verify EMT status in recombined and unrecombined cells.

As stated in 3.5 additional cell culture experiments should be conducted to evaluate the capability of the Fsp1^{mTmG} system to capture EMT-events *in vitro.* Those should include migration assays and comparing migratory potential of recombined and unrecombined cells. An analysis on protein levels could be added. The conducted TGF- ß experiment (see 3.5) could be modified to secure cell viability after longer treatment periods. One possibility could be a modification of the TGF-ß medium with small doses of FCS (e.g. 2-3%). However, this might lead to a not insignificant bias since FCS includes a more or less high amount of TGF-ß itself, which is a major reason for time dependent alteration of the recombination rate *in vitro* (see 3.6). The latency of the activation of the fluorescence signal found *in vitro* should always be considered when evaluating *in vivo* findings.

RNA sequencing and comparison of recombined and unrecombined PCCs, CTCs and metastatic cells and their genetic imprint could further support the veracity of the Fsp1^{mTmG} system and could also give insight on other possible genetic programs involved in the metastatic cascade. Also, single cell RNA sequencing of recombined and unrecombined CTCs could

increase the understanding of the processes involved in delamination and intravasation in those two subpopulations.

In a more general approach, the tumour formation and metastatic capacity of EMT and non-EMT cells could be studied by orthotopic and tail vein injection of the same amount of only recombined and non-recombined cells, respectively. In this experiment one could also investigate on the organotropism of EMT and non-EMT cells as already proposed in several studies.

Thesis conclusion:

In summary, this work evaluated the role of EMT dependent dissemination, invasion, and metastazation of PDAC cells in $Kras^{G12D}$ driven mouse models. It provides a thorough analysis of the veracity and accuracy of the underlying dual recombinase, dual fluorescence-based linage tracing system in detecting EMT-events *in vivo*. A non EMT-bound mechanism for metastases was found to be the dominant form of metastatic spread in the normal progression of PDAC. However, EMT activated cells had enhanced abilities to infiltrate the bloodstream and the peritoneal cavity but could not compete with non-EMT cells in regards to metastases quantity. A certain organotropism of EMT cells to form lung metastases could be observed. Further research is required to identify these processes to possibly make them accessible for future anti-metastatic treatments. Whether they involve the utilization of a partial EMT program of some sort remains unclear.

Acknowledgement

Hereby, I would like to thank everyone who contributed to the success of this thesis.

First, I thank Prof. Dr. Dieter Saur for giving me the chance to work on this interesting project, for his advice, valuable comments on the project and revision of the thesis.

I would like to thank Prof. Dr. Maximilian Reichert for his valuable mentorship, input and guidance in this project.

I owe my gratitude to Prof. Dr. Roland Schmid for giving me the opportunity to work in his department, the II. Medizinische Klinik at Klinikum rechts der Isar

Furthermore, I want to thank ….

… Dr. Kathleen Schuck for excellent supervision, input and support during my work.

… all animal caretakers for caring for the mice.

… all members of the Saur, Schneider and Reichert research groups for the great atmosphere in the lab and all the helpful advices throughout the years.

… Dido Egger and Tabea Leusser for revision of the thesis.

At last, I thank my family and my friends for all their support and motivation during my work.

References

Aceto, Nicola; Bardia, Aditya; Miyamoto, David T.; Donaldson, Maria C.; Wittner, Ben S.; Spencer, Joel A. et al. (2014): Circulating tumor cell clusters are oligoclonal precursors of breast cancer metastasis. In: *Cell* 158 (5), S. 1110–1122. DOI: 10.1016/j.cell.2014.07.013.

Aceto, Nicola; Toner, Mehmet; Maheswaran, Shyamala; Haber, Daniel A. (2015): En Route to Metastasis: Circulating Tumor Cell Clusters and Epithelial-to-Mesenchymal Transition. In: *Trends in cancer* 1 (1), S. 44–52. DOI: 10.1016/j.trecan.2015.07.006.

Adamska, Aleksandra; Domenichini, Alice; Falasca, Marco (2017): Pancreatic Ductal Adenocarcinoma: Current and Evolving Therapies. In: *International journal of molecular sciences* 18 (7). DOI: 10.3390/ijms18071338.

Aiello, Nicole M.; Bajor, David L.; Norgard, Robert J.; Sahmoud, Amine; Bhagwat, Neha; Pham, Minh N. et al. (2016): Metastatic progression is associated with dynamic changes in the local microenvironment. In: *Nature communications* 7, S. 12819. DOI: 10.1038/ncomms12819.

Aiello, Nicole M.; Maddipati, Ravikanth; Norgard, Robert J.; Balli, David; Li, Jinyang; Yuan, Salina et al. (2018): EMT Subtype Influences Epithelial Plasticity and Mode of Cell Migration. In: *Developmental cell* 45 (6), 681-695.e4. DOI: 10.1016/j.devcel.2018.05.027.

Ansari, Amir Mehdi; Ahmed, A. Karim; Matsangos, Aerielle E.; Lay, Frank; Born, Louis J.; Marti, Guy et al. (2016): Cellular GFP Toxicity and Immunogenicity: Potential Confounders in in Vivo Cell Tracking Experiments. In: *Stem cell reviews and reports* 12 (5), S. 553–559. DOI: 10.1007/s12015-016-9670-8.

Arnoletti, J. Pablo; Fanaian, Na'im; Reza, Joseph; Sause, Ryan; Almodovar, Alvin Jo; Srivastava, Milan et al. (2018): Pancreatic and bile duct cancer circulating tumor cells (CTC) form immune-resistant multi-cell type clusters in the portal venous circulation. In: *Cancer biology & therapy* 19 (10), S. 887–897. DOI: 10.1080/15384047.2018.1480292.

Arumugam, Thiruvengadam; Ramachandran, Vijaya; Fournier, Keith F.; Wang, Huamin; Marquis, Lauren; Abbruzzese, James L. et al. (2009): Epithelial to mesenchymal transition contributes to drug resistance in pancreatic cancer. In: *Cancer research* 69 (14), S. 5820–5828. DOI: 10.1158/0008-5472.CAN-08-2819.

Bhowmick, Neil A.; Chytil, Anna; Plieth, David; Gorska, Agnieszka E.; Dumont, Nancy; Shappell, Scott et al. (2004): TGF-beta signaling in fibroblasts modulates the oncogenic potential of adjacent epithelia. In: *Science (New York, N.Y.)* 303 (5659), S. 848–851. DOI: 10.1126/science.1090922.

Bockhorn, Maximilian; Jain, Rakesh K.; Munn, Lance L. (2007): Active versus passive mechanisms in metastasis: do cancer cells crawl into vessels, or are they pushed? In: *The Lancet Oncology* 8 (5), S. 444–448. DOI: 10.1016/S1470-2045(07)70140-7.

Boye, Kjetil; Maelandsmo, Gunhild M. (2010): S100A4 and metastasis: a small actor playing many roles. In: *The American journal of pathology* 176 (2), S. 528–535. DOI: 10.2353/ajpath.2010.090526.

Brabletz, Thomas (2012): To differentiate or not--routes towards metastasis. In: *Nature reviews. Cancer* 12 (6), S. 425–436. DOI: 10.1038/nrc3265.

Brabletz, Thomas; Kalluri, Raghu; Nieto, M. Angela; Weinberg, Robert A. (2018): EMT in cancer. In: *Nature reviews. Cancer* 18 (2), S. 128–134. DOI: 10.1038/nrc.2017.118.

Bresnick, Anne R.; Weber, David J.; Zimmer, Danna B. (2015): S100 proteins in cancer. In: *Nature reviews. Cancer* 15 (2), S. 96–109. DOI: 10.1038/nrc3893.

Cano, Carla E.; Motoo, Yoshiharu; Iovanna, Juan L. (2010): Epithelial-to-mesenchymal transition in pancreatic adenocarcinoma. In: *TheScientificWorldJournal* 10, S. 1947–1957. DOI: 10.1100/tsw.2010.183.

Che, Pulin; Yang, Youfeng; Han, Xiaosi; Hu, Meng; Sellers, Jeffery C.; Londono-Joshi, Angelina I. et al. (2015): S100A4 promotes pancreatic cancer progression through a dual signaling pathway mediated by Src and focal adhesion kinase. In: *Scientific reports* 5, S. 8453. DOI: 10.1038/srep08453.

Chen, Hongyan; Xu, Chengshan; Jin, Qing'e; Liu, Zhihua (2014): S100 protein family in human cancer. In: *American Journal of Cancer Research* 4 (2), S. 89–115.

Chen, Huihui; Lu, Wei; Huang, Chongjie; Ding, Kefeng; Xia, Dajing; Wu, Yihua; Cai, Mao (2017): Prognostic significance of ZEB1 and ZEB2 in digestive cancers: a cohort-based analysis and secondary analysis. In: *Oncotarget* 8 (19), S. 31435–31448. DOI: 10.18632/oncotarget.15634.

Chen, Yang; LeBleu, Valerie S.; Carstens, Julienne L.; Sugimoto, Hikaru; Zheng, Xiaofeng; Malasi, Shruti et al. (2018): Dual reporter genetic mouse models of pancreatic cancer identify an epithelial-to-mesenchymal transition-independent metastasis program. In: *EMBO molecular medicine* 10 (10). DOI: 10.15252/emmm.201809085.

Cheung, Kevin J.; Ewald, Andrew J. (2016): A collective route to metastasis: Seeding by tumor cell clusters. In: *Science (New York, N.Y.)* 352 (6282), S. 167–169. DOI: 10.1126/science.aaf6546.

Cheung, Kevin J.; Gabrielson, Edward; Werb, Zena; Ewald, Andrew J. (2013): Collective invasion in breast cancer requires a conserved basal epithelial program. In: *Cell* 155 (7), S. 1639–1651. DOI: 10.1016/j.cell.2013.11.029.

Chiba, Mitsuru; Kubota, Shiori; Sakai, Ayaka; Monzen, Satoru (2018): Cell-to-cell communication via extracellular vesicles among human pancreatic cancer cells derived from the same patient. In: *Molecular medicine reports* 18 (4), S. 3989–3996. DOI: 10.3892/mmr.2018.9376.

Conroy, Thierry; Desseigne, Françoise; Ychou, Marc; Bouché, Olivier; Guimbaud, Rosine; Bécouarn, Yves et al. (2011): FOLFIRINOX versus gemcitabine for metastatic pancreatic cancer. In: *The New England journal of medicine* 364 (19), S. 1817–1825. DOI: 10.1056/NEJMoa1011923.

Costa-Silva, Bruno; Aiello, Nicole M.; Ocean, Allyson J.; Singh, Swarnima; Zhang, Haiying; Thakur, Basant Kumar et al. (2015): Pancreatic cancer exosomes initiate pre-metastatic niche formation in the liver. In: *Nature cell biology* 17 (6), S. 816–826. DOI: 10.1038/ncb3169.

Craene, Bram de; Berx, Geert (2013): Regulatory networks defining EMT during cancer initiation and progression. In: *Nature reviews. Cancer* 13 (2), S. 97–110. DOI: 10.1038/nrc3447.

Fei, Fei; Qu, Jie; Zhang, Mingqing; Li, Yuwei; Zhang, Shiwu (2017): S100A4 in cancer progression and metastasis: A systematic review. In: *Oncotarget* 8 (42), S. 73219–73239. DOI: 10.18632/oncotarget.18016.

Fischer, Kari R.; Durrans, Anna; Lee, Sharrell; Sheng, Jianting; Li, Fuhai; Wong, Stephen T. C. et al. (2015): Epithelial-to-mesenchymal transition is not required for lung metastasis but contributes to chemoresistance. In: *Nature* 527 (7579), S. 472–476. DOI: 10.1038/nature15748.

Fischer, Richard; Breidert, Matthias; Keck, Tobias; Makowiec, Frank; Lohrmann, Christian; Harder, Jan (2012): Early recurrence of pancreatic cancer after resection and during adjuvant chemotherapy. In: *Saudi journal of gastroenterology : official journal of the Saudi Gastroenterology Association* 18 (2), S. 118–121. DOI: 10.4103/1319-3767.93815.

Goossens, Steven; Janzen, Viktor; Bartunkova, Sonia; Yokomizo, Tomomasa; Drogat, Benjamin; Crisan, Mihaela et al. (2011): The EMT regulator Zeb2/Sip1 is essential for murine embryonic hematopoietic stem/progenitor cell differentiation and mobilization. In: *Blood* 117 (21), S. 5620–5630. DOI: 10.1182/blood-2010-08-300236.

Gregory, Philip A.; Bert, Andrew G.; Paterson, Emily L.; Barry, Simon C.; Tsykin, Anna; Farshid, Gelareh et al. (2008): The miR-200 family and miR-205 regulate epithelial to mesenchymal transition by targeting ZEB1 and SIP1. In: *Nature cell biology* 10 (5), S. 593–601. DOI: 10.1038/ncb1722.

Grigore, Alexandru Dan; Jolly, Mohit Kumar; Jia, Dongya; Farach-Carson, Mary C.; Levine, Herbert (2016): Tumor Budding: The Name is EMT. Partial EMT. In: *Journal of clinical medicine* 5 (5). DOI: 10.3390/jcm5050051.

Grzelak, Candice A.; Goddard, Erica T.; Lederer, Emma E.; Rajaram, Kamya; Dai, Jinxiang; Shor, Ryann E. et al. (2022): Elimination of fluorescent protein immunogenicity permits modeling of metastasis in immune-competent settings. In: *Cancer cell* 40 (1), S. 1–2. DOI: 10.1016/j.ccell.2021.11.004.

Gupta, Gaorav P.; Massagué, Joan (2006): Cancer metastasis: building a framework. In: *Cell* 127 (4), S. 679–695. DOI: 10.1016/j.cell.2006.11.001.

Haeger, Anna; Wolf, Katarina; Zegers, Mirjam M.; Friedl, Peter (2015): Collective cell migration: guidance principles and hierarchies. In: *Trends in cell biology* 25 (9), S. 556–566. DOI: 10.1016/j.tcb.2015.06.003.

Hanahan, Douglas; Weinberg, Robert A. (2000): The Hallmarks of Cancer. In: *Cell* 100 (1), S. 57–70. DOI: 10.1016/S0092-8674(00)81683-9.

Hanahan, Douglas; Weinberg, Robert A. (2011): Hallmarks of cancer: the next generation. In: *Cell* 144 (5), S. 646–674. DOI: 10.1016/j.cell.2011.02.013.

Hartwell, Kimberly A.; Muir, Beth; Reinhardt, Ferenc; Carpenter, Anne E.; Sgroi, Dennis C.; Weinberg, Robert A. (2006): The Spemann organizer gene, Goosecoid, promotes tumor

metastasis. In: *Proceedings of the National Academy of Sciences of the United States of America* 103 (50), S. 18969–18974. DOI: 10.1073/pnas.0608636103.

Hay, E. D. (1995): An overview of epithelio-mesenchymal transformation. In: *Acta anatomica* 154 (1), S. 8–20. DOI: 10.1159/000147748.

Heerboth, Sarah; Housman, Genevieve; Leary, Meghan; Longacre, Mckenna; Byler, Shannon; Lapinska, Karolina et al. (2015): EMT and tumor metastasis. In: *Clinical and translational medicine* 4, S. 6. DOI: 10.1186/s40169-015-0048-3.

Helfman, D. M.; Kim, E. J.; Lukanidin, E.; Grigorian, M. (2005): The metastasis associated protein S100A4: role in tumour progression and metastasis. In: *British journal of cancer* 92 (11), S. 1955–1958. DOI: 10.1038/sj.bjc.6602613.

Herreros-Villanueva, Marta; Hijona, Elizabeth; Cosme, Angel; Bujanda, Luis (2012): Mouse models of pancreatic cancer. In: *World journal of gastroenterology* 18 (12), S. 1286–1294. DOI: 10.3748/wjg.v18.i12.1286.

Hingorani, Sunil R.; Petricoin, Emanuel F.; Maitra, Anirban; Rajapakse, Vinodh; King, Catrina; Jacobetz, Michael A. et al. (2003): Preinvasive and invasive ductal pancreatic cancer and its early detection in the mouse. In: *Cancer cell* 4 (6), S. 437–450. DOI: 10.1016/S1535-6108(03)00309-X.

Hingorani, Sunil R.; Wang, Lifu; Multani, Asha S.; Combs, Chelsea; Deramaudt, Therese B.; Hruban, Ralph H. et al. (2005): Trp53R172H and KrasG12D cooperate to promote chromosomal instability and widely metastatic pancreatic ductal adenocarcinoma in mice. In: *Cancer cell* 7 (5), S. 469–483. DOI: 10.1016/j.ccr.2005.04.023.

Hirai, Ichiro; Kimura, Wataru; Ozawa, Koichiro; Kudo, Shun; Suto, Koichi; Kuzu, Hiroshi; Fuse, Akira (2002): Perineural invasion in pancreatic cancer. In: *Pancreas* 24 (1), S. 15–25. DOI: 10.1097/00006676-200201000-00003.

Hoff, Daniel D. von; Ervin, Thomas; Arena, Francis P.; Chiorean, E. Gabriela; Infante, Jeffrey; Moore, Malcolm et al. (2013): Increased survival in pancreatic cancer with nab-paclitaxel plus gemcitabine. In: *The New England journal of medicine* 369 (18), S. 1691–1703. DOI: 10.1056/NEJMoa1304369.

Hong, Yupeng; Fang, Francia; Zhang, Qi (2016): Circulating tumor cell clusters: What we know and what we expect (Review). In: *International journal of oncology* 49 (6), S. 2206–2216. DOI: 10.3892/ijo.2016.3747.

Houg, Demi S.; Bijlsma, Maarten F. (2018): The hepatic pre-metastatic niche in pancreatic ductal adenocarcinoma. In: *Molecular cancer* 17 (1), S. 95. DOI: 10.1186/s12943-018-0842-9.

Hustinx, Steven R.; Leoni, Lorenzo M.; Yeo, Charles J.; Brown, Priscilla N.; Goggins, Michael; Kern, Scott E. et al. (2005): Concordant loss of MTAP and p16/CDKN2A expression in pancreatic intraepithelial neoplasia: evidence of homozygous deletion in a noninvasive precursor lesion. In: *Modern pathology : an official journal of the United States and Canadian Academy of Pathology, Inc* 18 (7), S. 959–963. DOI: 10.1038/modpathol.3800377.

Iacobuzio-Donahue, Christine A.; Fu, Baojin; Yachida, Shinichi; Luo, Mingde; Abe, Hisashi; Henderson, Clark M. et al. (2009): DPC4 gene status of the primary carcinoma correlates with patterns of failure in patients with pancreatic cancer. In: *Journal of clinical oncology : official journal of the American Society of Clinical Oncology* 27 (11), S. 1806–1813. DOI: 10.1200/JCO.2008.17.7188.

Jia, Fuxin; Liu, Mengmeng; Li, Xiao; Zhang, Fen; Yue, Shuqiang; Liu, Jiangwei (2019): Relationship between S100A4 protein expression and pre-operative serum CA19.9 levels in pancreatic carcinoma and its prognostic significance. In: *World journal of surgical oncology* 17 (1), S. 163. DOI: 10.1186/s12957-019-1707-4.

Jolly, Mohit Kumar; Ware, Kathryn E.; Gilja, Shivee; Somarelli, Jason A.; Levine, Herbert (2017): EMT and MET: necessary or permissive for metastasis? In: *Molecular oncology* 11 (7), S. 755–769. DOI: 10.1002/1878-0261.12083.

Kalluri, Raghu (2009): EMT: when epithelial cells decide to become mesenchymal-like cells. In: *The Journal of clinical investigation* 119 (6), S. 1417–1419. DOI: 10.1172/JCI39675.

Kalluri, Raghu (2016): The biology and function of fibroblasts in cancer. In: *Nature reviews. Cancer* 16 (9), S. 582–598. DOI: 10.1038/nrc.2016.73.

Kalluri, Raghu; Neilson, Eric G. (2003): Epithelial-mesenchymal transition and its implications for fibrosis. In: *The Journal of clinical investigation* 112 (12), S. 1776–1784. DOI: 10.1172/JCI20530.

Kalluri, Raghu; Weinberg, Robert A. (2009): The basics of epithelial-mesenchymal transition. In: *The Journal of clinical investigation* 119 (6), S. 1420–1428. DOI: 10.1172/JCI39104.

Kanda, Mitsuro; Matthaei, Hanno; Wu, Jian; Hong, Seung-Mo; Yu, Jun; Borges, Michael et al. (2012): Presence of somatic mutations in most early-stage pancreatic intraepithelial neoplasia. In: *Gastroenterology* 142 (4), 730-733.e9. DOI: 10.1053/j.gastro.2011.12.042.

Kawaguchi, Yoshiya; Cooper, Bonnie; Gannon, Maureen; Ray, Michael; MacDonald, Raymond J.; Wright, Christopher V. E. (2002): The role of the transcriptional regulator Ptf1a in converting intestinal to pancreatic progenitors. In: *Nature genetics* 32 (1), S. 128–134. DOI: 10.1038/ng959.

Kim, Seung; MacDonald, R. (2002): Signaling and transcriptional control of pancreatic organogenesis. In: *Current Opinion in Genetics & Development* 12 (5), S. 540–547. DOI: 10.1016/S0959-437X(02)00338-6.

Krebs, Angela M.; Mitschke, Julia; Lasierra Losada, María; Schmalhofer, Otto; Boerries, Melanie; Busch, Hauke et al. (2017): The EMT-activator Zeb1 is a key factor for cell plasticity and promotes metastasis in pancreatic cancer. In: *Nature cell biology* 19 (5), S. 518–529. DOI: 10.1038/ncb3513.

Krzykawski, M. P.; Krzykawska, R.; Paw, M.; Czyz, J.; Marcinkiewicz, J. (2019): A novel in vitro model of metastasis supporting passive shedding hypothesis from murine pancreatic cancer Panc-02. In: *Cytotechnology* 71 (5), S. 989–1002. DOI: 10.1007/s10616-019-00341-2.

Lambert, Arthur W.; Pattabiraman, Diwakar R.; Weinberg, Robert A. (2017): Emerging Biological Principles of Metastasis. In: *Cell* 168 (4), S. 670–691. DOI: 10.1016/j.cell.2016.11.037.

Lamouille, Samy; Xu, Jian; Derynck, Rik (2014): Molecular mechanisms of epithelial-mesenchymal transition. In: *Nature reviews. Molecular cell biology* 15 (3), S. 178–196. DOI: 10.1038/nrm3758.

Lee, Chang-Lung; Moding, Everett J.; Huang, Xiaofang; Li, Yifan; Woodlief, Loretta Z.; Rodrigues, Rafaela C. et al. (2012): Generation of primary tumors with Flp recombinase in FRT-flanked p53 mice. In: *Disease models & mechanisms* 5 (3), S. 397–402. DOI: 10.1242/dmm.009084.

Lv, Yinghao; Huang, Shuai (2019): Role of non-coding RNA in pancreatic cancer. In: *Oncology letters* 18 (4), S. 3963–3973. DOI: 10.3892/ol.2019.10758.

Maddipati, Ravikanth; Stanger, Ben Z. (2015): Pancreatic Cancer Metastases Harbor Evidence of Polyclonality. In: *Cancer discovery* 5 (10), S. 1086–1097. DOI: 10.1158/2159-8290.CD-15-0120.

Madisen, Linda; Garner, Aleena R.; Shimaoka, Daisuke; Chuong, Amy S.; Klapoetke, Nathan C.; Li, Lu et al. (2015): Transgenic mice for intersectional targeting of neural sensors and

effectors with high specificity and performance. In: *Neuron* 85 (5), S. 942–958. DOI: 10.1016/j.neuron.2015.02.022.

Mishra, Shrawan Kumar; Siddique, Hifzur Rahman; Saleem, Mohammad (2012): S100A4 calcium-binding protein is key player in tumor progression and metastasis: preclinical and clinical evidence. In: *Cancer metastasis reviews* 31 (1-2), S. 163–172. DOI: 10.1007/s10555-011-9338-4.

Morris, John P.; Wang, Sam C.; Hebrok, Matthias (2010): KRAS, Hedgehog, Wnt and the twisted developmental biology of pancreatic ductal adenocarcinoma. In: *Nature reviews. Cancer* 10 (10), S. 683–695. DOI: 10.1038/nrc2899.

Murakami, Takashi; Hiroshima, Yukihiko; Matsuyama, Ryusei; Homma, Yuki; Hoffman, Robert M.; Endo, Itaru (2019): Role of the tumor microenvironment in pancreatic cancer. In: *Annals of gastroenterological surgery* 3 (2), S. 130–137. DOI: 10.1002/ags3.12225.

Murray, Stephen A.; Gridley, Thomas (2006): Snail1 gene function during early embryo patterning in mice. In: *Cell cycle (Georgetown, Tex.)* 5 (22), S. 2566–2570. DOI: 10.4161/cc.5.22.3502.

Muzumdar, Mandar Deepak; Tasic, Bosiljka; Miyamichi, Kazunari; Li, Ling; Luo, Liqun (2007): A global double-fluorescent Cre reporter mouse. In: *Genesis (New York, N.Y. : 2000)* 45 (9), S. 593–605. DOI: 10.1002/dvg.20335.

Neoptolemos, John P.; Kleeff, Jörg; Michl, Patrick; Costello, Eithne; Greenhalf, William; Palmer, Daniel H. (2018): Therapeutic developments in pancreatic cancer: current and future perspectives. In: *Nature reviews. Gastroenterology & hepatology* 15 (6), S. 333–348. DOI: 10.1038/s41575-018-0005-x.

Nieto, M. Angela; Huang, Ruby Yun-Ju; Jackson, Rebecca A.; Thiery, Jean Paul (2016): EMT: 2016. In: *Cell* 166 (1), S. 21–45. DOI: 10.1016/j.cell.2016.06.028.

Nisticò, Paola; Bissell, Mina J.; Radisky, Derek C. (2012): Epithelial-mesenchymal transition: general principles and pathological relevance with special emphasis on the role of matrix metalloproteinases. In: *Cold Spring Harbor perspectives in biology* 4 (2). DOI: 10.1101/cshperspect.a011908.

Nomura, Alice; Majumder, Kaustav; Giri, Bhuwan; Dauer, Patricia; Dudeja, Vikas; Roy, Sabita et al. (2016): Inhibition of NF-kappa B pathway leads to deregulation of epithelial-mesenchymal transition and neural invasion in pancreatic cancer. In: *Laboratory investigation;*

a journal of technical methods and pathology 96 (12), S. 1268–1278. DOI: 10.1038/labinvest.2016.109.

Oida, Yasuhisa; Yamazaki, Hitoshi; Tobita, Kosuke; Mukai, Masaya; Ohtani, Yasuo; Miyazaki, Noriyuki et al. (2006): Increased S100A4 expression combined with decreased E-cadherin expression predicts a poor outcome of patients with pancreatic cancer. In: *Oncology reports* 16 (3), S. 457–463.

Orre, L. M.; Panizza, E.; Kaminskyy, V. O.; Vernet, E.; Gräslund, T.; Zhivotovsky, B.; Lehtiö, J. (2013): S100A4 interacts with p53 in the nucleus and promotes p53 degradation. In: *Oncogene* 32 (49), S. 5531–5540. DOI: 10.1038/onc.2013.213.

Owusu-Ansah, Kwabena Gyabaah; Song, Guangyuan; Chen, Ronggao; Edoo, Muhammad Ibrahim Alhadi; Li, Jun; Chen, Bingjie et al. (2019): COL6A1 promotes metastasis and predicts poor prognosis in patients with pancreatic cancer. In: *International journal of oncology* 55 (2), S. 391–404. DOI: 10.3892/ijo.2019.4825.

Peixoto, Renata D'Alpino; Speers, Caroline; McGahan, Colleen E.; Renouf, Daniel J.; Schaeffer, David F.; Kennecke, Hagen F. (2015): Prognostic factors and sites of metastasis in unresectable locally advanced pancreatic cancer. In: *Cancer medicine* 4 (8), S. 1171–1177. DOI: 10.1002/cam4.459.

Puisieux, Alain; Brabletz, Thomas; Caramel, Julie (2014): Oncogenic roles of EMT-inducing transcription factors. In: *Nature cell biology* 16 (6), S. 488–494. DOI: 10.1038/ncb2976.

Pylayeva-Gupta, Yuliya; Grabocka, Elda; Bar-Sagi, Dafna (2011): RAS oncogenes: weaving a tumorigenic web. In: *Nature reviews. Cancer* 11 (11), S. 761–774. DOI: 10.1038/nrc3106.

Rahib, Lola; Smith, Benjamin D.; Aizenberg, Rhonda; Rosenzweig, Allison B.; Fleshman, Julie M.; Matrisian, Lynn M. (2014): Projecting cancer incidence and deaths to 2030: the unexpected burden of thyroid, liver, and pancreas cancers in the United States. In: *Cancer research* 74 (11), S. 2913–2921. DOI: 10.1158/0008-5472.CAN-14-0155.

Reichert, Maximilian; Bakir, Basil; Moreira, Leticia; Pitarresi, Jason R.; Feldmann, Karin; Simon, Lauren et al. (2018): Regulation of Epithelial Plasticity Determines Metastatic Organotropism in Pancreatic Cancer. In: *Developmental cell* 45 (6), 696-711.e8. DOI: 10.1016/j.devcel.2018.05.025.

Ren, Bo; Cui, Ming; Yang, Gang; Wang, Huanyu; Feng, Mengyu; You, Lei; Zhao, Yupei (2018): Tumor microenvironment participates in metastasis of pancreatic cancer. In: *Molecular cancer* 17 (1), S. 108. DOI: 10.1186/s12943-018-0858-1.

Rhim, Andrew D.; Mirek, Emily T.; Aiello, Nicole M.; Maitra, Anirban; Bailey, Jennifer M.; McAllister, Florencia et al. (2012): EMT and dissemination precede pancreatic tumor formation. In: *Cell* 148 (1-2), S. 349–361. DOI: 10.1016/j.cell.2011.11.025.

Rodriguez-Aznar, Eva; Wiesmüller, Lisa; Sainz, Bruno; Hermann, Patrick C. (2019): EMT and Stemness-Key Players in Pancreatic Cancer Stem Cells. In: *Cancers* 11 (8). DOI: 10.3390/cancers11081136.

Roser Max; Ritchie Hannah (2018): Cancer. Hg. v. Ourworldindata.

Ryan, David P.; Hong, Theodore S.; Bardeesy, Nabeel (2014): Pancreatic adenocarcinoma. In: *The New England journal of medicine* 371 (11), S. 1039–1049. DOI: 10.1056/NEJMra1404198.

Savagner, Pierre (2015): Epithelial-mesenchymal transitions: from cell plasticity to concept elasticity. In: *Current topics in developmental biology* 112, S. 273–300. DOI: 10.1016/bs.ctdb.2014.11.021.

Schmidt-Hansen, Birgitte; Klingelhöfer, Jörg; Grum-Schwensen, Birgitte; Christensen, Annette; Andresen, Susanne; Kruse, Charlotte et al. (2004): Functional significance of metastasis-inducing S100A4(Mts1) in tumor-stroma interplay. In: *The Journal of biological chemistry* 279 (23), S. 24498–24504. DOI: 10.1074/jbc.M400441200.

Schönhuber, Nina; Seidler, Barbara; Schuck, Kathleen; Veltkamp, Christian; Schachtler, Christina; Zukowska, Magdalena et al. (2014): A next-generation dual-recombinase system for time- and host-specific targeting of pancreatic cancer. In: *Nature medicine* 20 (11), S. 1340–1347. DOI: 10.1038/nm.3646.

Schultheiß, Christoph; Binder, Mascha (2022): Overcoming unintended immunogenicity in immunocompetent mouse models of metastasis: the case of GFP. In: *Signal transduction and targeted therapy* 7 (1), S. 68. DOI: 10.1038/s41392-022-00929-9.

Seidler, Barbara; Schmidt, Annegret; Mayr, Ulrich; Nakhai, Hassan; Schmid, Roland M.; Schneider, Günter; Saur, Dieter (2008): A Cre-loxP-based mouse model for conditional somatic gene expression and knockdown in vivo by using avian retroviral vectors. In: *Proceedings of the National Academy of Sciences of the United States of America* 105 (29), S. 10137–10142. DOI: 10.1073/pnas.0800487105.

Shibue, Tsukasa; Weinberg, Robert A. (2017): EMT, CSCs, and drug resistance: the mechanistic link and clinical implications. In: *Nature reviews. Clinical oncology* 14 (10), S. 611–629. DOI: 10.1038/nrclinonc.2017.44.

Siegel, Rebecca L.; Miller, Kimberly D.; Jemal, Ahmedin (2019): Cancer statistics, 2019. In: *CA: a cancer journal for clinicians* 69 (1), S. 7–34. DOI: 10.3322/caac.21551.

Sun, Qiqing; Zhang, Bo; Hu, Qiangsheng; Qin, Yi; Xu, Wenyan; Liu, Wensheng et al. (2018): The impact of cancer-associated fibroblasts on major hallmarks of pancreatic cancer. In: *Theranostics* 8 (18), S. 5072–5087. DOI: 10.7150/thno.26546.

Thiery, Jean Paul; Acloque, Hervé; Huang, Ruby Y. J.; Nieto, M. Angela (2009): Epithelial-mesenchymal transitions in development and disease. In: *Cell* 139 (5), S. 871–890. DOI: 10.1016/j.cell.2009.11.007.

Thomas, Divya; Radhakrishnan, Prakash (2019): Tumor-stromal crosstalk in pancreatic cancer and tissue fibrosis. In: *Molecular cancer* 18 (1), S. 14. DOI: 10.1186/s12943-018-0927-5.

Vries, Annemieke de; Flores, Elsa R.; Miranda, Barbara; Hsieh, Harn-Mei; van Oostrom, Conny Th M.; Sage, Julien; Jacks, Tyler (2002): Targeted point mutations of p53 lead to dominant-negative inhibition of wild-type p53 function. In: *Proceedings of the National Academy of Sciences of the United States of America* 99 (5), S. 2948–2953. DOI: 10.1073/pnas.052713099.

Wang, Xinlong; Li, Yilong; Li, Jiating; Le Li; Zhu, Hong; Chen, Hua et al. (2019): Cell-in-Cell Phenomenon and Its Relationship With Tumor Microenvironment and Tumor Progression: A Review. In: *Frontiers in cell and developmental biology* 7, S. 311. DOI: 10.3389/fcell.2019.00311.

Wen, Zhang; Liu, Qiaofei; Wu, Jihua; Xu, Banghao; Wang, Jilong; Liang, Lizhou et al. (2019): Fibroblast activation protein α-positive pancreatic stellate cells promote the migration and invasion of pancreatic cancer by CXCL1-mediated Akt phosphorylation. In: *Annals of translational medicine* 7 (20), S. 532. DOI: 10.21037/atm.2019.09.164.

Xie, Ran; Schlumbrecht, Matthew P.; Shipley, Gregory L.; Xie, Susu; Bassett, Roland L.; Broaddus, Russell R. (2009): S100A4 mediates endometrial cancer invasion and is a target of TGF-beta1 signaling. In: *Laboratory investigation; a journal of technical methods and pathology* 89 (8), S. 937–947. DOI: 10.1038/labinvest.2009.52.

Xu, Jian; Lamouille, Samy; Derynck, Rik (2009): TGF-beta-induced epithelial to mesenchymal transition. In: *Cell research* 19 (2), S. 156–172. DOI: 10.1038/cr.2009.5.

Xue, Chengsen; Plieth, David; Venkov, Christo; Xu, Carol; Neilson, Eric G. (2003): The gatekeeper effect of epithelial-mesenchymal transition regulates the frequency of breast cancer metastasis. In: *Cancer research* 63 (12), S. 3386–3394.

Ying, Haoqiang; Kimmelman, Alec C.; Lyssiotis, Costas A.; Hua, Sujun; Chu, Gerald C.; Fletcher-Sananikone, Eliot et al. (2012): Oncogenic Kras maintains pancreatic tumors through regulation of anabolic glucose metabolism. In: *Cell* 149 (3), S. 656–670. DOI: 10.1016/j.cell.2012.01.058.

Zavadil, Jiri; Böttinger, Erwin P. (2005): TGF-beta and epithelial-to-mesenchymal transitions. In: *Oncogene* 24 (37), S. 5764–5774. DOI: 10.1038/sj.onc.1208927.

Zhang, Jun-Feng; Hua, Rong; Sun, Yong-Wei; Liu, Wei; Huo, Yan-Miao; Liu, De-Jun; Li, Jiao (2013): Influence of perineural invasion on survival and recurrence in patients with resected pancreatic cancer. In: *Asian Pacific journal of cancer prevention : APJCP* 14 (9), S. 5133–5139. DOI: 10.7314/apjcp.2013.14.9.5133.

Zheng, Xiaofeng; Carstens, Julienne L.; Kim, Jiha; Scheible, Matthew; Kaye, Judith; Sugimoto, Hikaru et al. (2015): Epithelial-to-mesenchymal transition is dispensable for metastasis but induces chemoresistance in pancreatic cancer. In: *Nature* 527 (7579), S. 525–530. DOI: 10.1038/nature16064.

Publications resulting from this work

Anna Lorentzen Paul F. Becker, Jan Kosla, Massimo Saini, Kathrin Weidele, Paolo Ronchi, Corinna Klein, Monika J. Wolf, Felix Geist, Bastian Seubert, Marc Ringelhan, Daniela Mihic-Probst, Knud Esser, Marko Roblek, Felix Kuehne, Gaia Bianco, Tracy O'Connor, **Quentin Müller**, Kathleen Schuck, Sebastian Lang, Daniel Hartmann, Saskia Spaich, Olaf Groß, Jochen Utikal, Sebastian Haferkamp, Martin R. Sprick, Amruta Damle-Vartak, Alexander Hapfelmeier, Norbert Hüser, Ulrike Protzer, Andreas Trumpp, Dieter Saur, Nachiket Vartak, Christoph A. Klein, Bernhard Polzer, Lubor Borsig & Mathias Heikenwalder. Single cell polarity in liquid phase facilitates tumour metastasis. Nature Commun. 9, 887 (Feb. 2018)